

**THERMOPHYSICAL CHARACTERIZATION OF COMPOSITE MATERIALS
UNDER TRANSIENT HEATING CONDITIONS**

By J. Roetling and J. Hanson

Prepared under Contract No. NAS1-10805 by

GENERAL ELECTRIC COMPANY
Re-entry and Environmental Systems Division
Philadelphia, Pennsylvania 19101

for

NATIONAL AERONAUTICS AND SPACE ADMINISTRATION

(NASA-CR-112082) THERMOPHYSICAL
CHARACTERIZATION OF COMPOSITE MATERIALS
UNDER TRANSIENT HEATING CONDITIONS J.
Roetling, et al (General Electric Co.)
[1972] 132 p

N72-26461

Unclas
CSCL 11D G3/18 31390

PRECEDING PAGE BLANK NOT FILMED
CONTENTS

Section	Page
Illustrations	v
Symbols	xi
SUMMARY	1
INTRODUCTION	3
MATERIALS	7
ATJ Graphite	7
Carbitex 700	7
RPP-4	8
MX 2600 Silica Phenolic	8
FM 5272 Cellulose Phenolic	8
TEST METHODS	9
Thermal expansion	9
Restrained Expansion Tests	14
Strength Measurement	21
Compression Measurements	21
Transient Thermal Conductivity Test	21
Analytic base of the GE-RESO transient numerical thermal conductivity technique	24
Sample geometry	26
Experimental procedure	27
Data Reduction	28
TEST RESULTS	35
Measurements on ATJ Graphite	35
Free thermal expansion of ATJ	35
Restrained expansion of ATJ	36
Transient thermal conductivity of ATJ	37
Measurements on MX 2600	37
Free thermal expansion of MX 2600	42
Restrained expansion of MX 2600	42
Strength measurements on MX 2600	44
Transient thermal conductivity of MX 2600 char	44
Measurements on FM 5272	45
Free thermal expansion of FM 5272	45
Restrained expansion of FM 5272	45
Strength measurements on FM 5272	75
Transient thermal conductivity of FM 5272 char	75

CONTENTS (Continued)

Section	Page
TEST RESULTS (continued)	
Measurements on Carbitex 700	83
Free thermal expansion of Carbitex 700	83
Restrained thermal expansion of Carbitex 700	84
Compressive stress-strain of Carbitex 700	85
Strength measurements on Carbitex 700	85
Transient thermal conductivity of Carbitex 700	86
Measurements on RPP-4	97
Free thermal expansion RPP-4	97
Restrained thermal expansion of RPP-4	98
Compression stress-strain tests on RPP-4	98
Strength measurements on RPP-4	100
Transient thermal conductivity of RPP-4	102
UTILIZATION OF TRANSIENT DATA IN THERMO-STRUCTURAL	
ANALYSIS	111
CONCLUSIONS	113
ATJ Graphite	113
MX 2600 Silica Phenolic	113
FM 5272 Cellulose Phenolic	114
Carbitex 700	114
RPP-4	115
General	115
APPENDIX	117
REFERENCES	119

ILLUSTRATIONS

Figure		Page
1	A Hypothetical Thermal Expansion Curve for Defining Terms	11
2	Experimental Arrangement for High Heating Rate Thermal Expansion Measurements	12
3	High Heating Rate Dilatometer	12
4	Close-up of Specimen and Induction Coil; High Heating Rate Dilatometer	13
5	Thermal Expansion Test on Nickel	13
6	MTI Servo-Controlled Electro-hydraulic Test Machine	18
7	Basic Control Circuit for the Restrained Expansion Test	18
8	Loading Arrangement, Restrained Expansion Test	19
9	Close-up of Restrained Expansion Specimen in the Test Machine	19
10	Coaxial Extensometer	20
11	Stress-Strain Relations in the Restrained Expansion Test	20
12	Tensile Specimen	22
13	Tensile Specimen with Unassembled Grips	22
14	Transient Thermal Conductivity Model	31
15	Unassembled Specimen Holder and Specimen; Transient Thermal Conductivity Test	32
16	Instrumented Transient Thermal Conductivity Model	32
17	Small Arc Facility, Showing the Specimen Mounted on the Pneumat- ically Activated Sting	33
18	Hyperthermal Arc Facility, Showing the Dual Specimen Setup	33
19	Data Reduction Technique, Thermal Conductivity	34
20	Thermal Expansion of ATJ Graphite, with Grain, at $T=0.033$ K/s	35
21	Thermal Expansion of ATJ, with Grain, Comparison of Static and Transient Methods	38
22	Effective Thermal Expansion of ATJ, with Grain, $T=27.8$ K/s, $R=55\%$	39
23	Effective Thermal Expansion of ATJ, with Grain, $T=27.8$ K/s, $R=75\%$	39
24	Effective Thermal Expansion of ATJ, with Grain, Comparison, Showing Effect of Restraint	40
25	Modulus of Restrained ATJ Graphite, with Grain	40
26	Thermal Conductivity of ATJ, Perpendicular to Grain	41
27	Heating Rate Data for ATJ Thermal Conductivity Test	41
28	Thermal Expansion of MX 2600 With Lamina, Low Heating Rate Rate (0.033 K/s)	46
29	Thermal Expansion of MX 2600 Across Lamina, Low Heating Rate	46
30	Thermal Expansion of MX 2600, Comparison of With and Across Lamina	47

ILLUSTRATIONS (Continued)

Figure		Page
31	Thermal Expansion of MX 2600, With Lamina at 5.55 K/s (600° F/min)	47
32	Thermal Expansion of MX 2600, With Lamina at 13.9 K/s (1500° F/min)	48
33	Thermal Expansion of MX 2600, Effect of Heating Rate, With Lamina	48
34	Restrained Expansion of MX 2600, With Lamina, Heating rate = 2.9 K/s (310° F/min) R = 65%	49
35	Restrained Expansion of MX 2600, With Lamina, Heating rate = 2.9 K/s (310° F/min) R = 30%	49
36	Restrained Expansion of MX 2600, With Lamina, Heating rate = 5.0 K/s (540° F/min.) R = 65%	50
37	Restrained Expansion of MX 2600, With Lamina, Heating rate = 5.0 K/s (540° F/min.) R = 30%	50
38	Restrained Expansion of MX 2600, Across Lamina, Heating rate = 2.9 K/s (310° F/min) R = 85%	51
39	Restrained Expansion of MX 2600, Across Lamina, Heating rate = 2.9 K/s (310° F/min) R = 55%	51
40	Restrained Expansion of MX 2600, Across Lamina, Heating rate = 5.0 K/s (540° F/min) R = 65%	52
41	Restrained Expansion of MX 2600, Across Lamina, Heating rate = 5.0 K/s (540° F/min) R = 60%	52
42	Effect of Restraint and Heating Rate on Effective Thermal Expansion of MX 2600, With Lamina	53
43	Effect of Restraint and Heating Rate on Effective Thermal Expansion of MX 2600, Across Lamina	53
44	MX 2600 Specimen after Testing at High Heating Rate and High Restraint (Note two "Blow-outs")	54
45	Restrained Expansion Tests on Thick Walled Specimen MX 2600, with Lamina, Heating Rate = 2.9 K/s R = 30%	54
46	Modulus of Restrained MX 2600, With Lamina, Heating Rate = 2.9 K/s (310° F/min) R = 65%	55
47	Modulus of Restrained MX 2600, With Lamina, Heating Rate = 2.9 K/s (310° F/min) R = 30%	55
48	Modulus of Restrained MX 2600, With Lamina, Heating Rate = 5.0 K/s (540° F/min) R = 65%	56
49	Modulus of Restrained MX 2600, With Lamina, Heating Rate = 5.0 K/s (540° F/min) R = 30%	56

ILLUSTRATIONS (Continued)

Figure		Page
50	Modulus of Restrained MX 2600, Across Lamina Heating Rate = 2.9 K/s (310° F/min) R = 85%	57
51	Modulus of Restrained MX 2600, Across Lamina Heating Rate = 2.9 K/s (310° F/min) R = 55%	57
52	Modulus of Restrained MX 2600, Across Lamina Heating Rate = 5.0 K/s (540° F/min) R = 85%	58
53	Modulus of Restrained MX 2600, Across Lamina Heating Rate = 5.0 K/s (540° F/min) R = 60%	58
54	Modulus of Restrained MX 2600, With Lamina, Thick Wall Specimen, Heating Rate = 2.9 K/s (310° F/min) R = 30%	59
55	Summary of Modulus Data, MX 2600, Across Lamina	59
56	Summary of Modulus Data, MX 2600, With Lamina	60
57	Strength Measurements, MX 2600, With Lamina,	60
58	Thermal Conductivity of MX 2600, Silica Phenolic Char, With Lamina, Transient Measurement	61
59	Thermal Conductivity of MX 2600, Silica Phenolic Char, Across Lamina, Transient Measurement	61
60	Thermal Conductivity of MX 2600 Silica Phenolic Char, From Rocket Nozzle (Approx. 30-Degree Orientation)	62
61	Thermal Conductivity of MX 2600 Silica Phenolic Char, Summary of Transient Data	62
62	Thermal Conductivity of MX 2600 Silica Phenolic Char, Summary of Heating Rate Data	63
63	Thermal Expansion of FM 5272, Across Lamina, Low Heating Rate (0.033K/s) (3.6° F/min)	64
64	Thermal Expansion of FM 5272, With Lamina, Low Heating Rate (0.033K/s) (3.6° F/min)	64
65	Thermal Expansion of FM 5272, Comparison of With and Across Lamina	65
66	Thermal Expansion Specimens After Testing in the Brinkmann Dilatometer	65
67	Thermal Expansion of FM 5272, With Lamina at 5.55 K/s (600° F/min)	66
68	Thermal Expansion of FM 5272, With Lamina at 13.9 K/s (1500° F/min)	66
69	Thermal Expansion of FM 5272, Effect of Heating Rate	67

ILLUSTRATIONS (Continued)

Figure		Page
70	Restrained Expansion of FM 5272, With Lamina, Heating Rate = 2.9 K/s (310° F/Min) R = 90%	67
71	Restrained Expansion of FM 5272, With Lamina, Heating Rate = 2.9 K/s (310° F/Min) R = 60%	68
72	Restrained Expansion of FM 5272, With Lamina, Heating Rate = 5.0 K/s (540° F/Min) R = 90%	69
73	Restrained Expansion of FM 5272, With Lamina Heating Rate = 5.0 K/s (540° F/Min) R = 70%	69
74	Restrained Expansion of FM 5272, Across Lamina Heating Rate = 2.9 K/s (310° F/min) R = 95%	70
75	Restrained Expansion of FM 5272, Across Lamina Heating Rate = 2.9 K/s (310° F/min) R = 90%	71
76	Restrained Expansion of FM 5272, Across Lamina Heating Rate = 2.9 K/s (310° F/min) R = 82%	71
77	Restrained Expansion of FM 5272, Across Lamina Heating Rate = 2.9 K/s (310° F/min) R = 65%	72
78	Restrained Expansion of FM 5272, Across Lamina Heating Rate = 5.0 K/s (540° F/min) R = 90%	72
79	Restrained Expansion of FM 5272, Across Lamina Heating Rate = 5.0 K/s (540° F/min) R = 80%	73
80	Restrained Expansion Tests on Thick Wall Specimen of FM 5272, Heating rate = 2.9 K/s (310° F/min) R = 60%	73
81	Summary of Restrained Expansion Data FM 5272, Across Lamina	74
82	Summary of Restrained Expansion Data FM 5272, With Lamina	74
83	Modulus of Restrained FM 5272, With Lamina, Heating Rate = 2.9 K/s (310° F/min) R = 90%	76
84	Modulus of Restrained FM 5272, With Lamina, Heating Rate = 2.9 K/s (310° F/min) R = 60%	76
85	Modulus of Restrained FM 5272, With Lamina, Heating Rate = 5.0 K/s (540° F/min) R = 90%	77
86	Modulus of Restrained FM 5272, With Lamina, Heating Rate = 5.0 K/s (540° F/min) R = 70%	77
87	Modulus of Restrained FM 5272, Across Lamina, Heating Rate = 2.9 K/s (310° F/min) R = 95%	78
88	Modulus of Restrained FM 5272, Across Lamina, Heating Rate = 2.9 K/s (310° F/min) R = 90%	78
89	Modulus of Restrained FM 5272, Across Lamina, Heating Rate = 2.9 K/s (310° F/min) R = 82%	79
90	Modulus of Restrained FM 5272, Across Lamina, Heating Rate = 2.9 K/s (310° F/min) R = 65%	79

ILLUSTRATIONS (Continued)

Figure		Page
91	Modulus of Restrained FM 5272, Across Lamina, Heating Rate = 5.0 K/s (540° F/min) R = 90%	80
92	Modulus of Restrained FM 5272, Across Lamina, Heating Rate = 5.0 K/s (540° F/min) R = 80%	80
93	Modulus of Restrained FM 5272, With Lamina, Thick Wall Specimen, Heating Rate = 2.9 K/s (310° F/min) R = 70%	81
94	Summary of Modulus Data, FM 5272, With Lamina	81
95	Summary of Modulus Data, FM 5272, Across Lamina	82
96	FM 5272 Restrained Expansion Specimen after Testing at High Heating Rate	82
97	Strength Measurements, FM 5272 With Lamina	83
98	Thermal Expansion of Carbitex 700, Across Lamina, 0.033K/s (3.6° F/min)	88
99	Thermal Expansion of Carbitex 700, With Lamina, 0.033K/s (3.6° F/min)	88
100	Thermal Expansion of Carbitex 700, With Lamina, 13.9 K/s (1500° F/min)	89
101	Thermal Expansion of Carbitex 700, With Lamina, 27.8 K/s (3000° F/min)	89
102	Summary of Free Thermal Expansion Data, Carbitex 700, With Lamina	90
103	Restrained Expansion of Carbitex 700, With Lamina, Heating Rate = 13.9 K/s (1500° F/min) R = 55%	90
104	Restrained Expansion of Carbitex 700, With Lamina, Heating Rate = 27.8 K/s (3000° F/min) R = 55%	91
105	Restrained Expansion of Carbitex 700, With Lamina, Heating Rate = 27.8 K/s (3000° F/min) R = 75%	91
106	Summary of Restrained Expansion Data, Carbitex 700, With Lamina	92
107	Modulus of Restrained Carbitex 700, With Lamina	93
108	Compressive Stress-Strain Behavior of Carbitex 700 to 1800 K With Lamina (Average curves, not loaded to failure)	94
109	Compressive Stress-Strain Behavior of Carbitex 700 to 1800 K Across Lamina (Average curves, not loaded to failure)	95
110	Thermal Conductivity of Carbitex 700, Transient Test With Lamina	96

ILLUSTRATIONS (Continued)

Figure		Page
111	Thermal Conductivity of Carbitex 700, Transient Test, Across Lamina	96
112	Thermal Conductivity of Carbitex 700, Transient Test Summary of Heating Rate Data	97
113	Thermal Expansion of RPP-4, With and Across Lamina at 0.033 K/s (3.6° F/min)	102
114	Thermal Expansion of RPP-4, With Lamina, 13.9 K/s (1500° F/min)	103
115	Thermal Expansion of RPP-4, With Lamina, 27.8 K/s (3000° F/min)	103
116	Mean Thermal Expansion Coefficient of RPP-4, With Lamina	104
117	Restrained Thermal Expansion of RPP-4, With Lamina, Heating Rate = 13.9 K/s (1500° F/min) R = 65%	104
118	Restrained Thermal Expansion of RPP-4, With Lamina, Heating Rate = 27.8 K/s (3000° F/min) R = 65%	105
119	Summary of Free and Restrained Thermal Expansion Data, RPP-4, With Lamina	105
120	Modulus of Restrained RPP-4, With Lamina, R = 65%	106
121	Compressive Stress-Strain Behavior of RPP-4 to 1800 K (Average curves, not loaded to failure), With Lamina	107
122	Compressive Stress-Strain Behavior of RPP-4 to 1800 K (Average curves, not loaded to failure), Across Lamina	107
123	Thermal Conductivity of RPP-4 Transient Tests, Across Lamina	108
124	Thermal Conductivity of RPP-4 Transient Tests, With Lamina	108
125	Thermal Conductivity of RPP-4 Transient Tests, Summary of Heating Rate Data	109

SYMBOLS

A	Pre-exponential Constant (Collision frequency)
C_p	Specific Heat at Constant Pressure
C_{pg}	Specific Heat of Pyrolysis Gas
E	Modulus of elasticity
ΔE	Activation Energy
H_K	Latent Heat of Gas Cracking
ΔH	Heat of Decomposition
L	Length
ΔL	Change in Length
$\Delta L/L$	Strain (Change in length per unit length); usually thermal strain (i. e. , expansion).
$\left(\frac{\Delta L}{L}\right)_{\text{eff}}$	The effective (or apparent) thermal expansion which is derived from the restrained expansion test
\dot{m}	Mass Flux
P	Pressure
ρ_c	Char Density
R	Gas Constant (conductivity equation) or Restraint in Restrained Expansion Test
t	Time
T	Temperature
$\phi(T)$	A temperature dependent change in dilatometer dimensions
ΔT	Temperature Change

dT/dt or \dot{T}	Heating Rate (Time rate of change of temperature)
X	Depth in Material
α	Thermal Expansion Coefficient
α'	Mean Thermal Expansion Coefficient
β	Area Ratio
λ	Thermal Conductivity
ξ	The thermal strain which is permitted to occur under partially restrained expansion
ρ	Density
ρ_g	Gas Density
σ	Stress

SUMMARY

Thermophysical property measurements were made under transient heating conditions on several materials being considered for use in SCOUT rocket motors. The materials included were ATJ graphite, MX 2600 silica phenolic, FM 5272 cellulose phenolic, and two carbon-carbon composites: Carbitex 700 and RPP-4. The ATJ was included as a reference or base line material to check performance of the transient tests as it was not expected to be sensitive to heating rate.

Measurements included in the program were thermal conductivity, strength, compressive stress-strain (carbon-carbon only), thermal expansion and the "effective thermal expansion" under partially restrained conditions. Development of this latter measurement was a major part of the program. It consisted of partially restraining the expansion of a specimen as it was heated, measuring the load and strain which occurred (together with a simultaneous modulus determination by superimposing a small cyclic load) and using these quantities to calculate what the "effective thermal expansion" would have to be to produce the observed stress and deformation. For materials which are sensitive to heating rate, such as reinforced phenolics, it was believed that this would provide a more realistic determination of the thermal expansion as it more nearly simulates the conditions experienced in end use. The measurement was successfully performed and, to the best of our knowledge, is a technique which has not been used previously.

Measurements on the graphitic materials indicated no heating rate effects up to the maximum temperature employed (about 1900 K). Measurements of the "effective thermal expansion" of these materials were in agreement with the usual free or unrestrained measurement results for levels of restraint up to about 55 percent. At higher restraint levels, (i. e., 65 to 75 percent) the "effective expansion" is slightly lower at high temperatures. The reason for this deviation is not known. It may be associated with nonlinearity of the stress strain behavior or possibly even an increase in hysteresis affecting the cyclically determined modulus. However, the excellent agreement at the lower restraint levels provided additional confidence for applying the technique to the heating rate sensitive phenolics.

As was expected, the phenolic materials were sensitive to heating rate, the free expansion increasing markedly with rate. In the case of FM 5272 it was also found that the "effective thermal expansion" in the lamina direction was considerably less than the free expansion at the same rate. It is expected that this is also the case in the across laminate direction (for both FM 5272 and MX 2600) but no fast-heating free expansion measurements were made in this direction. The effective thermal expansion of MX 2600 in the with laminate direction was only slightly lower than the free expansion, possibly because of the restraining effect of the silica fibers limiting the free expansion. For both phenolics it was noted that a combination of high heating rate and high restraint in the across-laminate direction tended to result in a higher

effective thermal expansion, probably as a result of restricting the escape of decomposition products. This also resulted in pieces of the MX 2600 being violently blown out of the specimen surface.

Transient thermal conductivities measured on the carbon-carbon materials were in agreement with the steady state, low temperature data and extended the data to about 2000 K. Measurements on the phenolics were made by first preparing char under very fast heating conditions. In the case of the FM 5272, the char was so soft and weak that it disintegrated rapidly even at fairly low flow rates.

INTRODUCTION

The SCOUT system consists of a family of solid propellant rocket motors which are utilized in a number of three to five stage vehicles. In general, these motors have provided highly satisfactory service but are constantly being upgraded for improved performance and reliability. As noted in Reference 1, many new and improved materials have become available since the earliest SCOUT flights and these have provided the basis for reassessment of both materials and design of the SCOUT motors.

One of the most important areas associated with thermostructural analysis and reliability assessment of rocket nozzle materials is that of reliable and reproducible environmental response data. It is, of course, important that the data employed in analyses be representative of the material under whatever conditions exist in the end use application being analyzed. The effect of temperature, for example, is recognized and taken into account. However, other factors such as time at temperature, rate of strain and rate of change of temperature can often be very important but may be neglected. Since an analysis based on invalid data can be misleading, the effects of environment upon material properties should be carefully examined. Some classes of materials are more sensitive than others to these environmental factors and when this is the case, it becomes apparent that certain of the engineering design data should be generated under conditions that approach the heating and loading rates encountered in the end use application. As compared to "static" tests, these transient tests are considerably more difficult to perform, require more time, and tend to be less precise, but the resulting data are far more meaningful.

In considering the dependence of material properties on time or rate, it should be noted that there are at least two distinct types of rate effects which one may be concerned with. One of these is connected with flow of the material. For example, the flow stress of aluminum increases with increasing strain rate (ref. 2), a phenomenon that may be explained in terms of thermal activation of dislocation motion. Similarly, the deformation of a polymer will frequently result in the motion of molecules past one another, i. e., viscous flow of the material and viscosity may also be treated (ref. 3) as a thermally activated or rate process. Since higher stresses are required to cause viscous flow to occur more rapidly, many polymer mechanical properties, such as the yield stress (ref. 4) are dependent on the strain rate. This type of time dependence is associated with material flow and although this flow is temperature dependent it is generally regarded as being independent of time at temperature* or heating rate except in those cases where the material is being altered. This qualification, "the material is being altered," introduces a second type of time dependence and is the one with which this program was primarily concerned.

*It is possible that a finite time is required for response to a temperature rise so that time at temperature effects may be observed at extreme heating rates and very short times.

If a polymeric material such as a phenolic is heated to a sufficiently high temperature, it will undergo chemical changes that affect its properties. It is possible, for example, for additional cross-linking to occur which would increase the modulus over that which would exist in the absence of such a reaction. Since reactions of this type are rate processes, one would expect that if the material could be heated very rapidly, the modulus would decrease during heating, but would then rise to some intermediate value as the cross-linking reaction progressed. Such an effect has been observed at this laboratory during studies on an epoxy adhesive. A very similar effect has been observed on heating certain crystallizable (but initially amorphous) polymers. With these polymers, Young's modulus (above T_g) increases as the degree of crystallization increases, and the rate of crystallization increases as the temperature is increased. In addition, these materials often show an incubation period (also temperature dependent) before the onset of crystallization.

With thermoset polymers, such as the phenolics, a degradation reaction occurs at elevated temperatures. The onset of such a reaction is accompanied by a weight loss and hence may be followed by thermogravimetric analysis (TGA). As this reaction progresses, gases are evolved that diffuse to the surface to escape, and the remaining material reduces to a carbonaceous char. Since the degradation is again a rate process, one finds that the onset of the reaction is shifted to a higher temperature as the heating rate is increased. At the higher rate, the weight loss (or extent of reaction) will be less at any given temperature, but the rate of reaction at that temperature will be higher.

In an earlier program, it had been observed that when carbon phenolic or silica phenolic laminates were heated slowly, some thermal expansion occurred up to about 450 K, after which the material contracted. The change from expansion to contraction corresponds to the onset of thermal degradation. At high heating rates, it was observed that a sharp increase in the thermal expansion coefficient occurred in about the same temperature region as that where contraction started at low rate. It is believed that at high heating rates, the resin initially softens and then a rapid evolution of gases occurs. These gases cannot escape readily and create a pressure within the material which causes rapid expansion and the opening of fissures. Properties other than the thermal expansion are also affected by heating rate, since the structure of the material is affected.

In considering the heating rates to which a material may be subjected within a rocket motor, it may be noted that propellant flame temperature in the SCOUT motors is roughly 3600 K. The heating rate which the material experiences will depend on the thermal conductivity, time, the distance of a given point below the heated surface, etc. However, past experience with ablation testing of a carbon phenolic material indicates that a 3600 K surface temperature may be expected to result in heating rates of about 10 to 200 K/s in the region of 2.5 to 10 mm (0.1 to 0.4 inch) below the surface.

The program described in the following report was concerned with the investigation of several materials of interest to the SCOUT program to determine whether the properties of these materials were sensitive to heating rate and to provide meaningful property data on these materials.

General Electric Company personnel who have made significant contributions to this program include J. Roetling (Program Manager), L. Sponar, J. Hanson, J. Brazel, B. Kennedy and S. Schlusberg.

The program was administered by the Thermal Protection Materials Branch of NASA/Langley Research Center. Mr. J. P. Howell, Heat Shield Section, acted as Technical Monitor.

MATERIALS

Five materials were included in this study. These were as follows:

ATJ Graphite

ATJ graphite is a fine grain, high strength, premium quality graphite produced by the Union Carbide Corporation. It is probably one of the most uniform of the high performance graphites which became available in the early 1960's and can be machined to very close tolerances with fine surface finish. ATJ has been used as a rocket motor nozzle (throat) insert material and in general has proven very successful in this application. However, polycrystalline graphites may be considered to be fairly brittle materials and there has been some concern that if a crack did initiate it would propagate catastrophically. Hence there has been interest in materials which would possess the excellent thermal shock resistance and ablation performance of ATJ while providing greater resistance to fracture propagation.

In general, ATJ graphite was not expected to show any significant dependence of properties upon heating rate. It was therefore included in this program more for demonstration purposes than to provide new data. That is, if the properties of the ATJ were insensitive to heating rate, then one would expect good agreement between static test data and transient test data if the latter tests are properly conducted. In this respect, it was known from past experience (ref. 5) that the thermal conductivity of ATJ as obtained by the GE transient technique was in agreement with steady-state determinations. However, it was less certain that mechanical properties would be independent of heating rate. It is known, for example, that when polycrystalline graphites are strained at room temperature they acquire a "permanent" set (ref. 6) which can be recovered by annealing at about 1300 K or higher. The reasons for this set and its recovery by annealing are not certain but may involve a change in the crystal structure (a stress induced change from hexagonal to rhombohedral structure of a very small percentage of the material). Because this set can be annealed out at relatively low temperature and because such a crystalline change is probably best treated as a rate process, it was considered possible that some heating rate effects might be seen. However, it seemed probable that if any such rate effects did exist they would be small.

Carbitex 700

Carbitex 700 is a carbon composite material consisting of graphite base fibers in a graphite matrix. The fibrous base is in the form of a square weave fabric which

is laid-up in a layered flat construction. Although the material included in this program was a flat lay up, Carbitex can also be produced by tape and filament winding techniques. It is manufactured by the Carborundum Company.

Carbon-carbon composite materials such as Carbitex are of interest as rocket motor throat insert materials since they appear to combine the many desirable properties of graphite with a much improved resistance to fracture propagation.

Carbitex is available in a wide variety of sizes. The particular panels which were purchased for use on this program were approximately 20 x 20 x 5.1 cm. (8 x 8 x 2 inches) in size, the 5.1 cm dimension being perpendicular to the fabric plane (i.e., across laminate).

RPP-4

RPP-4 is also a carbon-carbon composite and was also obtained in a flat lay up construction. It was manufactured by LTV Aerospace Corporation. The panels purchased for this program were cut into cubes approximately 5.1 cm on a side before the final impregnation and firing. This was done in order to obtain an impregnation which would be comparable to that which would exist on SCOUT throat inserts fabricated from this material.

MX 2600 Silica Phenolic

MX 2600 is also a flat lay-up material consisting of layers of silica fiber fabric impregnated with a phenolic resin. It has been used in rocket motors such as the Algol II-B as entrance insulation and exit cone insulation (ref. 1). Being a phenolic material, it was expected to show significant heating rate effects.

FM 5272 Cellulose Phenolic

FM 5272 cellulose phenolic is also a laminated material and was obtained as a flat lay up. The cellulose laminates are in the form of kraft paper. This material has been under consideration for use as insert backup insulation on submerged nozzles and as an exit cone insulation (ref. 1).

TEST METHODS

The measurements included in this program consisted of thermal expansion determinations at both high and low heating rates, strength measurements under fast heating conditions, transient thermal conductivity measurements, and the measurement of an "effective thermal expansion" under partially restrained conditions. This latter measurement also included a modulus determination. In cases where no heating rate sensitivity existed, some of the restrained expansion tests were replaced by compressive stress-strain measurements. Each of these test methods is described below.

Thermal Expansion

By thermal expansion measurement, we generally mean the measurement of thermal strain under free or unrestrained conditions. By way of definition of terms, consider the thermal expansion curve illustrated in Figure 1. It is the usual practice to measure the thermal strain, $\Delta L/L$ (i.e., the increase in length per unit length resulting from heating), as a function of temperature. The instantaneous thermal expansion coefficient, α , is the slope of the tangent to the curve at any point (e.g., the slope of the line CD at the point B). The mean or secant thermal expansion coefficient, α' , between the points A and B is the slope of the line AB. Hence the increase in thermal strain due to an increase in temperature from T_0 to T_n is:

$$\begin{aligned} \left(\frac{\Delta L}{L}\right)_{T_n} - \left(\frac{\Delta L}{L}\right)_{T_0} &= \int_{T_0}^{T_n} \alpha \, dT \\ &= \alpha' (T_n - T_0) \end{aligned} \tag{1}$$

where α must be expressed as a function of temperature in order to perform the integration. As noted above, thermal strain is usually measured under conditions of free expansion.

For the measurement of thermal expansion at low heating rates, a commercial dilatometer (Brinkmann) was employed which utilized either a fused quartz or sintered alumina system to support the specimen inside a furnace. Choice of the system employed depends upon the maximum temperature, the quartz being limited to about 1370K and the alumina to about 1650 K. Relative expansion of the specimen is measured by means of an LVDT. Expansion of the quartz or alumina system is determined by testing a platinum standard. This permits the measured (relative) expansion to be corrected, yielding the expansion of the material being tested.

The basic experimental arrangement for high heating rate thermal expansion measurement is shown in Figure 2, an LVDT again being used to measure expansion. If the specimen is electrically conducting, such as ATJ graphite for example, it is heated directly by means of induction heating. If the specimen is a nonconductor, heating is accomplished by placing a graphite susceptor between the specimen and the induction coil. Figure 3 is a photograph of the apparatus. In use, it is enclosed in a bell jar to provide an inert atmosphere (argon was used in the present program). Figure 4 is a close up of the induction coil and specimen. Note that the induction coil is wound on a fused quartz tube. This quartz tube is used to support the susceptor when the test specimen is not an electrical conductor. It is of interest to note that the susceptor temperature is often well above the softening point of the quartz tube but the cooling water which flows through the coil also provides adequate cooling of the fused quartz tube.

It is seen that the primary difference between the fast and slow heating methods is in the method of heating employed. The induction heating, employed in the fast heating test, not only provides the requisite fast heating but limits the heating to the vicinity of the specimen. This permits most of the apparatus to be fabricated from fused quartz, which material has the great advantage of a very low thermal expansion coefficient ($\alpha = 5.5 \times 10^{-7} \text{ K}^{-1}$, 290 K to 300 K). Use of ceramic inserts between the specimen and the quartz permits the specimen to be heated to about 1980 K.

When the test specimen is directly heated by induction, practically all of the measured expansion is due to specimen expansion since the fixture is heated only at the points of contact. This is illustrated in Figure 5 which compares an uncorrected fast heating expansion measurement on a nickel specimen with the corrected data from the Brinkmann dilatometer. Nickel, which shows no transitions between room temperature and its melting point, should be insensitive to heating rate. Thus the two curves should differ only by the extent to which the apparatus expands. It is seen that expansion of the fixture is negligible up to about 1000 K and introduces an error of only about three percent at 1400 K. Above 1400 K, this error may be expected to increase steadily and a correction becomes necessary. Two possible correction techniques which may be used are:

- (1) Conduct measurements on a material whose thermal expansion is known and independent of heating rate. For example, nickel could be used up to about 1600 K. From this, apparatus expansion could be determined.
- (2) Conduct measurements using two different specimen lengths at the same heating rate. The contributions from the connecting rods should be the same for the two specimen sizes, allowing this contribution to be eliminated. For example, if ΔL_1 is the total expansion that occurs when the specimen length is L_1 , and $\phi(T)$ is the contribution from the connecting rods, then:

$$\Delta L_1 = \alpha \cdot \Delta T \cdot L_1 + \phi(T) \quad (2)$$

Similarly, for a length L_2

$$\Delta L_2 = \alpha \cdot \Delta T \cdot L_2 + \phi(T) \quad (3)$$

and hence,

$$\Delta L_1 - \Delta L_2 = \alpha \cdot \Delta T \cdot (L_1 - L_2) \quad (4)$$

This circumvents the necessity of finding a heating rate independent standard (or reference) material with high temperature capability and is the technique that was employed on this program. It may be noted that this technique is particularly suitable when direct induction heating of the specimen is employed. When a susceptor is employed, the length of the susceptor must be changed when the specimen length is changed in order to keep the end effect constant.

Test specimens employed with both the Brinkmann and high heating rate dilatometer were rods, approximately 0.63 cm in diameter. Length of the Brinkmann specimens was 5.08 cm. The two specimen lengths employed in the fast heating tests were 5.08 cm and 1.27 cm.

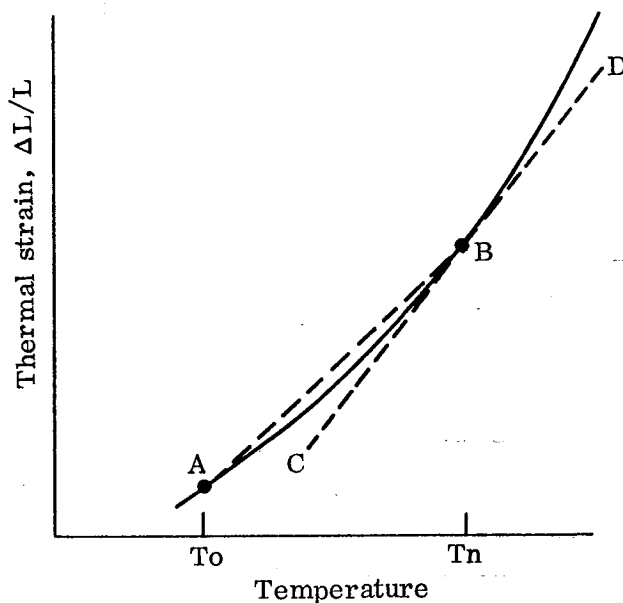


Figure 1. A Hypothetical Thermal Expansion Curve for Defining Terms

Restrained Expansion Tests

Although thermal expansion is normally measured under conditions of free or unrestrained expansion, this condition seldom exists in end use applications. In a typical application, a material may be heated on one surface and a thermal gradient created through the thickness. While expansion normal to this surface is unrestrained, the expansion parallel to the surface is restrained by the cooler underlying material. Thus the hot material experiences a compressive stress and the cool material experiences a tensile stress. It is situations such as this, where a thermal stress is developed, that are of primary interest.

Under high heating rate conditions, the expansion of a reinforced thermoset polymer such as a phenolic is due in part to an internal pressure that develops as gas is generated by thermal decomposition of the resin. Under conditions of unrestrained expansion, fissures can open which allow the gases to escape. If the expansion is restrained, such fissures are not as readily developed, and one would expect that the resultant internal pressure would be higher. Consequently, one might expect that the "effective thermal expansion" for the restrained case would not necessarily be the same as the thermal expansion measured under unrestrained conditions. By "effective thermal expansion," we mean the value which should be used in thermal stress analyses in order to correctly calculate the stresses which occur. For example, if one used data obtained from a free expansion measurement and used this to calculate the stress developed when the material was not able to expand freely, one might find that this calculated stress was incorrect. An alternative then would be to measure the stress when the specimen was restrained and calculate what the "effective thermal expansion" would have to be in order to produce the observed stress.

If a specimen is heated from T_0 to T_n and is totally restrained from expanding, a compressive stress, σ , is developed which is given by:

$$\sigma = -E \alpha' (T_n - T_0) \quad (5)$$

where α' is the secant or mean thermal expansion coefficient between T_0 and T_n and E is the modulus, measured at T_n .

It is apparent from equation (5) that if the restraining force and temperature are measured, the product $E \alpha'$ is readily obtained. A separate measurement of either E or α' is then necessary if the individual quantities are required.

Although this would seem to be a simple measurement to perform, the condition of total restraint is not particularly easy to achieve. The condition can be practically achieved with a test machine having closed-loop servo control and controlled by an extensometer on the specimen. However, what is more important is the fact that total restraint, like free expansion, is a condition which is not normally encountered in end use applications. Of primary interest is the case of partially restrained expansion.

Equation (5) gives the stress which is developed if a specimen is completely restrained from expanding when it is heated. If, instead, a partial expansion is permitted, then the equation becomes:

$$\sigma = -E (\alpha' \Delta T - \xi) \quad (6)$$

where

- α' is the secant thermal expansion coefficient for this temperature interval,
- ξ is the thermal strain which does occur, and
- E is the modulus at the temperature T_n .

Note that the condition $\xi = 0$ corresponds to complete restraint of the specimen and equation (6) reduces to equation (5), whereas at $\sigma = 0$, $\xi = \alpha' \cdot \Delta T$, which is the free expansion condition. We are concerned here with the case where neither σ nor ξ is zero. In this case, if σ , ξ , ΔT and E are all measured quantities, the effective thermal expansion coefficient is given by:

$$\alpha' = \frac{E \xi - \sigma}{E \cdot \Delta T} \quad (7)$$

From this one may also calculate an effective expansion (i.e., $\Delta L/L_0$) for comparison with the free-expansion curves, or for use in analyses if this is the data form preferred. Thus from (7) we have:

$$\left(\frac{\Delta L}{L_0} \right)_{\text{eff}} = \alpha' \cdot \Delta T = \frac{E \cdot \xi - \sigma}{E} \quad (8)$$

(Note that σ is negative for compressive stress).

Measurements of this type were performed using an MTI servo-controlled, hydraulic powered testing machine. This test machine and the associated apparatus employed in these tests is shown in Figure 6. Basically the servo control was used to prevent expansion of the specimen (extensometer control), but as load is developed, a part of the signal from the load cell is combined with the extensometer signal. This combined signal is matched to a reference signal as is shown in the control diagram given in Figure 7, allowing an expansion to occur which was proportional to the load developed.

Operation of the test was essentially as follows: The test specimen was placed between two platens, one of which connected to a load cell, the other to the hydraulic ram. An extensometer provided a signal proportional to any changes in specimen length and the load cell provided a signal proportional to load. The specimen was heated

by induction heating and as it attempted to expand it was partially restrained by the test machine, thus causing a load to be developed. The load and strain signals were combined so that the machine permitted an expansion to occur which was proportional to the load developed. The degree to which expansion of the specimen was restrained was controlled by the relative amplitude of the load and strain signals. For example, if the load signal was reduced to zero, then the machine would control on strain only and would hold expansion to essentially zero (complete restraint). On the other hand, if the load signal was very large compared to the strain signal then we would have had load control and if set at low load would essentially have had free expansion.

In conducting this test, the combined load-strain signal was kept matched to a dc reference signal (fig. 7) as the specimen was heated, and the load and strain were recorded. However, examination of equation (8) shows that to calculate the effective $\Delta L/L_0$, the modulus must also be known. For materials such as the phenolics, the modulus can also be dependent on heating rate and may, in a test such as this, also depend on the degree to which the specimen is restrained. Thus the ideal arrangement appeared to be to make a simultaneous determination of the modulus. To do this, a small amplitude square wave signal was superimposed upon the dc reference signal (frequency about 0.4 cps). This resulted in corresponding cyclic variations in both the load and strain, from which the modulus was calculated.

Since restraint of the specimen resulted in the development of a compressive load, the specimen design had to be such as to minimize the possibility of buckling. A hollow cylindrical specimen was used because this allowed a large diameter to length ratio to prevent buckling and at the same time kept the thickness of the material down to maintain uniform heating.

The load arrangement employed is illustrated in Figure 8. The cylindrical specimen is held between two pyrolytic graphite end caps which serve to support the extensometer and which act to insulate the platens and alignment piece from the specimen. The alignment piece is, essentially, a hardened steel hemisphere which is used to obtain uniform loading of the specimen. The platens are water cooled and the lower platen is equipped with a pan which is filled with water to provide cooling of the alignment piece. A close up view of the specimen and platens is shown in Figure 9.

The upper platen is an integral part of the load cell and is mounted in the "fixed" cross-head of the test machine.* The section just above the upper platen (load link) is equipped with strain gages and is calibrated to provide a load signal. A hole through the entire cell along its axis permits use of a coaxial extensometer.

Details of the coaxial extensometer are shown in Figure 10. The extensometer is coaxial with the specimen and is supported by the pyrolytic end caps on the specimen

*Actually this crosshead can be moved for initial positioning, but it remains fixed during testing.

(fig. 9). The extensometer support points lie in the same planes as the ends of the specimen. Since the rod extending through the specimen is made of fused quartz, a ceramic insulator is provided to protect the rod from direct heat from the specimen.

To check operation of the extensometer, a specimen of ATJ was equipped with strain gages, placed in the test machine, and was loaded in compression. Strain was measured by means of the strain gages and by the extensometer. Strain measurements made by the two methods were in agreement within three percent.

To further clarify the restrained expansion test, consider the stress-strain diagram shown in Figure 11. The curves OA and OB represent tension and compression stress-strain curves respectively at room temperature. If a specimen is heated and allowed to expand in a free or unrestrained condition, the expansion is along the line OC. If the specimen is heated and totally restrained from expanding, a compressive stress is developed at zero strain. That is, we progress along the line OD. At the elevated temperature, the tensile stress-strain curve is represented by the curve CC' and the compressive curve by CD. In the case of a partially restrained expansion, heating the specimen results in some thermal strain and a compressive stress, so that progression is along the line OE. Superposition of a cyclic load (for modulus determination) corresponds to small motions along the line CD at the point E. Note that because of the increased temperature, together with the fact that the specimen may be highly stressed (i.e., the measurement is not at the initial or zero stress region of the stress strain curve), the slope of the line CD at E may be quite different from that of BOA at the point O. If the stress strain curve is not linear, the modulus at E may also differ from that at the point C.

As noted earlier, the specimens used in the restrained expansion tests were cylindrical. Dimensions were 5.08 cm (2.0 inches) length and 2.86 cm (1.125 inches) outside diameter. Most of the tests were conducted on specimens which had an inside diameter of 2.22 cm (0.875 inch) (i.e., a wall thickness of 0.32 cm (0.125 inch)). However, the ATJ specimens were made with an inside diameter of 1.91 cm (0.75 inch) (wall thickness of 0.475 cm (0.187 inch)). This greater thickness was also employed in a few tests on the other materials in order to determine whether any size effects existed. Such a size effect might exist, for example, if the greater thickness hindered the escape of gases generated by the decomposition of resin.

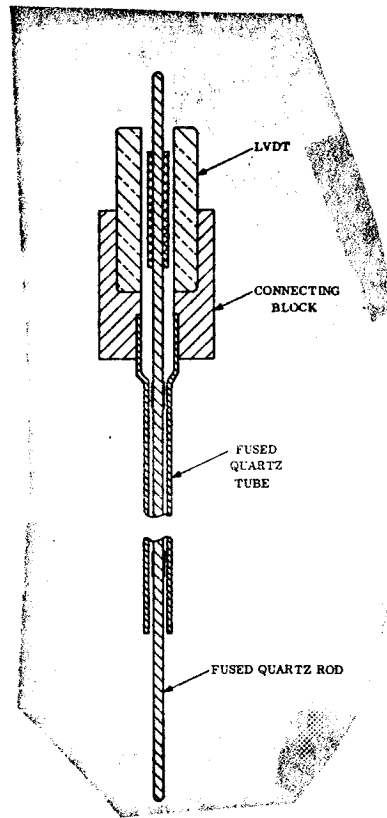


Figure 10. Coaxial Extensometer

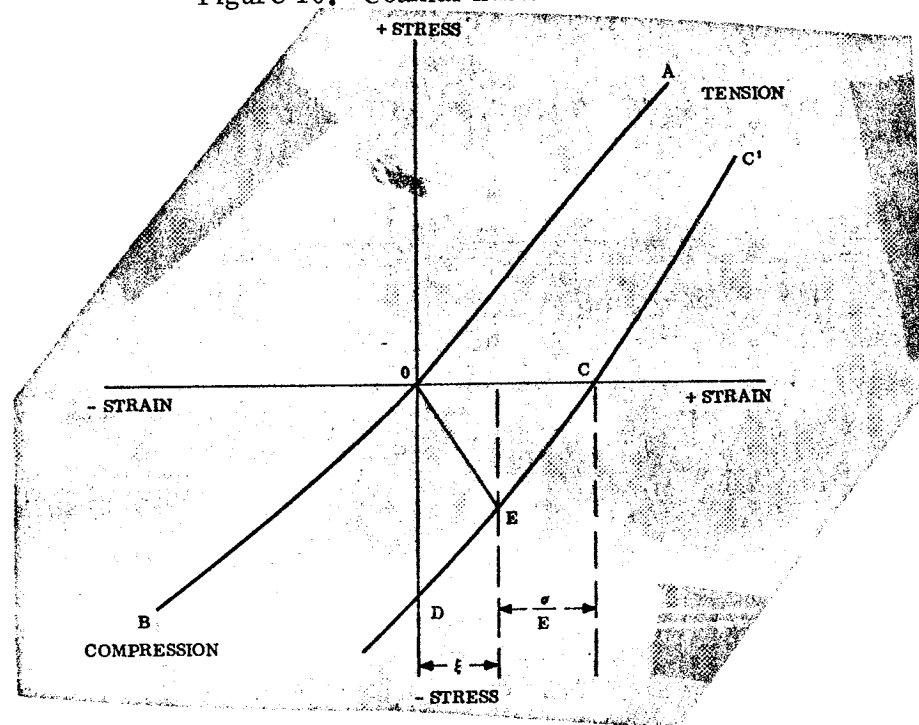


Figure 11. Stress-Strain Relations in the Restrained Expansion Test

Strength Measurement

Preliminary strength measurements were made at room temperature by means of a flexure test. At elevated temperatures, a tensile measurement was employed. Because of the small size of the RPP-4 panels and to conserve material, a small specimen with conical ends was adopted. This basic specimen design had proven satisfactory in earlier testing of polycrystalline graphites. Specimen dimensions are shown in Figure 12. Figure 13 shows a specimen and the specimen grips before assembly.

In the elevated temperature tests, specimens were heated rapidly to the desired temperature using induction heating (as was done in the other tests) and then loaded fairly rapidly. Strain rates employed were on the order of 0.01 sec^{-1} for the graphitic materials and about one-tenth of this for the phenolics. These loading rates were sufficiently fast that the specimens were not at elevated temperature for more than a few seconds but were slow enough to avoid the problems which can accompany high strain rate testing (ref. 7).

Compression Measurements

Compressive stress strain measurements were made using the same specimens and the same basic apparatus as was used to perform the restrained expansion measurements. This required some changes in circuitry but was straight forward. Feed-back signal from the load cell was disconnected so that the control signal was obtained from the extensometer and the fixed reference signal was replaced by a linear ramp. Thus, once the specimen was at temperature, the ramp was initiated and the strain increased linearly. Both load and strain were recorded.

These tests were not conducted to stresses high enough to fail the specimen. It was learned early in the program that such a specimen failure could result in damage to the extensometer with resultant loss of control of the test machine and possible damage to the load cell and induction coil. "Disasters" of this nature had occurred on at least two occasions and considerable caution was exercised to prevent any further occurrences of this nature.

Transient Thermal Conductivity Test

Time dependent thermal transport effects have long been observed in ablative heat shield phenomena. The high performance of the ablative class of materials was usually lumped in a high "Q-Star" — the effective heat of ablation, the heat required to remove a mass or thickness of material. However, until the advent of ablators that generated char layers of sufficient refractoriness to cling tenaciously to the underlying

degrading and virgin material layers, the char's contribution to net heat accommodation was insignificant or marginal. The nylon phenolic system was comprehensively described by Kratsch, Hearne, and McChesney (ref. 8) who, although they had no transiently derived thermal conductivity data and only rudimentary thermophysical degradation data, demonstrated the sensitivity of thermal performance predictions to the parameters used to describe transport in the char layer, and especially heat absorption and generation of transpiring gas species in the critical decomposition zone.

The implications of char and virgin material thermal conductivity were directly treated by Shaw, Garner, and Florence (ref. 9) for refractory-reinforced phenolics, using experimental data generated in our laboratory. They showed the effect on heat shield weight of using transiently derived data as opposed to conventional steady-state thermal conductivities. It was shown that shield overdesigns of as much as 25 percent could originate from plausibly high steady state char thermal conductivity data.

These investigations documented the impact of thermophysical parameter evaluation on re-entry heat shields. Transient methods of making thermal conductivity measurements had been developed by the early 1960's, e.g., Parker's now widespread "flash diffusivity method" (ref. 10). However, these methods all require appreciable heating times to get the sample, however prepared, up to temperature; then the sample must be ascertained to be isothermal so that the small temperature differential imposed across the small thickness of material can be attributed completely to the radiation imposed on the front face. For ablative, thermally degradable heat shield materials, this protracted heating period is usually much longer than that experienced by the material in flight and will change the structure. The small thickness - typically 0.158 cm (1/16 inch) or less - required to satisfy optimum experimental design conditions was observed to permit through transmission of the incident radiant energy, producing much higher apparent thermal conductivities. These phenomena were studied by Cunningham, et. al. (ref. 11), who were able to reduce the heating cycle down to 15 minutes as compared to the 2 to 3 minutes observed for ballistic re-entry vehicle heating times.

The optimum technique then for valid characterization of thermally degradable materials would be one which:

- (1) Made its measurement on the material in the anticipated end use environment (e.g., pressure, temperature, heating rate).
- (2) In a period of time representative of end use (i.e., a transient technique).
- (3) Tested the material in its flight-representative form (e.g., completely charred but not graphitized).

Analytic base of the GE-RESO transient numerical thermal conductivity technique. -
The partial differential equation for heat transport in the condensed phase of a thermally degradable heat shield is:

$$\begin{aligned}
 \underbrace{\frac{\partial}{\partial X} \left(\lambda \frac{\partial T}{\partial X} \right)}_{\text{heat conducted}} = & \underbrace{\rho C_P \frac{\partial T}{\partial t}}_{\text{enthalpy rise}} + \underbrace{\Delta H (\rho - \rho_c) A \exp(-\Delta E/RT)}_{\text{absorbed in reaction}} + \\
 & C_{Pg} \left[\underbrace{(1-\beta)^{3/2} \rho_g \frac{\partial T}{\partial t}}_{\text{energy stored in evolved gases}} + \dot{m} \frac{\partial T}{\partial t} \right] + \dot{m} \left[\underbrace{\frac{\partial H_k}{\partial T} \frac{\partial T}{\partial X} + \frac{\partial H_k}{\partial P} \frac{\partial P}{\partial X}}_{\text{evolved gas}} \right] + \\
 & \underbrace{\rho_g (1-\beta)^{3/2} \left[\frac{\partial H_k}{\partial T} \frac{\partial T}{\partial t} + \frac{\partial H_k}{\partial P} \frac{\partial P}{\partial t} \right]}_{\text{"cracking"}}
 \end{aligned}
 \tag{9}$$

where

- λ = thermal conductivity*
- T = temperature
- X = depth in material
- ρ = density
- C_P = specific heat of solid at constant pressure
- ΔH = heat of decomposition
- ρ = density (as a function of temperature, pressure, heat treatment)
- ρ_c = density of char
- A = pre-exponential constant (collision frequency)
- ΔE = activation energy

* λ is the recently adopted symbol for thermal conductivity in the SI (System Internationale) replacing the more familiar k which it was feared was being confused with the Boltzmann constant.

R = universal gas constant

C_{Pg} = specific heat of pyrolysis gas

β = area ratio: $\frac{\text{char solid area}}{\text{char solid area} + \text{char pore area}}$

ρ_g = gas density

\dot{m} = mass flux

t = time

H_k = latent heat of gas cracking

P = pressure

This is the full model used in the GE REKAP (Reaction Kinetics Ablation Program) to describe thermal response in a heat shield from its front face, where other boundary layer and surface phenomena must be matched, through the char, the degrading material, the virgin material and the back face boundary of the shield. As such, it is a complicated equation, describing an even more complicated set of physical and chemical phenomena. Impressive success has been achieved in fitting it to flight, ground test, and laboratory data.

In the cooler, virgin material which has not reached the temperature of the first "knee" in its TGA analysis, frequently just 50 to 100 K above its cure temperature, no degradation effects or gas generation occur so that only the first two terms of the general equation pertain (i.e., conduction and enthalpy rise).

Coming forward into the hotter reaction zone, defined approximately as the temperatures between the upper and lower knees of the TGA, the full equation must be used for the material's description. Because of the exceptionally large energy accommodation possibilities, it is this reaction zone that has been the subject of most modeling efforts for ablators, especially before the advent of the phenolic systems whose highly carbonaceous chars contributed insulative, cracking, and high-emittance effects. However, because of the complexity of this state, most analyses are primarily boundary matches to the data and analyses of the virgin and char zones. Laboratory efforts at really significant contributions to the calorimetric thermochemistry of this zone have been only partially successful and then, only for a few materials. One of the more sophisticated of these studies, including direct laboratory determinations of the heat of gas formation, was performed by GE-RESO on the Voyager Lander Heat Shield Study in 1967 (ref. 12).

The char layer presents only slightly less complexity in itself, with only the removal of the decomposition term but the addition of a surface boundary matching problem and the experimental difficulties of extreme high-temperature technology which are involved in obtaining meaningful ablation or laboratory data. The very "refractoriness" of the char - its resistance to heat - makes measurements on charring cap (over a degradation and virgin substrate) operationally all but impossible. Consider the terms in the complete equation, minus only the degradation term.

If char thermal conductivity were being sought, the portion of total energy accommodation involved in this parameter, \dot{q}_{net} , is (ref. 9) on the order of 10 percent of the total heating rate for a low-angle, low heat flux trajectory. It would be even lower for ballistic entry. Thus char thermal conductivity would appear to be too completely masked by other contributions to heat flux when a complete simulation sample is tested. This problem has been circumvented in the development of the GE-RESD transient technique by the following procedure that assures both the representative validity* of the char material and the test technique.

First, the char sample is prepared in a plasma jet or recovered from a flight vehicle. Then the char cap is removed for instrumentation and test. At this point in its temperature-time history, the specimen is no different from the cap on the complete system. But when subsequently heated, no transpiration or cracking effects occur and the energy balance equation again reduces to the heat conduction equation (in one dimension):

$$\frac{\partial}{\partial X} \left(\lambda \frac{\partial T}{\partial X} \right) = \rho C_P \frac{\partial T}{\partial t} \quad (10)$$

In arriving at this formulation, it is assumed that high heating rate, transient heat flow within the body obeys Fourier's hypothesis and solid conduction is the predominant mode of heat transfer, (i.e., although gas percolation effects have been removed, other phenomena such as direct radiant transfer are lumped into an "effective" thermal conductance, the form in which they can be used in subsequent performance analyses). The implications of non-Fourier effects at high heating rates have been discussed for representative shield materials by Brazel and Nolan (Ref. 13).

The coefficients ρ , C_P , and λ are dependent functions of position, material state, and temperature within the body.

Sample geometry. - A fairly sophisticated sample holder is needed for the transient thermal conductivity test (Figure 14). It shields the sample from heating on all sides but the front surface and also provides a protective housing for the thermocouple lead junctions. The sample is instrumented with six thermocouples which, in order to

*Originally developed for heat shields, it is also directly applicable to rocket nozzle material analysis.

minimize measurements error, enter the cylindrical sample radially to a depth of 0.5 cm along isothermal planes. Two types of ultra miniature thermocouple sensors were purchased (from Robinson-Halpern) for this test. W-W/26Re thermocouples, in 0.02 cm diameter tantalum sheathing are used in the three uppermost temperature measurement positions because of their high temperature capability and chromel-alumel thermocouples, in 0.02 cm diameter stainless steel sheathing, are used at the three lower measurement positions. The thermocouple lead wires leave the holder through a hole in the mounting lug. Figure 15 shows an unassembled specimen holder with the specimen ready for instrumentation and Figure 16 shows the instrumented specimen.

Experimental procedure. - Initially, it was proposed that either a small Tandem Gerdien arc facility or a CO₂ laser would be used as a heat source for the thermal conductivity tests. As it turned out, the particular laser available did not have sufficient power to produce the heating rates required when the beam was diverged to the specimen size. As a result, the small arc facility, which had previously been used as a heat source for the transient thermal conductivity tests was again used (Figure 17). The test model was mounted on a pneumatically activated sting which moved the specimen into the arc flow for a preset heating time.

Midway through the testing program, a transformer failed in the power supply of the small arc and could not be repaired in time to complete this program. The next step was to try an oxyacetylene torch as a heat source but the heat flux output was too low to be useful. We therefore utilized the hyperthermal arc facility and were eventually able to complete the major part of our testing at that facility. Figure 18 shows the orifice of the arc and two samples mounted on pneumatic stings on either side of the arc flow. Thus duel specimen setup conserved the number of times the arc needed to be lit and accelerated the testing schedule. The major disadvantage of this facility was the increased erosion of the sample due to the much higher flow. The greatest erosion occurred at the interface of the guard ring and the specimen and resulted in early thermocouple failure. When the retaining lip on the guard ring eroded through, it allowed the arc flow to enter the holder and burn off the exposed portion of the thermocouple sensors at the side of the specimen.

The last set of samples, cellulose phenolic char, needed a heat flux lower than that which could readily be obtained with the larger thermal arc facility. We therefore used a Linde torch facility, which is intermediate in heat flux between the oxyacetylene torch and the hyperthermal arc facility.

The recording instrument used with all the transient thermal conductivity tests, was an 18 channel CEC oscillograph recorder. This recording system contained an internal calibration circuit which greatly facilitated the test setup and improved the resultant accuracy.

Data reduction. - As stated above, the specimen geometry is such that essentially one dimensional heat flow can be assumed and the defining differential equation is:

$$\rho C_P \frac{\partial T}{\partial t} = \frac{\partial}{\partial X} \left(\lambda \frac{\partial T}{\partial X} \right) \quad (11)$$

In the past, λ as a function of temperature has been calculated from the measured data by the technique which is briefly described below. Equation (11) expanded is:

$$\rho C_P \frac{\partial T}{\partial t} = \lambda \frac{\partial^2 T}{\partial X^2} + \frac{\partial \lambda}{\partial X} \left(\frac{\partial T}{\partial X} \right) \quad (12)$$

At any given instant in time equation (12) can be written:

$$\frac{d\lambda}{dX} = \left[\frac{a_3 - \lambda a_2}{a_1} \right] \quad (13)$$

where a_1 , a_2 , a_3 are all functions of X and are known.

$$a_1 = \frac{\partial T}{\partial X} \quad a_2 = \frac{\partial^2 T}{\partial X^2} \quad a_3 = \rho C_P \frac{\partial T}{\partial t}$$

Then, knowing the boundary condition λ_0 at some point X_0 , equation (13) was readily solved by the Runge-Kutta numerical technique for the conductivity as a function of depth, X , in the test material. Since T as a function of X is known in the sample at that particular time, then λ was found as a function of T by cross-plotting. A more detailed description of this technique can be found in Reference 5.

The one possible disadvantage of this data reduction scheme was that it required the second derivative of temperature with respect to time as an input. Since T was only known at six points in the material, the exact shape of the curve of T versus X was not known. Hence, errors likely resulted when the first derivative was taken and were compounded drastically when the second derivative was taken.

The data reduction technique employed on this program utilized the heat conduction equation in a different form, as shown below. Integrating both sides of equation (11) with respect to X :

$$\int_{X_6}^X \rho C_P \frac{\partial T}{\partial t} dX = \int_{X_6}^X \frac{\partial}{\partial X} \left(\lambda \frac{\partial T}{\partial X} \right) dX = \left(\lambda \frac{\partial T}{\partial X} \right)_X - \left(\lambda \frac{\partial T}{\partial X} \right)_{X_6} \quad (14)$$

then

$$\left(\lambda \frac{\partial T}{\partial X} \right)_X = \int_{X_6}^X \rho C_P \frac{\partial T}{\partial t} dX + \left(\lambda \frac{\partial T}{\partial X} \right)_{X_6} \quad (15)$$

where X is any point between the first thermocouple location, X_1 , and the last thermocouple location, X_6 .

This equation simply states that rate of energy flow through the sample at a depth of X, $(\lambda \partial T / \partial X)_X$, is equal to the rate at which energy is being stored in the material between the point X and X_6 , the integral term, plus the rate at which energy is flowing past the point X_6 , $(\lambda \partial T / \partial X)_{X_6}$.

Then, from equation (15),

$$\lambda_X = \frac{\int_{X_6}^X \rho C_P \frac{\partial T}{\partial t} dX + \lambda_{X_6} \left. \frac{\partial T}{\partial X} \right|_{X_6}}{\left. \frac{\partial T}{\partial X} \right|_X} \quad (16)$$

Equation (16) is the equation used for data reduction. To start reduction from the six thermocouple voltage traces, a temperature versus time curve was drawn for each thermocouple position (Figure 19). Then a time, t_1 , was selected at which the conductivity versus temperature was to be calculated. $\partial T / \partial t$ was then graphically determined at t_1 , for each thermocouple position, $X_1 \dots X_6$ and a curve was plotted of $\partial T / \partial t$ versus X. Also the function of T versus X at $t = t_1$, was plotted. And from this curve, a plot of $\partial T / \partial X$ versus X at $t = t_1$ was obtained. C_p for the material was usually known or could be estimated as a function of temperature and using the T versus X curve a cross plot could be performed to obtain a C_p versus X plot. The last curve needed was in general ρ versus X, but in all cases considered here, ρ was constant.

A computer program was written to perform the calculation in equation (16). The inputs needed were functions; T, $\partial T / \partial X$, $\partial T / \partial t$, C_p and ρ (if needed) as a function of X between $X = X_1$ and $X = X_6$. Also, an input was needed for λ_{X_6} if $\partial T / \partial X \big|_{X_6} \neq 0$. The value of λ_6 could usually be obtained by steady state means, except in the case of the char samples where t_1 was selected such that $\partial T / \partial X \big|_{X_6}$ was essentially zero, in which case that term containing

λ_{X_6} dropped out of the equation. The output of the computer program was a table of temperature and λ at approximately 10 points through the sample. To get more data, the above process was repeated at two or three different times for each sample.

The technique we used here is the same as that used by E. D. Smyly* with the exception of the use of the computer.

*E. D. Smyly, Southern Research Institute, Personal Communication to J. Brazel, GE, RESD 10/10/69.

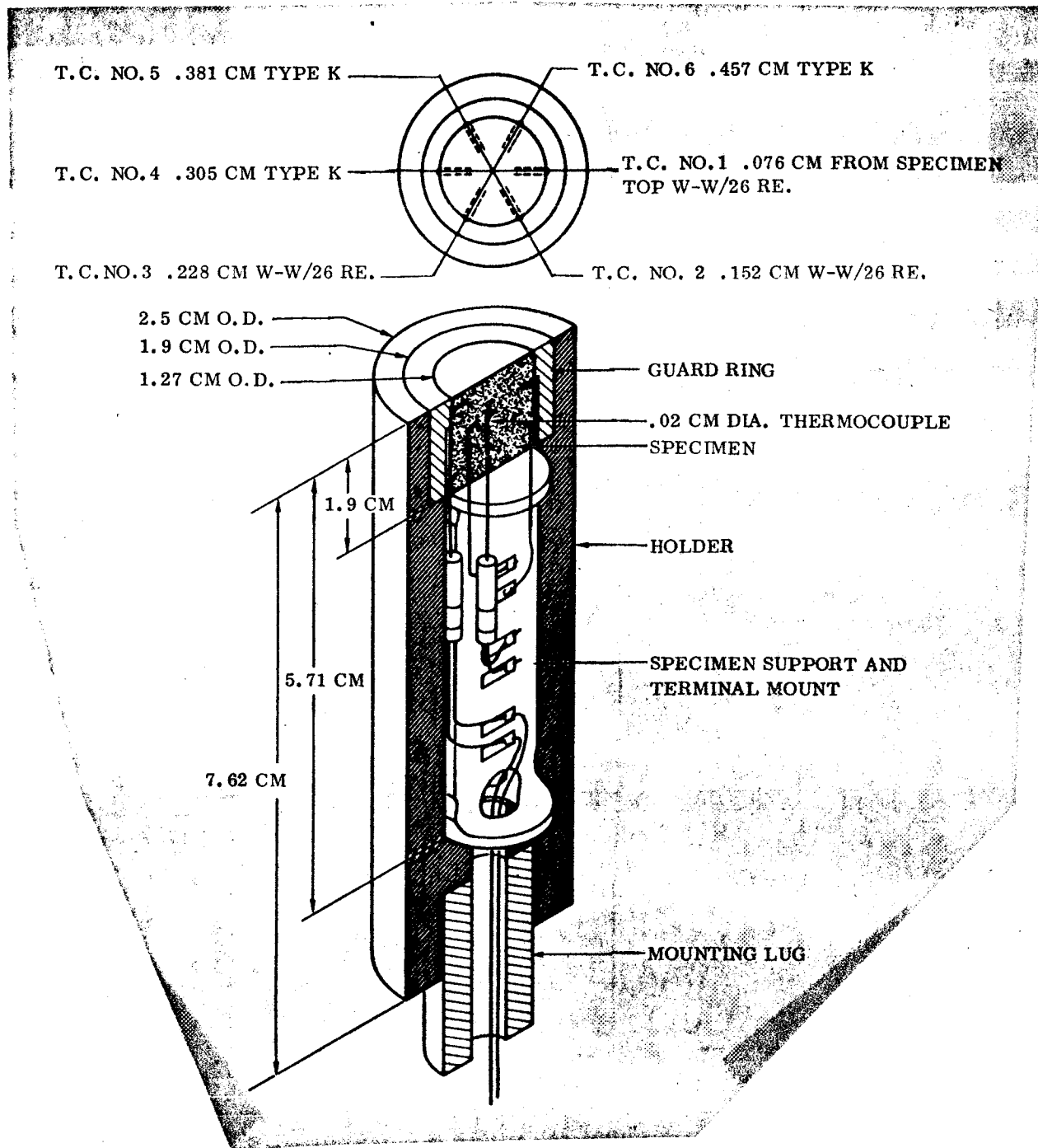


Figure 14. Transient Thermal Conductivity Model

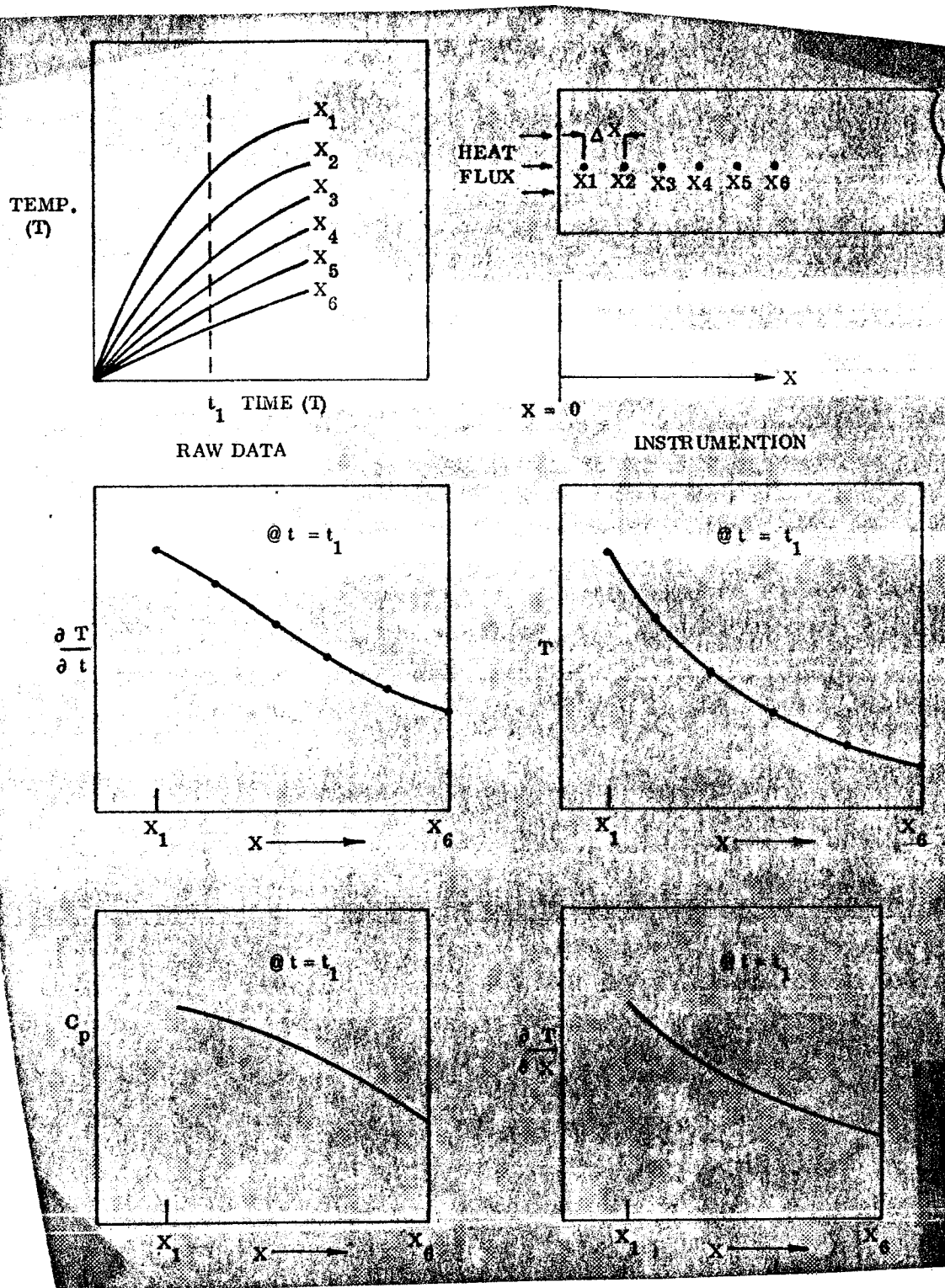


Figure 19. Data Reduction Technique, Thermal Conductivity

TEST RESULTS

Measurements on ATJ Graphite

Density and modulus measurements were made on the ATJ for comparison with available data on this material. Results were as follows:

Density: 1720 kg/m^3 (Mean of five measurements). This density is typical.

Modulus: 11.2 GN/m^2 ($1.62 \times 10^6 \text{ psi}$) (Mean of two ultrasonic measurements made on thermal expansion specimens at a frequency of $0.73 \pm 0.02 \text{ MHz}$). This value is typical of the with-grain tensile modulus of ATJ. Actually, ATJ with grain tensile moduli have been reported which range as low as 6.5 GN/m^2 and as high as 13.3 GN/m^2 . A value of 11.8 has been used at GE-RESO as the maximum for design purposes. Moduli reported from compression tests have generally run lower with values as low as 4.86 GN/m^2 being reported.

Free thermal expansion of ATJ. - Two with-grain specimens of ATJ graphite were measured using the Brinkmann dilatometer at a heating rate of 0.033 K/s (3.6° F/min). The results of these measurements are given in Figure 20 and are representative for this material. Figure 21 compares the static or low rate test data with data obtained at a rate of 27.8 K/sec (3000° F/min). The fast heating curve is the result of

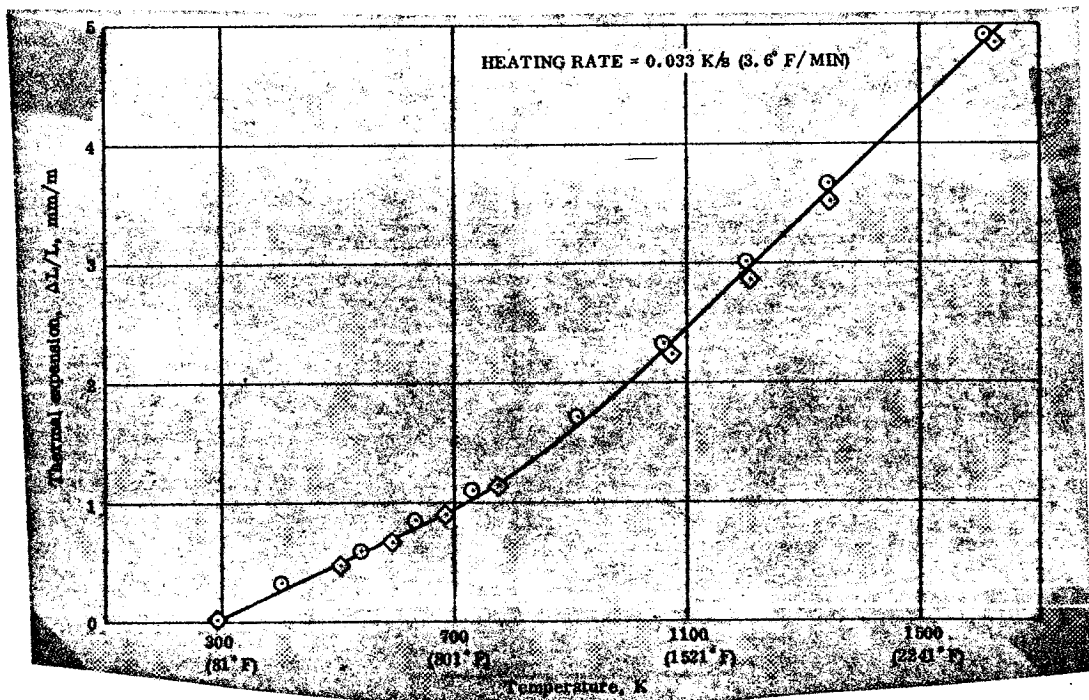


Figure 20. Thermal Expansion of ATJ Graphite, With Grain, at $T = 0.033 \text{ K/s}$

eight tests on four long (5.08 cm) (2.0 inches) and four short (1.27 cm) (0.5 inch) specimens. The four test results at each length were averaged and the difference of these taken to eliminate end effects (i.e., expansion of the fixture at the points of contact with the specimen) as is described in a previous section of this report. The differences between the fast and slow heating curves are not significant and are probably close to the limit of resolution of the apparatus.

The range indicated on each of the data points of the high heating rate curve is the square root of the sum of the squares of the ranges for the long and short specimens. That is:

$$\text{Range of } \frac{\Delta L}{L} = \sqrt{\frac{(\text{Range of } \Delta L_1)^2 + (\text{Range of } \Delta L_2)^2}{L_1 - L_2}} \quad (17)$$

where L_1 is the length of the long specimen and L_2 is the length of the short specimen (See Test Methods section).

Restrained expansion of ATJ. - The results of restrained expansion tests on ATJ graphite are given in Figures 22 and 23, where the effective thermal expansion, $(\Delta L/L)_{\text{eff}}$, is plotted as a function of temperature. As noted in a previous section $(\Delta L/L)_{\text{eff}}$, is calculated using the relation:

$$\left(\frac{\Delta L}{L}\right)_{\text{eff}} = \frac{E\xi - \sigma}{E} \quad (8)$$

where

E = modulus

ξ = the expansion which is allowed to occur

σ = compression stress developed as a result of restraining the thermal expansion.

This equation assumes a linear stress-strain relation.

For a restraint of 55 percent (i. e., the quantity $-\sigma/E$ is 55 percent of $(\Delta L/L)_{\text{eff}}$ and the actual expansion allowed, ξ , is 45 percent*), the effective thermal expansion is in excellent agreement with the free expansion data. At a restraint of 75 percent, however, the effective thermal expansion is low at temperatures above about 1000K but the difference is small. A comparison of free and restrained expansions is given in Figure 24. The reason for this deviation at the higher stress levels is not certain but is believed to be the result of non-linearity of the stress-strain relation.

In general, it may be said that no heating rate effect is observed for the ATJ and that the free and restrained expansion test yield the same result.

As a part of the restrained expansion tests, modulus measurements were made by superimposing a small cyclic load on the specimen as it was heated. This provided the modulus-temperature data needed for equation (8). The results of these modulus measurements are given in Figure 25. The values obtained at room temperature appear to be typical for compressive data for ATJ and the scatter is also typical.

Considering the modulus data, the scatter was such that there appeared to be no justification for drawing any kind of curve other than a straight line through the data points. This is illustrated by the points shown on the curves obtained at 55 percent restraint. In using these modulus data, it should be kept in mind that at room temperature the modulus is measured at low stress but the measurement is made at increasingly negative stress as the temperature increases. This may be seen by referring to Figure 11.

Transient thermal conductivity of ATJ. - The graphite specimens were instrumented with a thermocouple spacing of 0.15 cm (0.017 inch) and were tested with a heat flux of 1.25×10^7 watts/meter² with the Tandem Gerdien Arc Facility. The results are shown in Figure 26. The data agree well with the steady state conductivity curve although considerable scatter is observed. This scatter, however, is normal for this type of conductivity measurement.

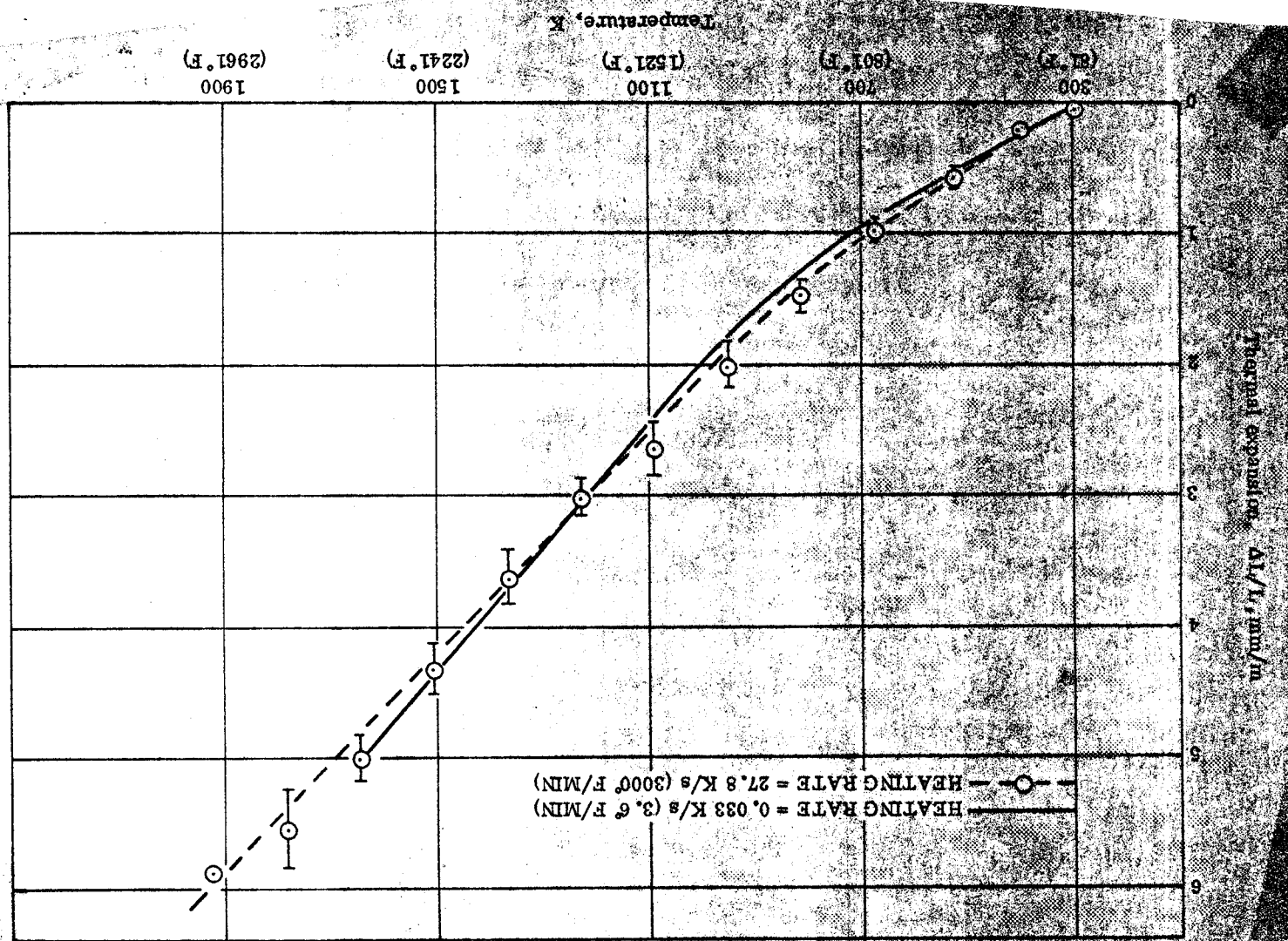
The heating rates involved in the transient thermal conductivity test are shown in Figure 27.

Measurements on MX 2600

Density of the MX 2600 silica phenolic used on this program was 1710 kg/m³ (107 lb/ft³). Ultrasonic measurements indicated a with-laminate modulus of about 21 GN/m² (3.0×10^6 psi). However, as will be noted below, the modulus obtained in the restrained

*The degree of restraint, %R, may be defined as $\%R = 100 \frac{(-\sigma/E)}{(\xi - (\sigma/E))}$

Figure 21. Thermal Expansion of ATJ, With Grain; Comparison of Static and Transient Methods



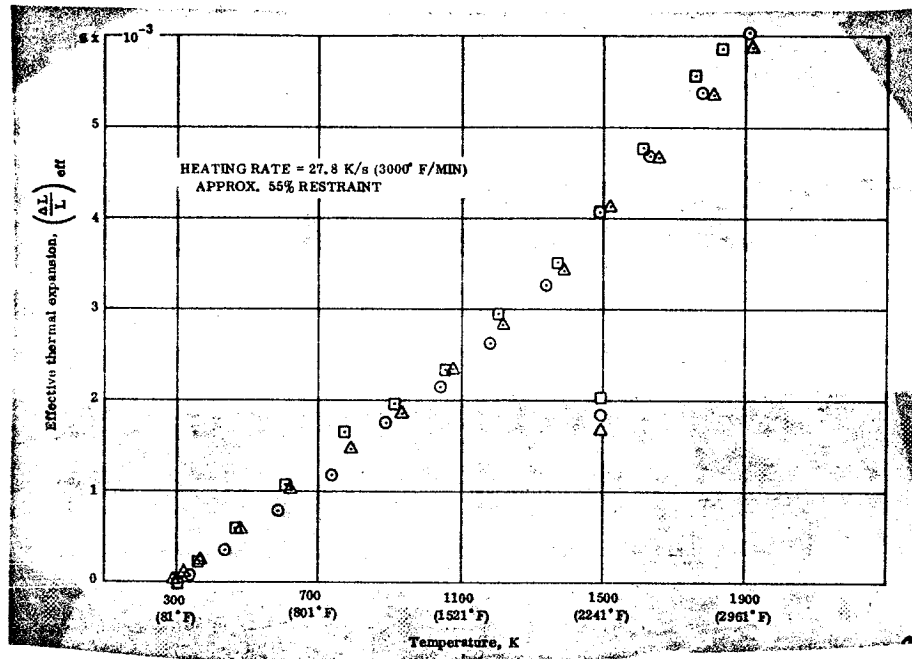


Figure 22. Effective Thermal Expansion of ATJ, with Grain T = 27.8 K/s, R=55%

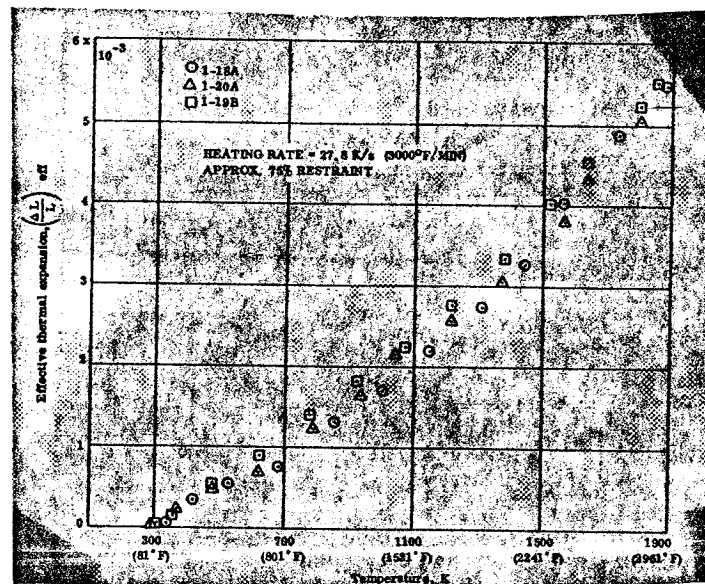


Figure 23. Effective Thermal Expansion of ATJ, with Grain T = 27.8 K/s, R=75%

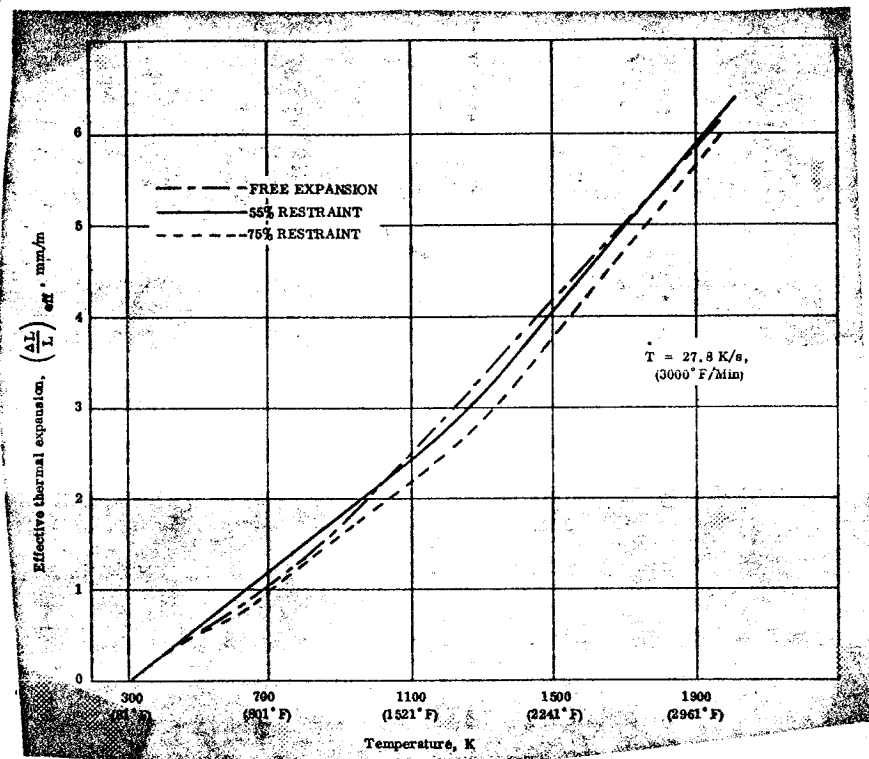


Figure 24. Effective Thermal Expansion of ATJ, With Grain Comparison, Showing Effect of Restraint

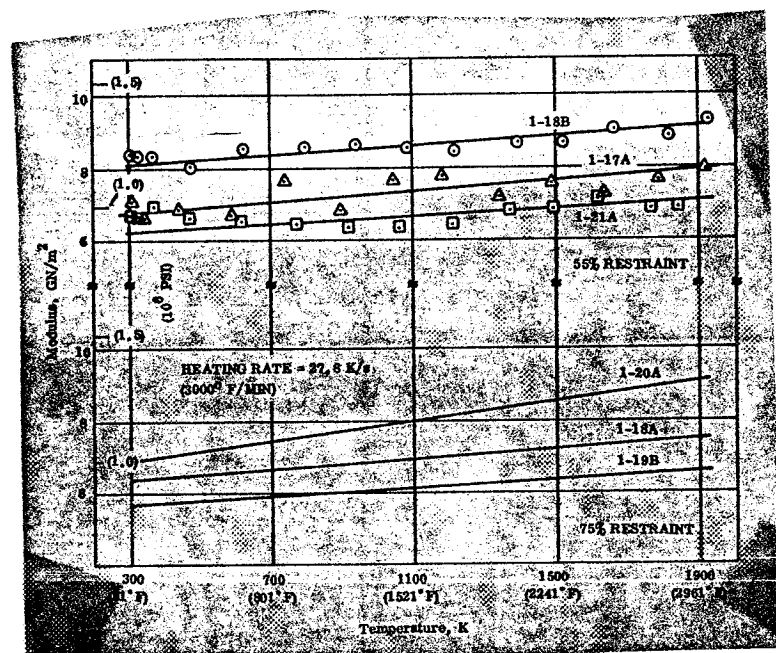


Figure 25. Modulus of Restrained ATJ Graphite, With Grain

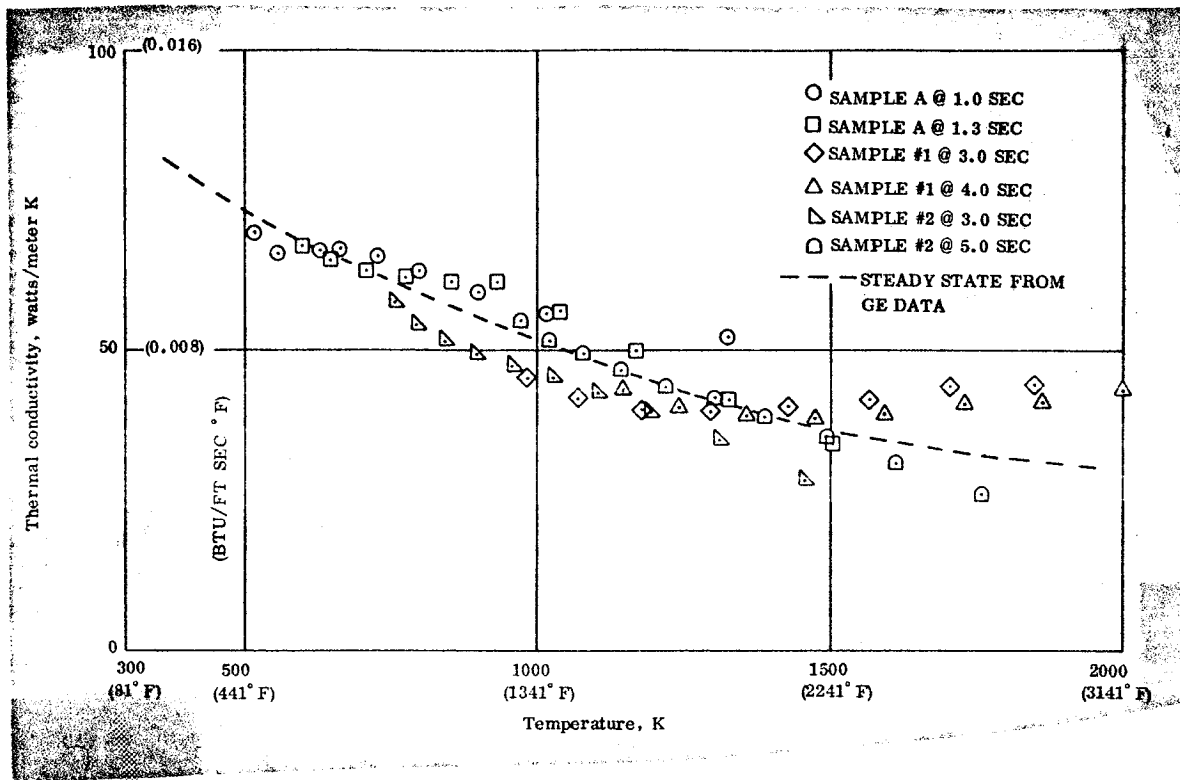


Figure 26. Thermal Conductivity of ATJ, Perpendicular to Grain

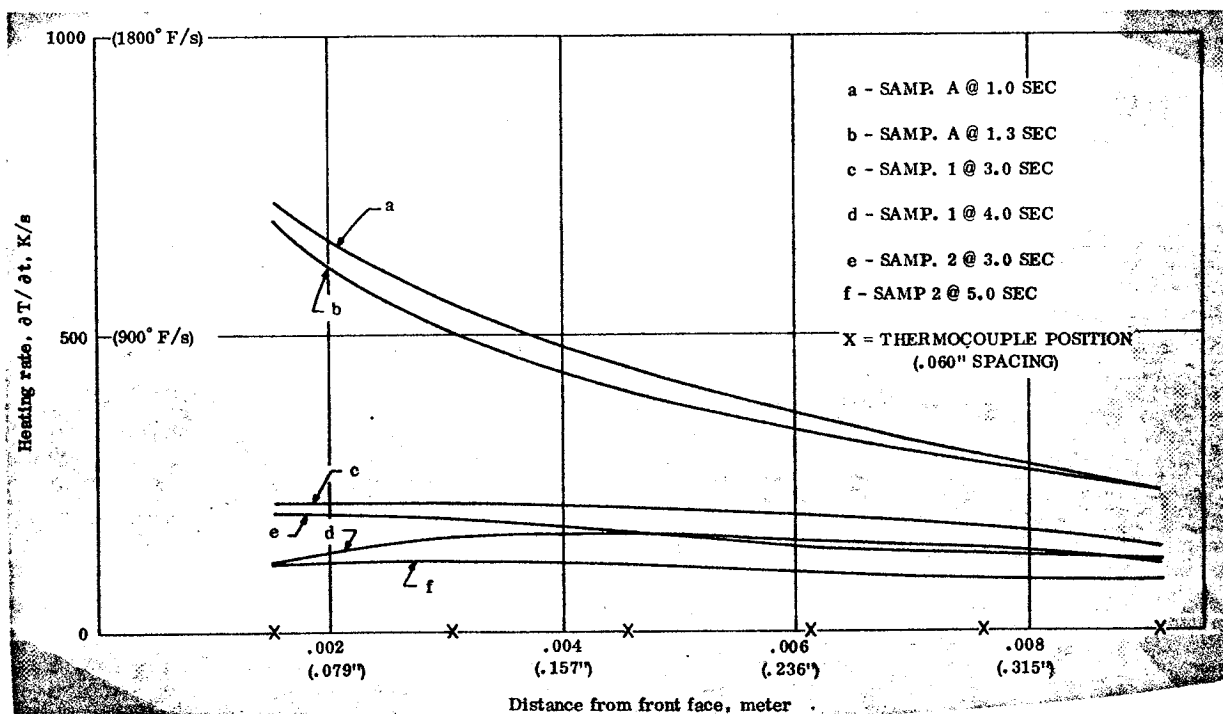


Figure 27. Heating Rate Data for ATJ Thermal Conductivity Test

expansion tests was much less than this. Reference 1 gives the modulus as 13.8 GN/m^2 but moduli obtained from ultrasonic measurements are usually high compared to tensile or flexure test data so this difference is not surprising.

Free thermal expansion of MX 2600. - Thermal expansion data for MX 2600 Silica Phenolic, obtained under slow heating conditions are given in Figures 28 and 29 (2 runs in each direction). As is usually observed with phenolics, the material initially expands, then contracts as the resin degrades. The expansion observed at this low heating rate is quite small in both directions and the expansion portions of the two curves are compared in Figure 30, where the scale is expanded. Note that the expansion in the across laminate direction is somewhat larger, no doubt as a result of with-laminate expansion being restrained by the silica fibers.

The results of free expansion measurements in the with laminate direction under fast heating conditions are shown in Figures 31 and 32. Each of these curves is an average based on measurements on three long and three short specimens. A comparison of the results at the three heating rates is given in Figure 33. Note that as the rate is increased the peak expansion tends to increase and tends to shift to somewhat higher temperature. The effect seen here is quite small, however, because of the restraining effect of the silica fibers. Based on previous measurements of this type, one would expect to see much larger rate effects for measurements in the across laminate direction.

Restrained expansion of MX 2600. - Restrained expansion measurements were made in both the with and across laminate directions at two heating rates and at two degrees of restraint. The rates employed were lower than were used with electrically conducting materials in order to avoid steep thermal gradients. The results of the with-laminate measurements are shown in Figures 34 through 37. In considering these four curves it will be noted that:

- a. The results for these two heating rates are essentially the same at the same degree of restraint.
- b. The peak expansion is slightly higher at the lower degree of restraint and the effective expansion continues somewhat higher at the higher temperatures. Thus it will be noted that after peaking the effective thermal expansion becomes zero between 600 and 700 K and 65 percent restraint, between 700 and 800 K at 30 percent restraint, and between 800 and 900 K in the free expansion case (at the comparable heating rate of 5.55 K/s.).

The results of across laminate restrained expansion measurements are shown in Figures 38 through 41. Considerably more scatter is evident here than was observed in the with laminate measurements. In running these tests the load was observed to go through two or three peaks in a number of the runs. Why this occurred is not known, but it is possible that internal gas pressure would build-up, release, and then build-up again.

The greater scatter which occurred makes it difficult to pick out definite trends. However, it is evident that the effective thermal expansion at both high heating rates is considerably higher than the free thermal expansion obtained at low rate. No high heating rate free expansion measurements were made in the across grain direction, but based on past experience it seems probable that such a test would have yielded an expansion much larger than the effective expansion obtained in the restrained tests. Considering the effect of heating rate further, it is seen that the tests at 5K/s tend to yield higher effective expansions than are obtained at 2.9 K/s. This is particularly evident at the higher restraint, whereas at the lower restraint a high effective expansion occurred in only one of three runs.

In considering these results, which are summarized in Figures 42 and 43, it may be noted that when a with laminate specimen is restrained in the WL direction, it is still able to expand in the across-laminate (AL) direction. However, when an AL specimen is restrained in the AL direction, the fibers provide restraint in the WL direction. As a result, a high degree of restraint in the AL direction can result in high internal pressures. This same effect would not occur for high restraints in the WL direction.* In relation to this, and supporting the idea that high internal pressures result when high AL restraints exist, it was of interest to note that at the higher degree of AL restraint (85%) and the higher heating rate, pieces were blown off of the specimen with explosive force. This usually occurred shortly after the load had peaked and was starting to decrease and was evidenced by several (usually 2 or 3) loud reports. A typical specimen, showing two ruptured regions, is shown in Figure 44. It is apparent that this type of blow out could lead to an apparently high ablation rate if the material was restrained in the across laminate direction.

To check on possible specimen thickness effects, three runs were made on with-laminate specimens having thicker walls. Because of the greater thickness, the measurements were made at the lower heating rate (2.9 K/s) to avoid excessive gradients in the specimen. For some reason, greater scatter occurred (fig. 45), but in general the effective thermal expansion was comparable to that obtained with the thinner walled specimens under the same conditions of restraint and heating rate.

Modulus data, obtained from the cyclic load variations imposed during the restrained expansion tests, are given in Figures 46 through 56. In general the moduli in the AL direction are lower than the WL direction and decrease more rapidly with increase in temperature.

*In fact, the opposite might occur as the WL stress could promote interlaminar separation.

Strength measurements on MX 2600. - Room temperature strength measurements were made by means of a flexure test (quarter-point loading) with results as follows (with laminate direction):

74.2 MN/m ²
51.5
65.5
57.2
64.1
<hr/>
Mean 62.5 MN/m ² (9070 psi)

At elevated temperatures, tensile measurements were made at two heating rates (2.8 and 7.0 K/s). These results are shown in Figure 57. The difference in heating rates employed did not appear to have any effect on the observed strength.

Transient thermal conductivity of MX 2600 char. - The silica phenolic specimens for the transient thermal conductivity test were charred by means of the tandem Gerdien Arc facility. The specimens were premachined to the approximate desired sample dimension and mounted in graphite holders. They were then exposed to a flux of 1.25×10^7 watts/meter² for a duration of 25 seconds.

The density of a charred specimen was measured as a function of position by removing layers from the end of the cylindrical specimen in a lathe and weighing the remainder. The density was found to be a constant value of about 1410 kg/meter³ over the entire 2 cm of char depth.

The specific heat of front and aft sections of another charred specimen were measured with the Perkin-Elmer Differential Scanning Calorimeter at a temperature of 340 K and both found to be a ≈ 800 Joules/Kg. K. This specific heat data agrees exactly with the specific heat measurements previously done on another silica phenolic char. Therefore, for the purposes of data reduction, the specific heat of the sample was assumed to be only a function of temperature, not position in sample, and that the specific heat varied with temperature as had previously been measured.

A sample of silica phenolic char, 30-degree orientation, from a SCOUT rocket nozzle was supplied by J. Howell of NASA/Langley Research Center. A char density profile was measured and it too was uniform through the thickness but a slightly higher value, 1540 kg/m³, than the previously mentioned arc produced char.* The specific heat of the sample measured the same as the arc char at 340 K.

*This could be due to initial density differences or as a result of some difference in heat flux.

The silica phenolic specimens were instrumented with a thermocouple spacing of 0.076 cm and tested in the Tandem Geridien Arc Facility with a heat flux of 5.6×10^6 watts/meter². The results of the tests are shown in Figures 58 through 62. The conductivity curves in the two orthogonal directions are slightly lower than the previously measured data on silica phenolic char. In general, the results are what would be expected; at low temperature the conductivity in the with grain direction is about twice that of the across grain direction and both tend to increase with temperature as most low conductivity materials do.

The conductivity of the rocket nozzle material, 30-degree orientation, falls between the conductivity of the two orthogonal directions at lower temperature, as it should, but goes higher than both at higher temperatures.

Measurements on FM 5272

Density measurements on specimens from the panel of FM 5272 cellulose phenolic gave a value of 1320 kg/m³ (82 lb/ft³). The with laminate modulus, as determined from ultrasonic wave velocity was 8.15 GN/m² (1.18×10^6 psi).

Free thermal expansion of FM 5272. - The results of free thermal expansion measurements, made at low heating rate in the Brinkmann dilatometer are shown in Figures 63 and 64. It will be noted that the peak expansion across laminate is considerably larger than the with laminate expansion and that both peaks are larger than were observed for the MX 2600. Figure 65 gives a comparison of the expansion portion of the curves with an expanded scale.

In addition to the greater expansion shown by FM 5272 (as compared to MX 2600), this material also showed a much larger shrinkage as the resin degraded. This is evident in Figure 66 which shows specimens of Carbitex, MX 2600 and FM 5272 after testing in the Brinkmann dilatometer. All specimens were the same length and diameter before being tested.

Figures 67 and 68 show the results of high heating rate, free expansion tests on FM 5272 in the with laminate direction. As with the MX 2600, each of these curves represents measurements on six long and six short specimens. A comparison, showing the effect of heating rate on free thermal expansion is shown in Figure 69. It is apparent that not only are the peak expansions considerably larger than those observed for MX 2600, but the effect of heating rate is much greater. As is typical, the peak is not only larger but is shifted to higher temperature as the heating rate is increased.

Restrained expansion of FM 5272. - The results of restrained thermal expansion tests on FM 5272 in the with laminate direction are given in Figures 70 through 73. It is interesting to note that the peak effective expansions obtained are not much different

Figure 28. Thermal Expansion of MX 2600
With Lamina, Low Heating Rate (0.033 K/s)

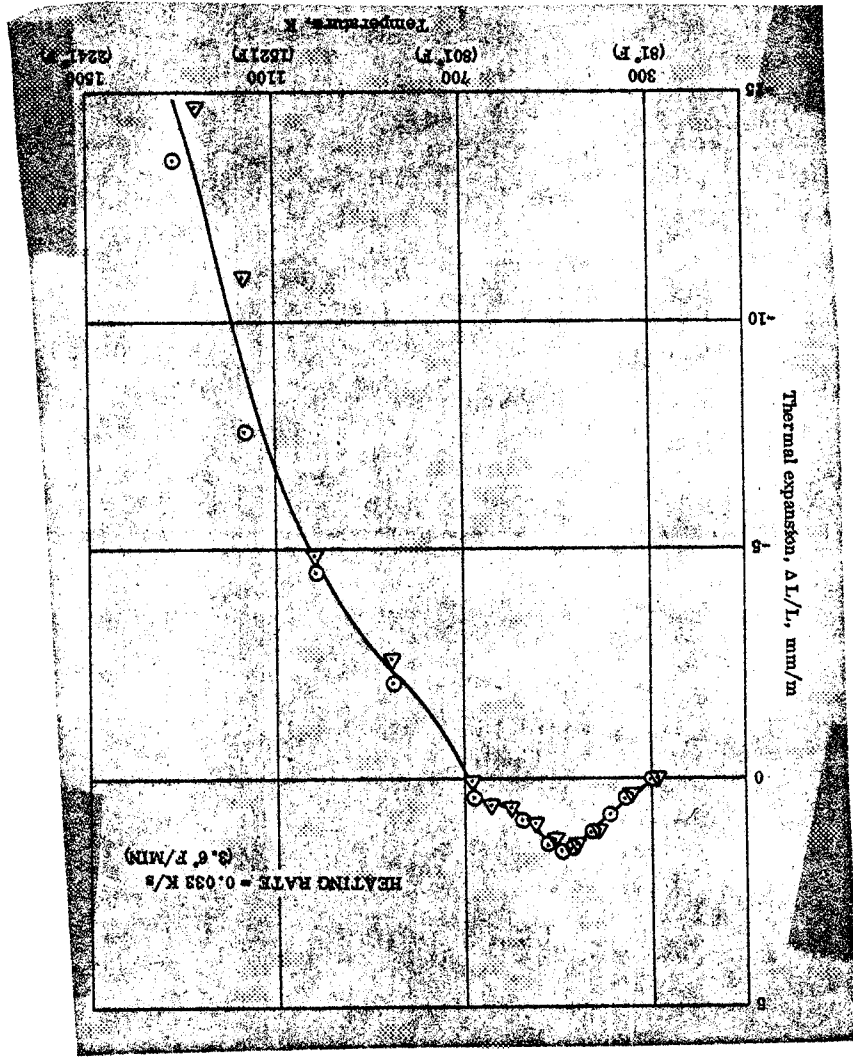
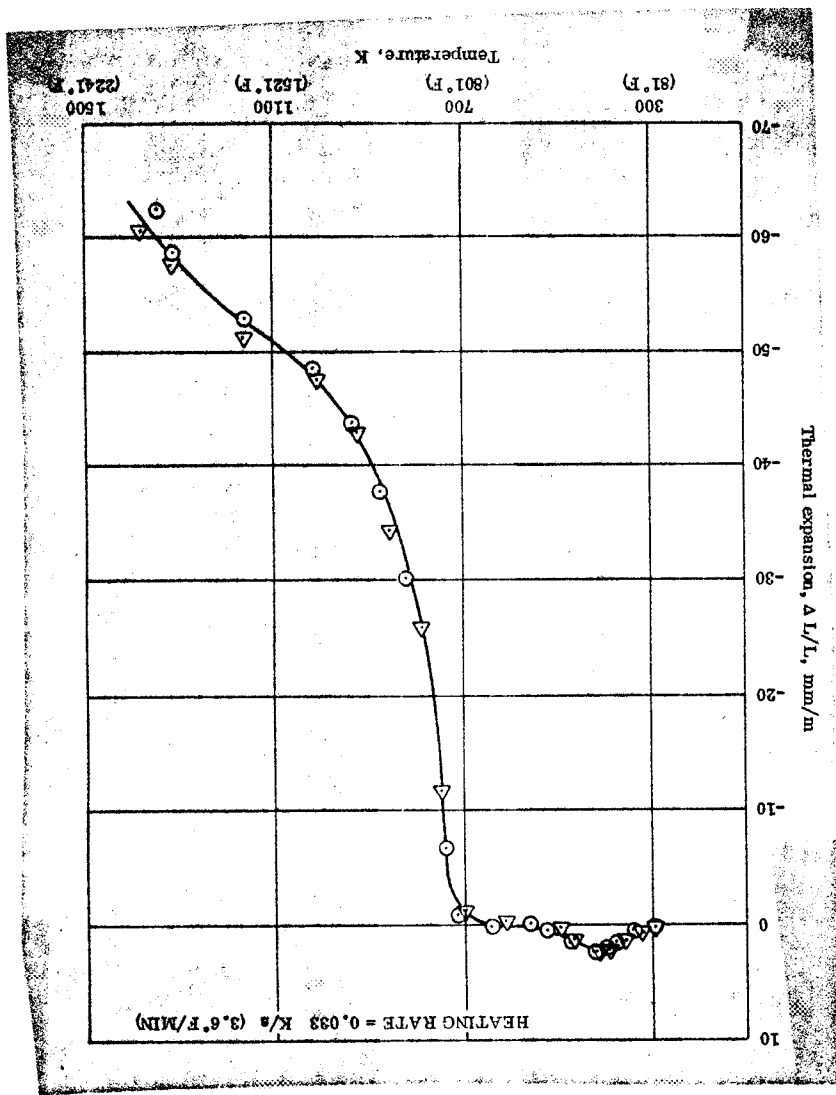


Figure 29. Thermal Expansion of MX 2600
Across Lamina, Low Heating Rate



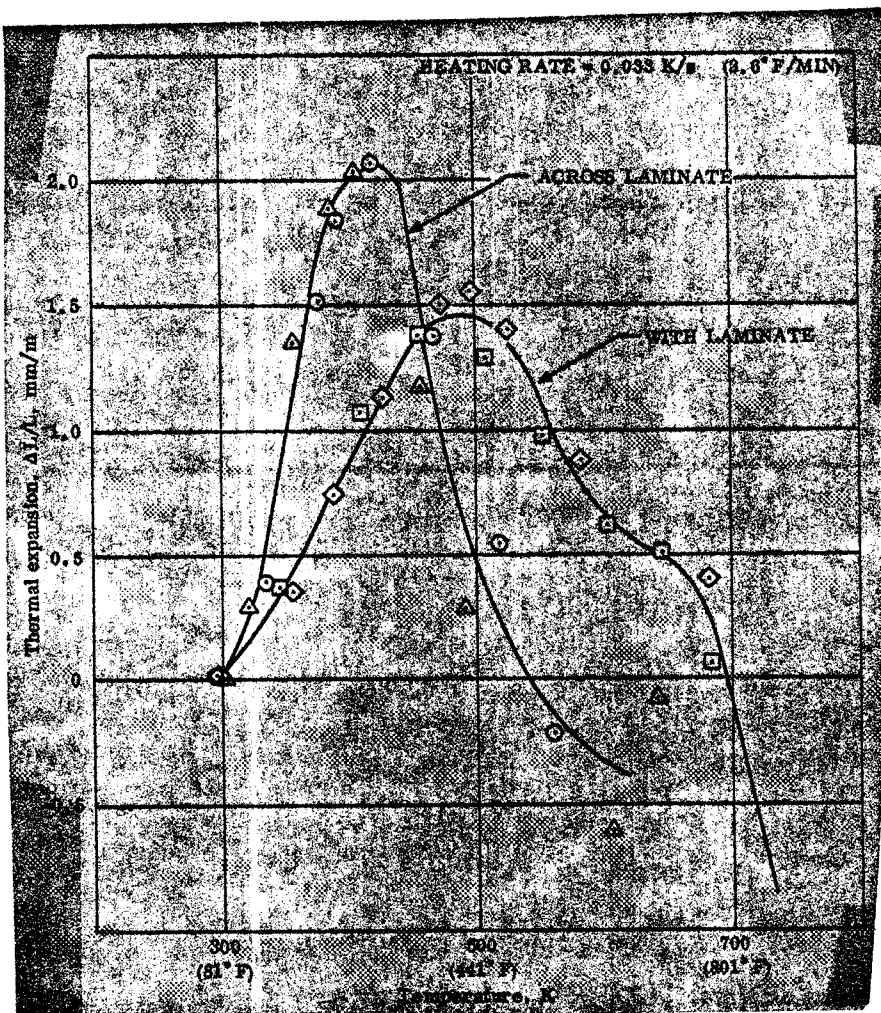


Figure 30. Thermal Expansion of MX 2600
Comparison of With and Across Lamina

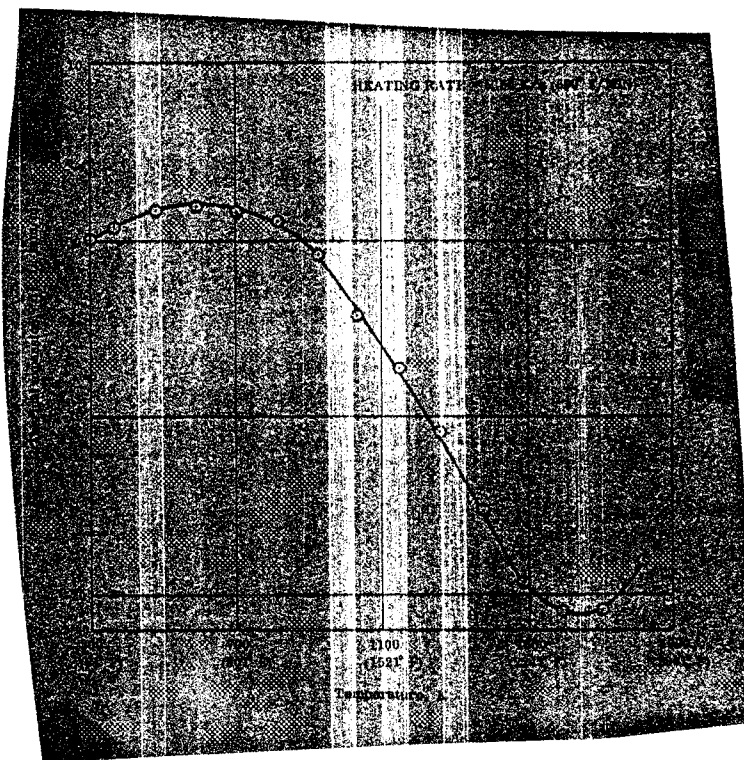


Figure 31. Thermal Expansion of MX 2600
With Lamina at 5.55 K/s (600°F/min)

Figure 32. Thermal Expansion of MX 2600
With Lamina at 13.9 K/s (1500° F/min)

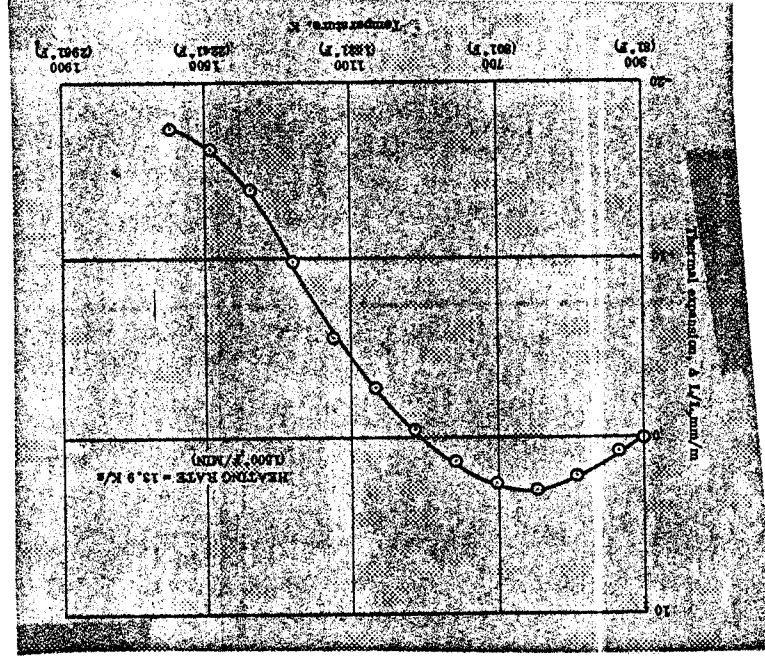
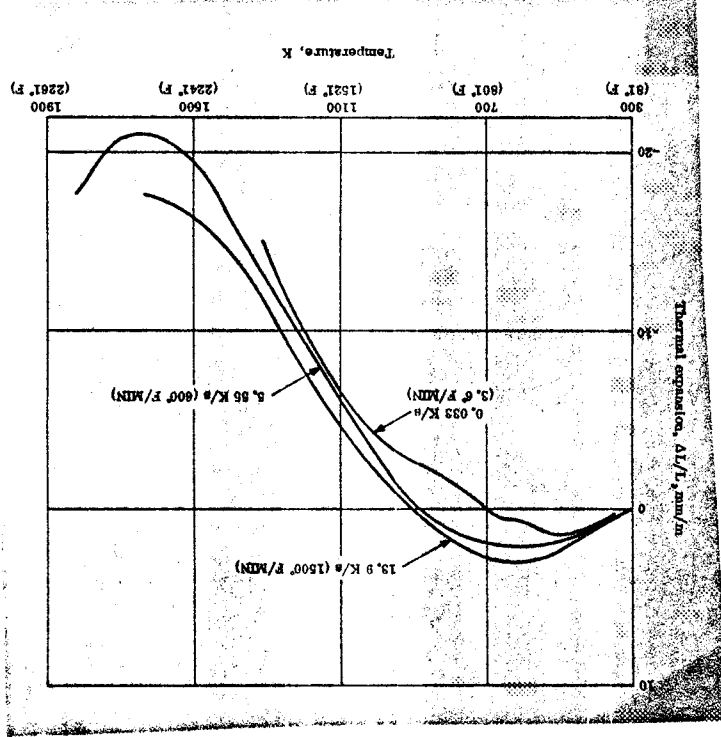


Figure 33. Thermal Expansion of MX 2600
Effect of Heating Rate, With Lamina



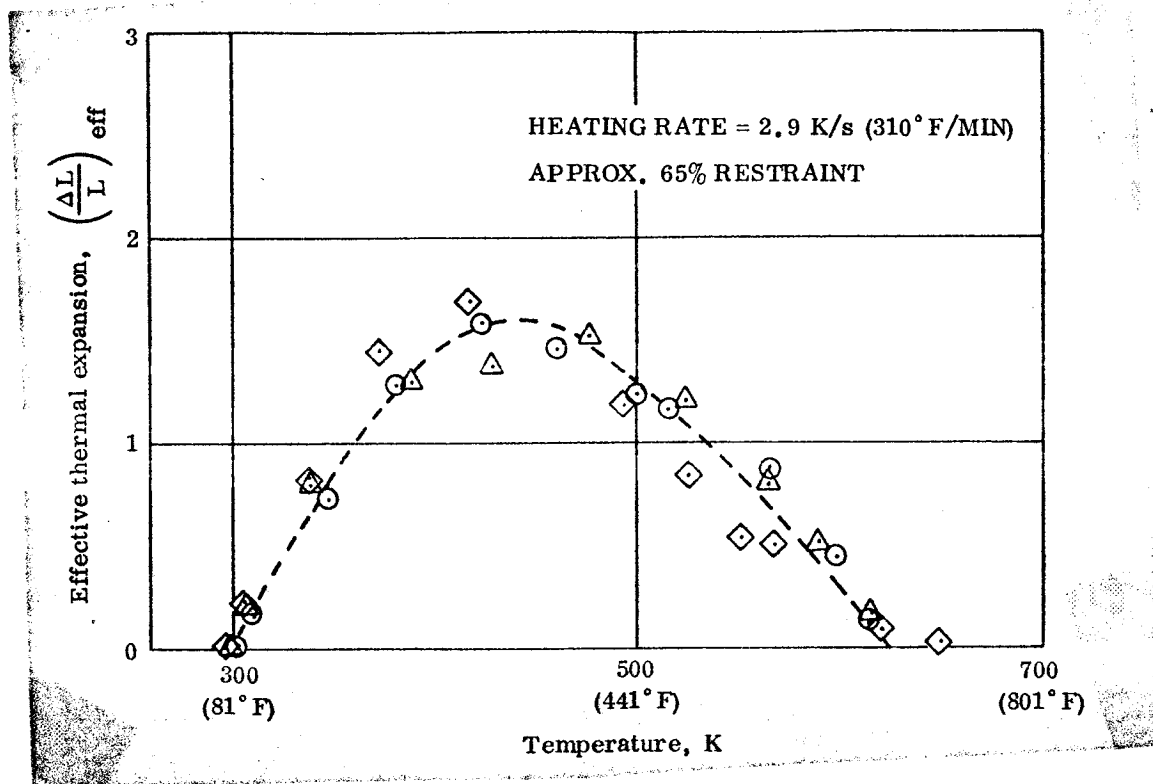


Figure 34. Restrained Expansion of MX 2600, With Lamina
Heating Rate = 2.9 K/s (310° F/min) R = 65%

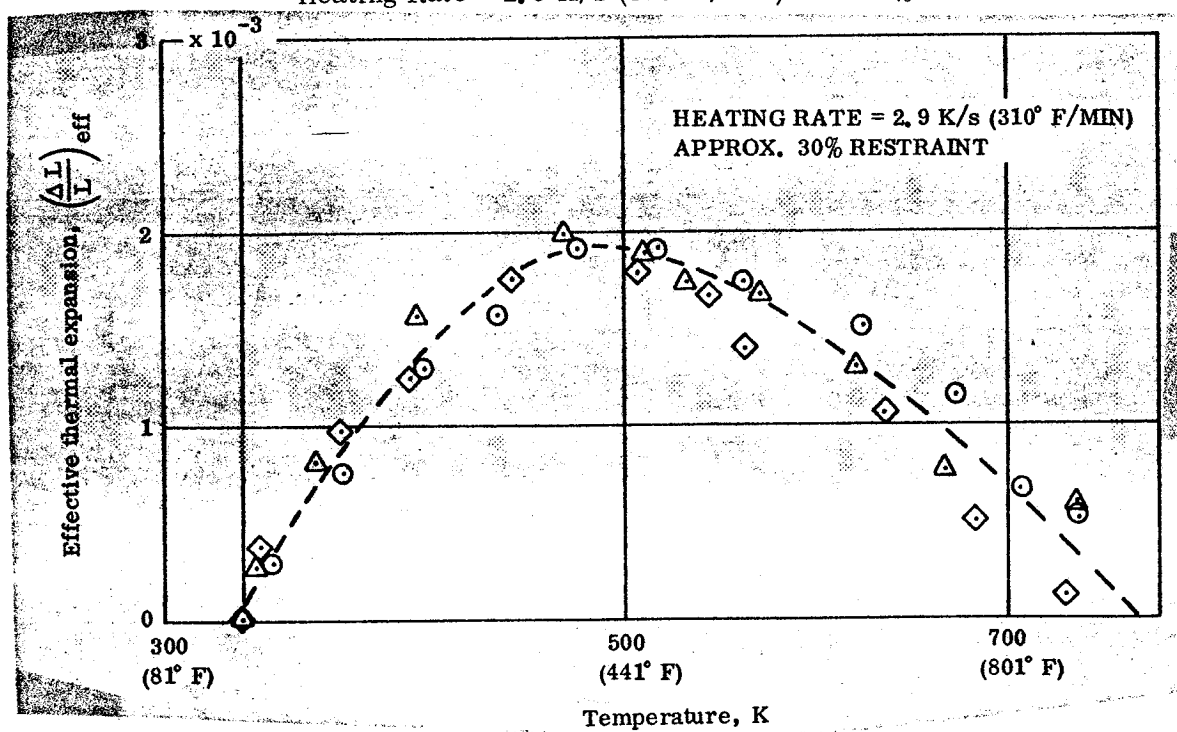


Figure 35. Restrained Expansion of MX 2600, With Lamina
Heating Rate = 2.9 K/s (310° F/min) R = 30%

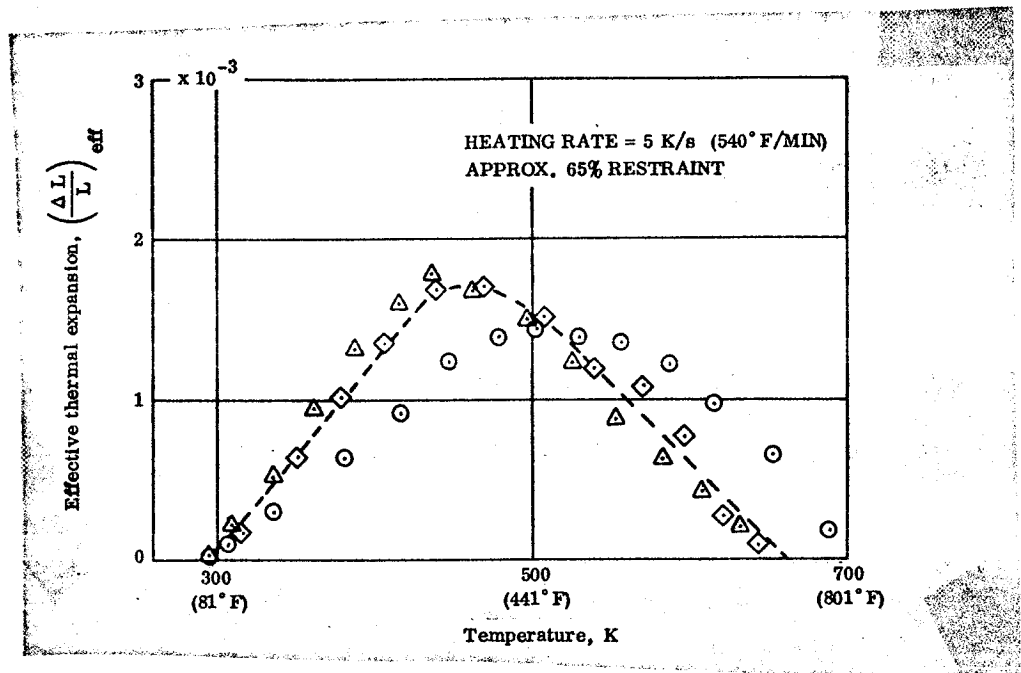


Figure 36. Restrained Expansion of MX 2600, With Lamina
Heating Rate = 5.0 K/s (540° F/min) R = 65%

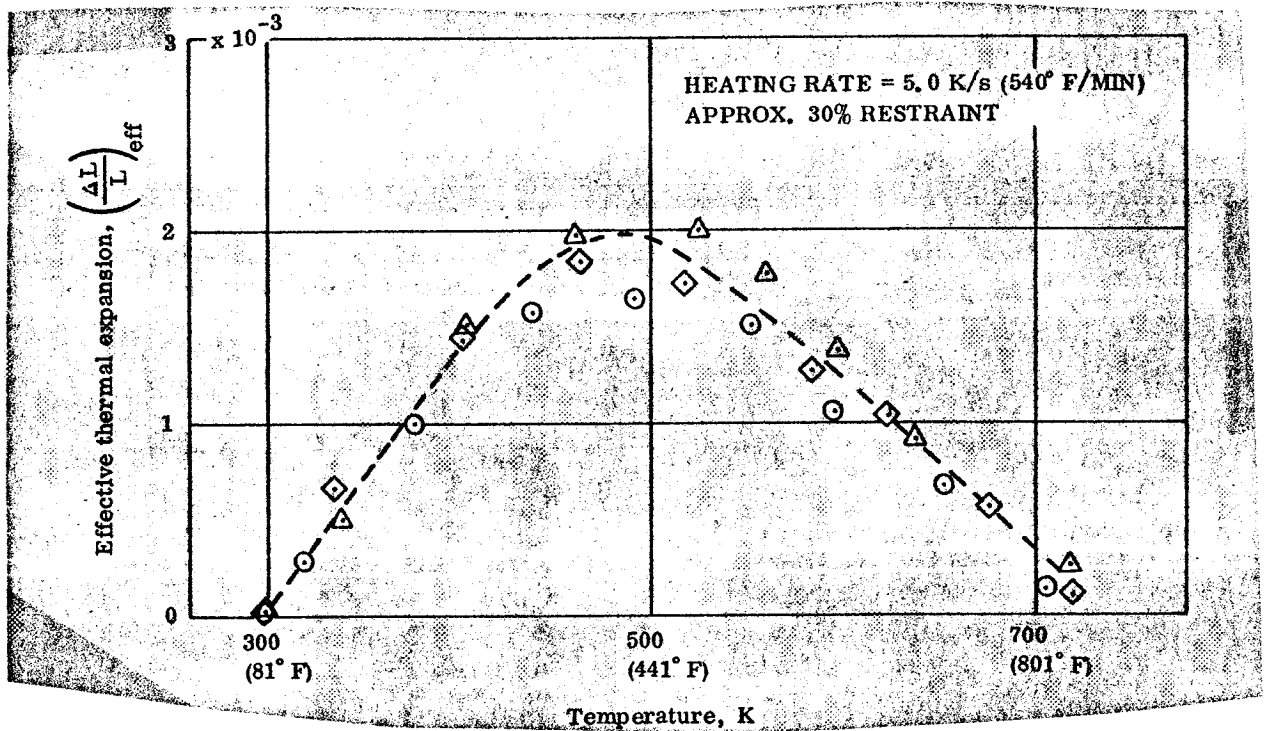


Figure 37. Restrained Expansion of MX 2600, With Lamina
Heating Rate = 5.0 K/s (540° F/min) R = 30%

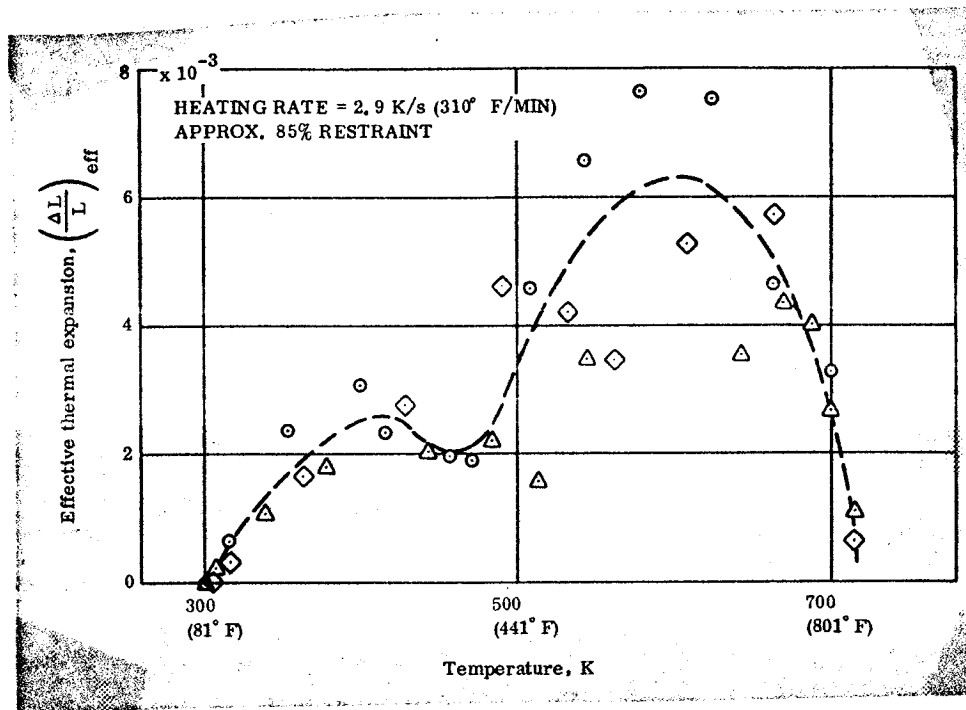


Figure 38. Restrained Expansion of MX 2600, Across Lamina
Heating Rate = 2.9 K/s (310° F/min) R = 85%

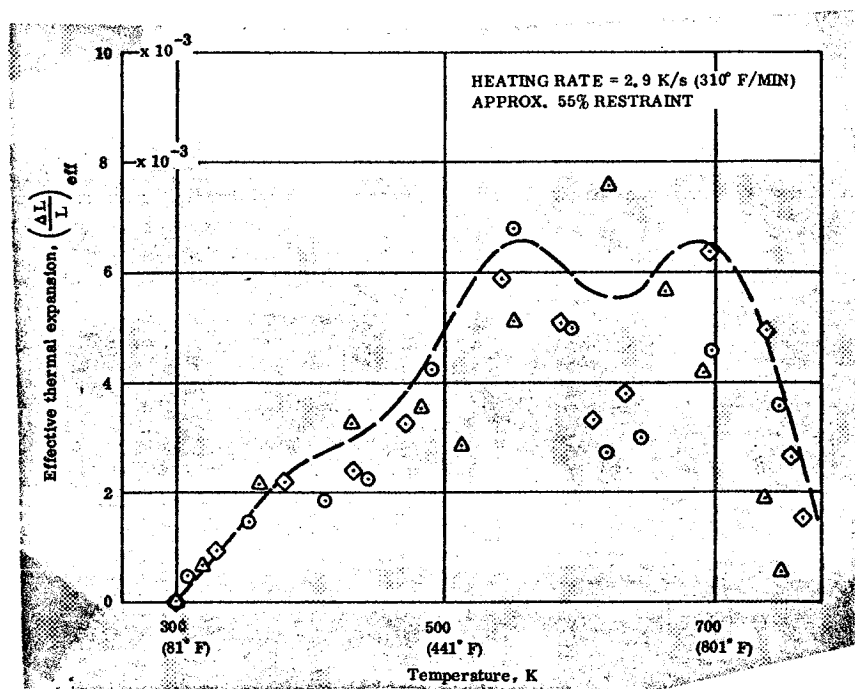


Figure 39. Restrained Expansion of MX 2600, Across Lamina
Heating Rate = 2.9 K/s (310° F/min) R = 55%

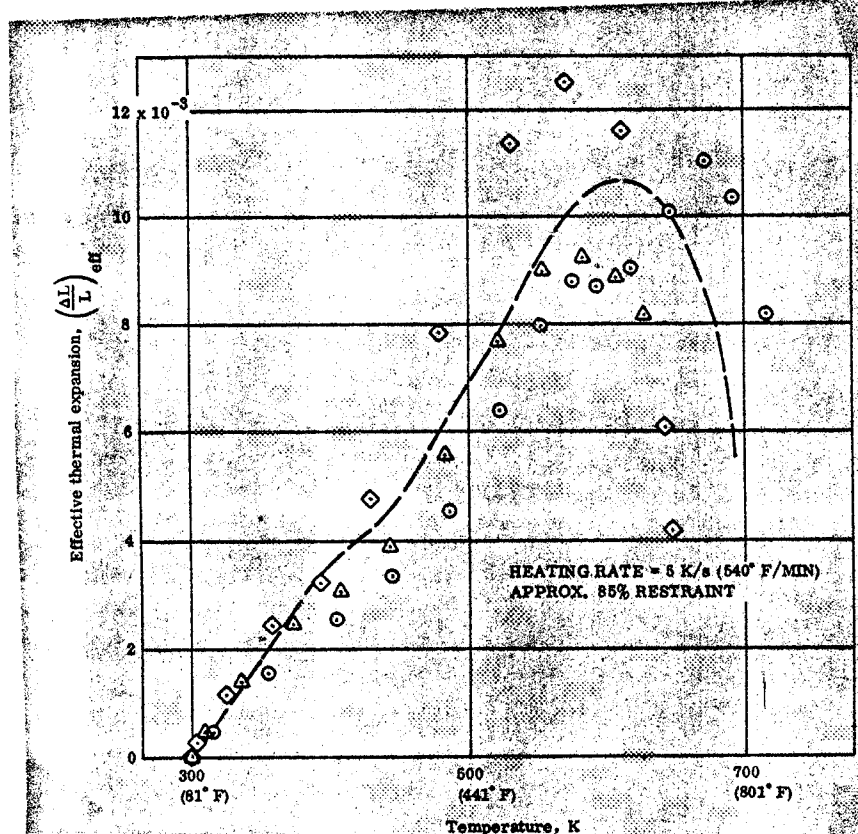


Figure 40. Restrained Expansion of MX 2600,
Across Lamina Heating Rate = 5.0 K/s
(540° F/min) R = 85%

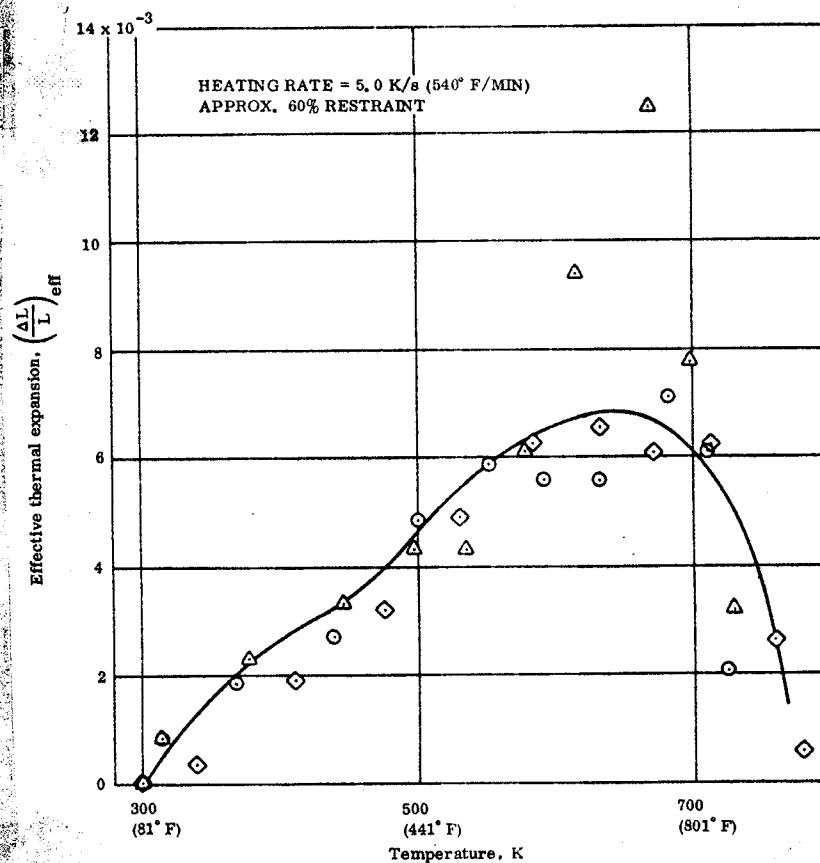


Figure 41. Restrained Expansion of MX 2600,
Across Lamina Heating Rate = 5.0 K/s
(540° F/min) R = 60%

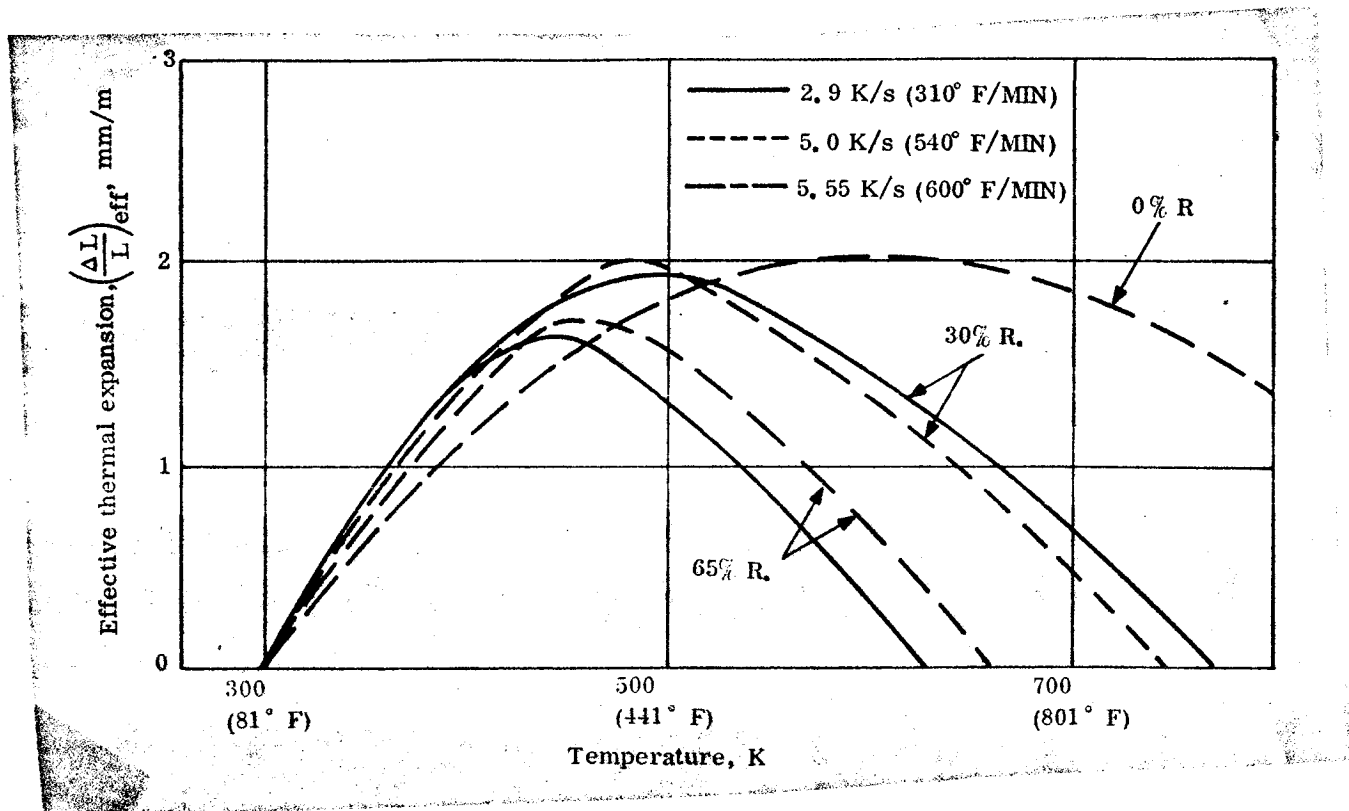


Figure 42. Effect of Restraint and Heating Rate on Effective Thermal Expansion of MX 2600, With Lamina

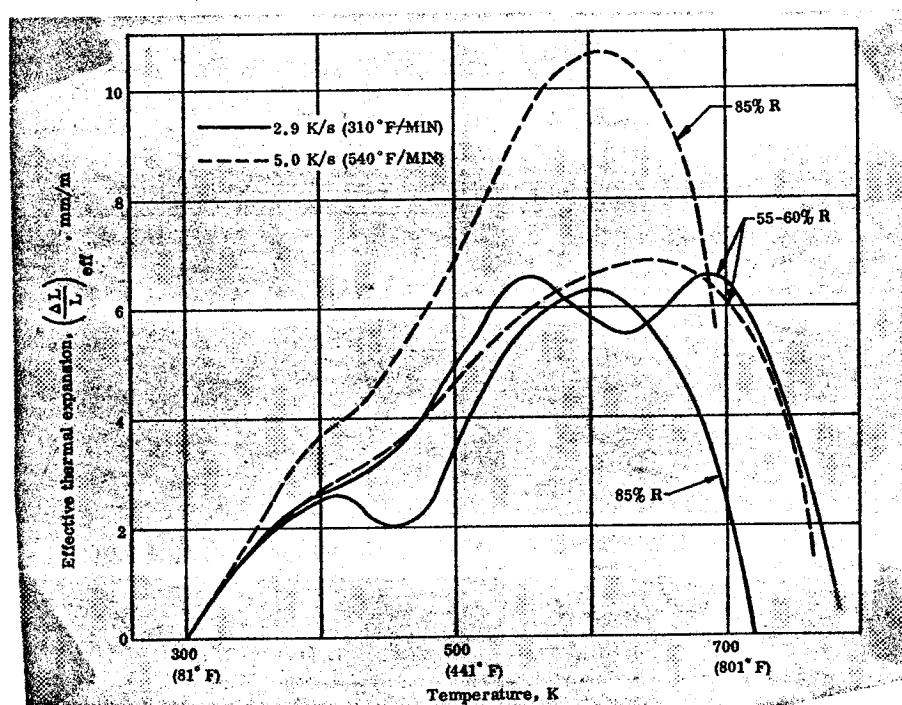


Figure 43. Effect of Restraint and Heating Rate on Effective Thermal Expansion of MX 2600, Across Lamina

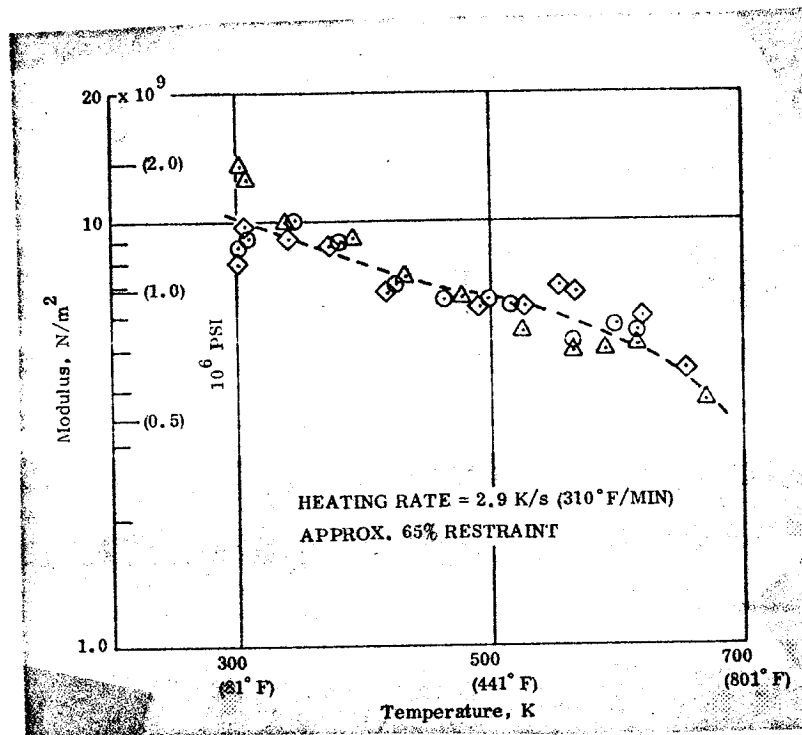


Figure 46. Modulus of Restrained MX 2600, With Lamina,
Heating Rate = 2.9 K/s (310°F/min) R = 65%

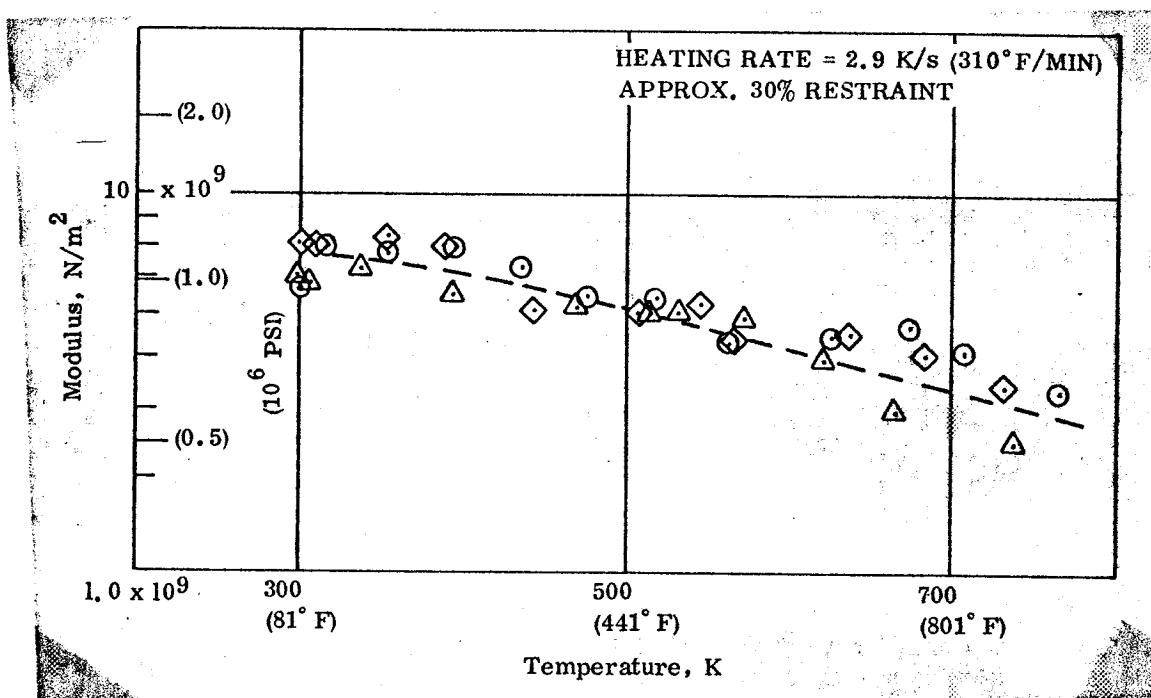


Figure 47. Modulus of Restrained MX 2600, With Lamina,
Heating Rate = 2.9 K/s (310°F/min) R = 30%

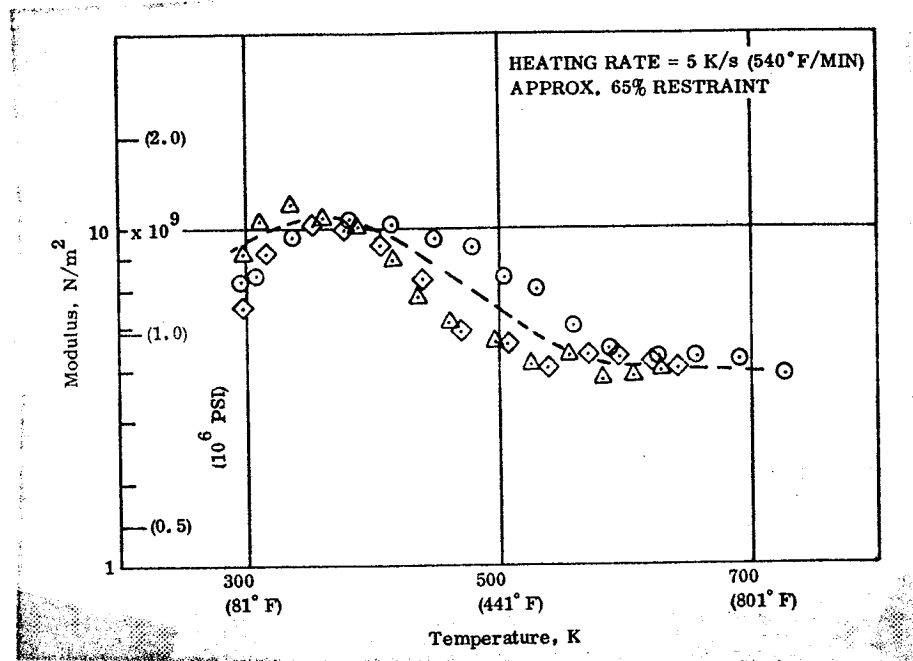


Figure 48. Modulus of Restrained MX 2600, With Lamina,
Heating Rate = 5.0 K/s (540° F/min) R = 65%

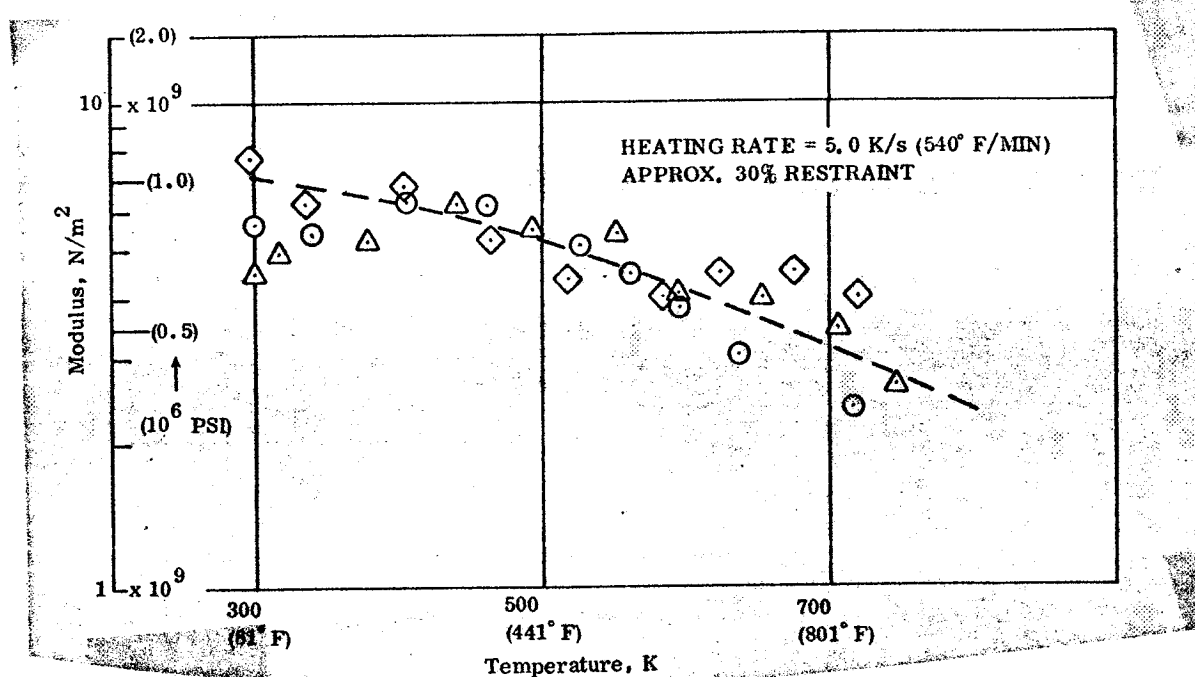


Figure 49. Modulus of Restrained MX 2600, With Lamina,
Heating Rate = 5.0 K/s (540° F/min) R = 30%

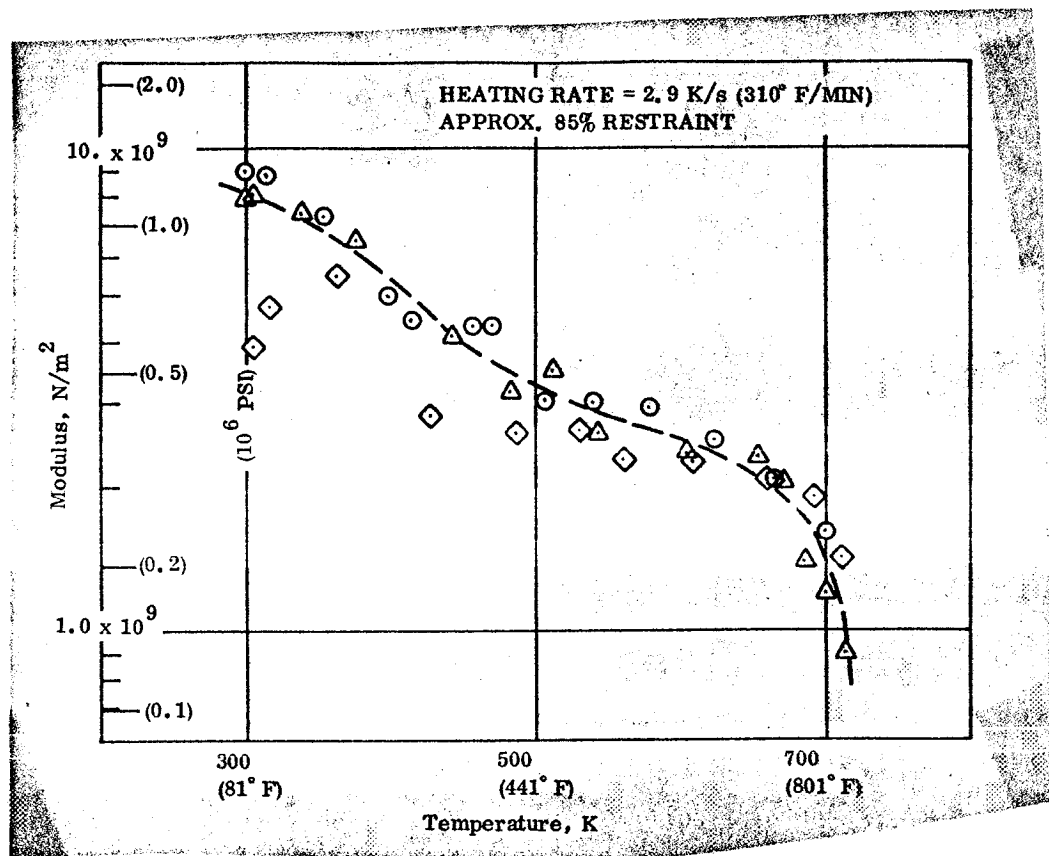


Figure 50. Modulus of Restrained MX 2600, Across Lamina
Heating Rate = 2.9 K/s (310° F/min) R = 85%

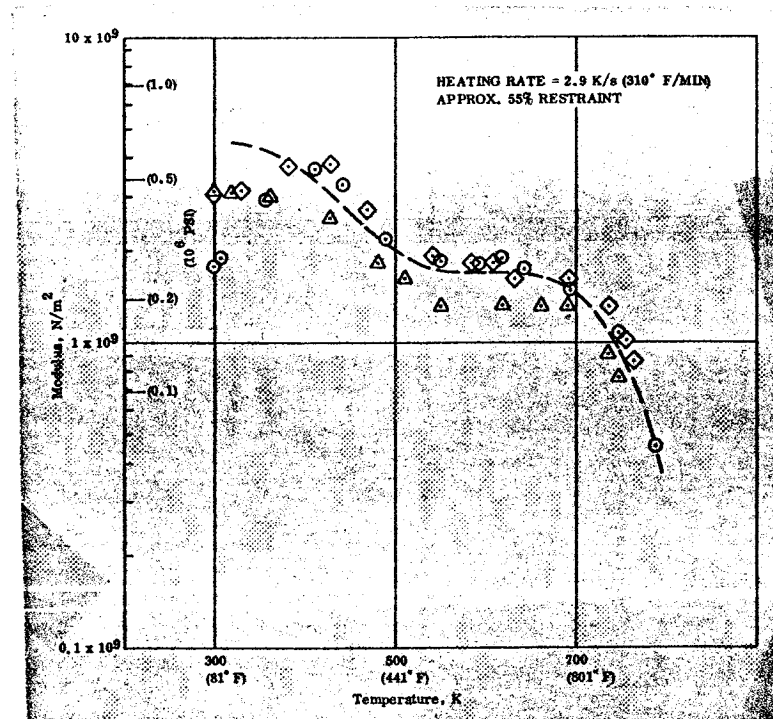


Figure 51. Modulus of Restrained MX 2600, Across Lamina
Heating Rate = 2.9 K/s (310° F/min) R = 55%

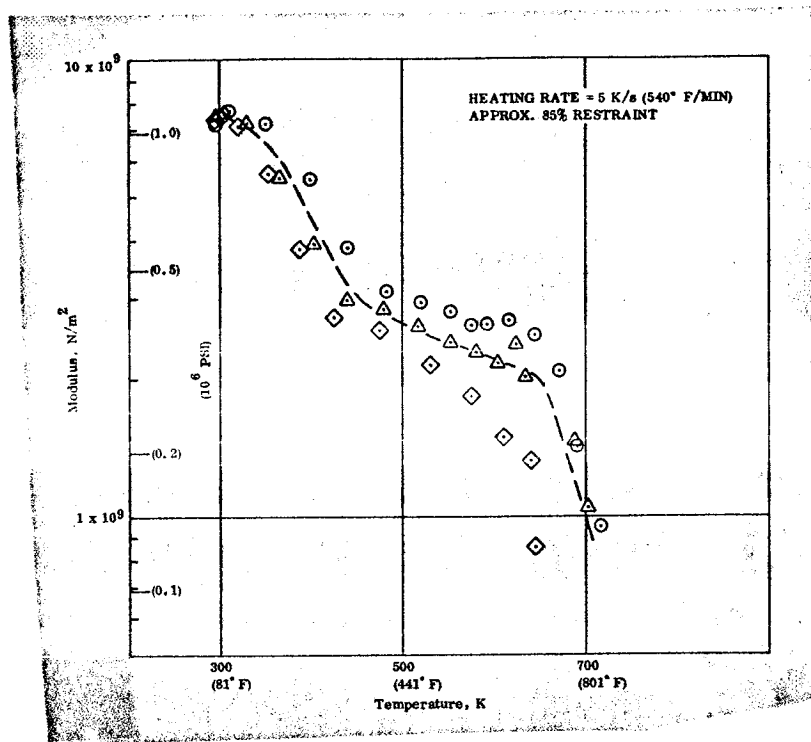


Figure 52. Modulus of Restrained MX 2600, Across Lamina
Heating Rate = 5.0 K/s (540° F/min) R = 85%

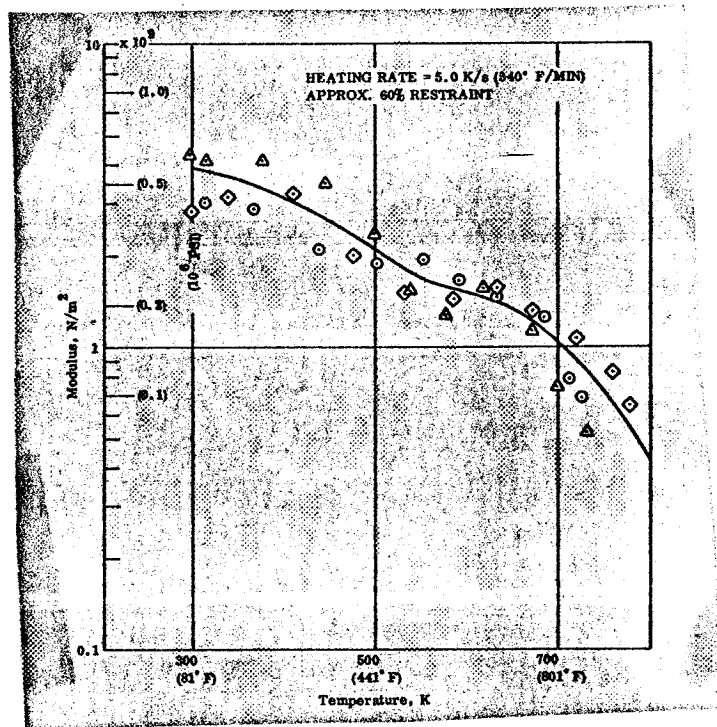


Figure 53. Modulus of Restrained MX 2600, Across Lamina
Heating Rate = 5.0 K/s (540° F/min) R = 60%

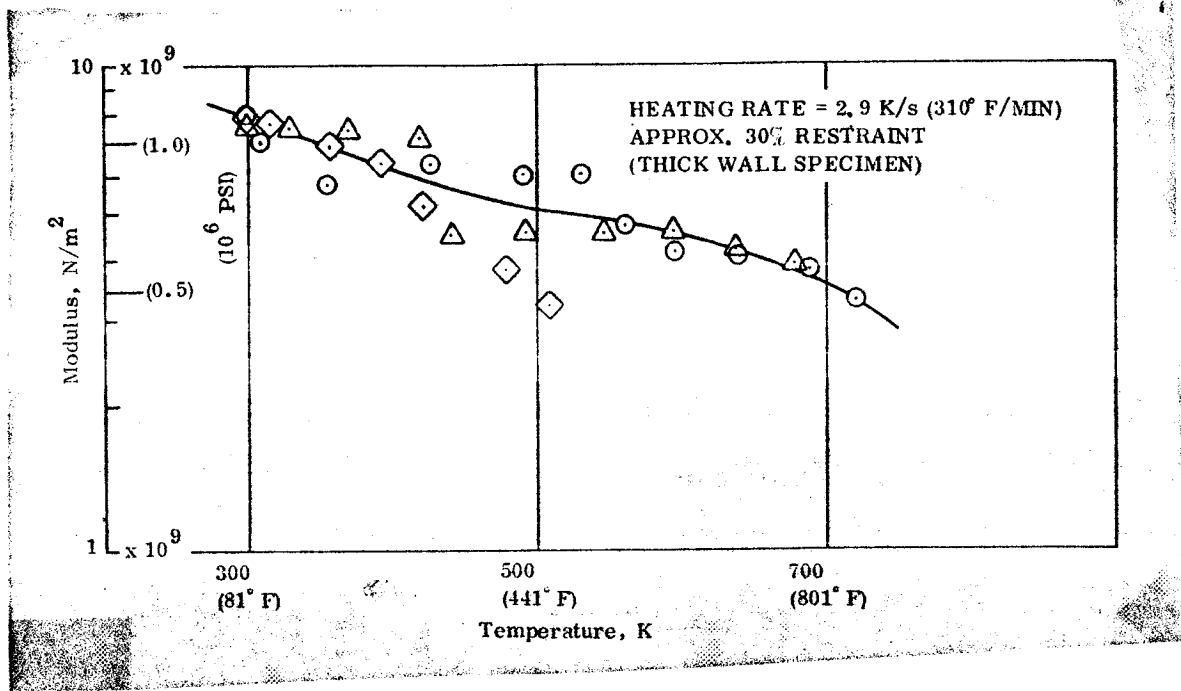


Figure 54. Modulus of Restrained MX 2600, with Lamina, Thick Wall Speciman, Heating Rate = 2.9 K/s (310° F/min) R = 30%

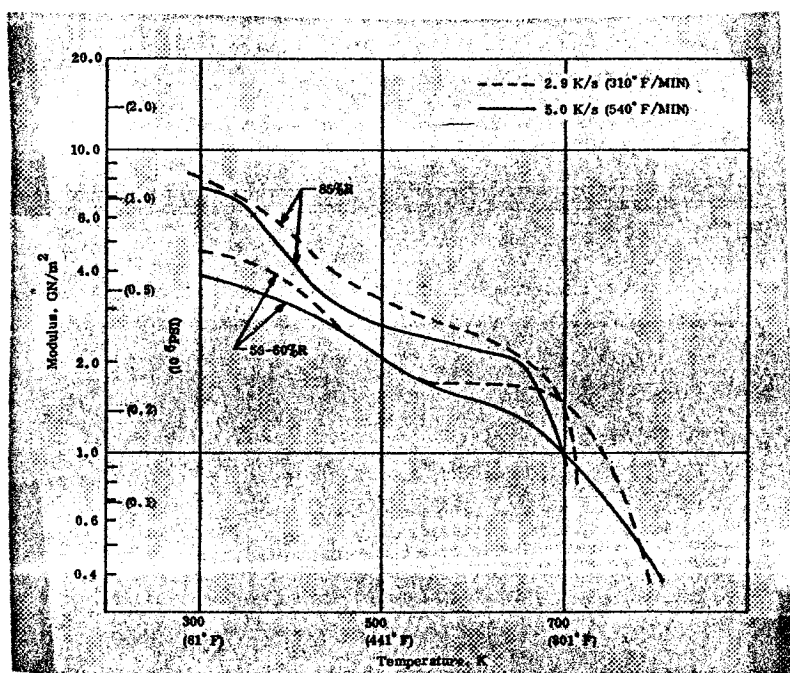


Figure 55. Summary of Modulus Data, MX 2600, Across Lamina

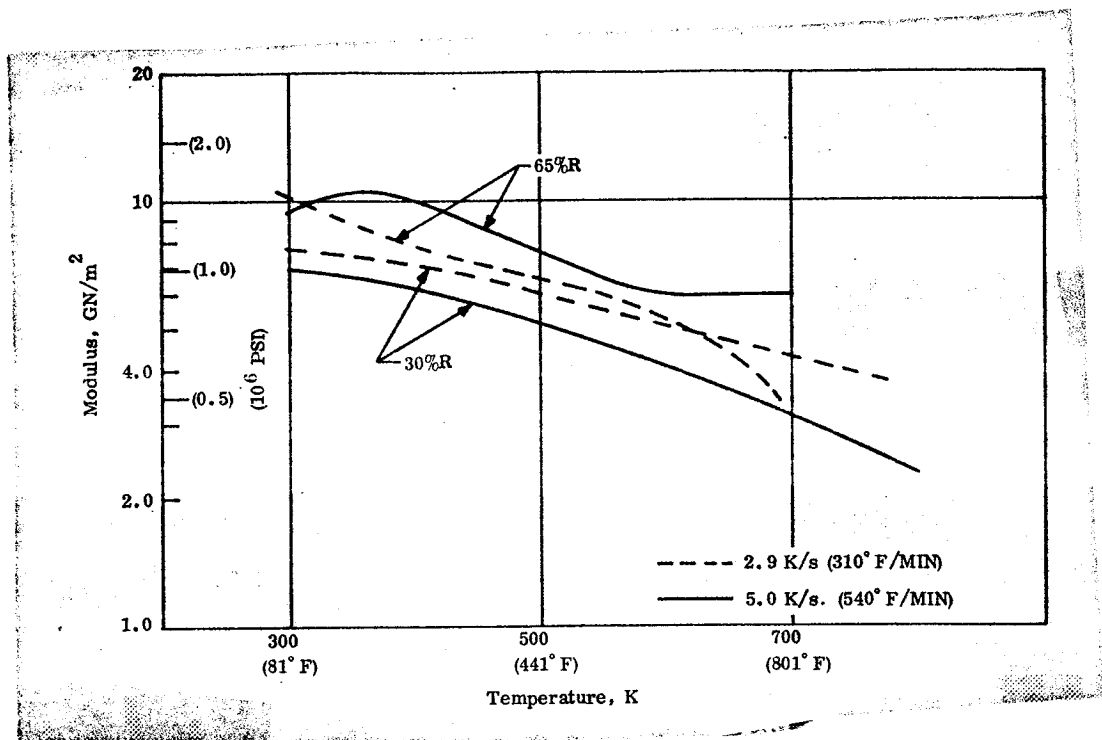


Figure 56. Summary of Modulus Data, MX 2600, With Lamina

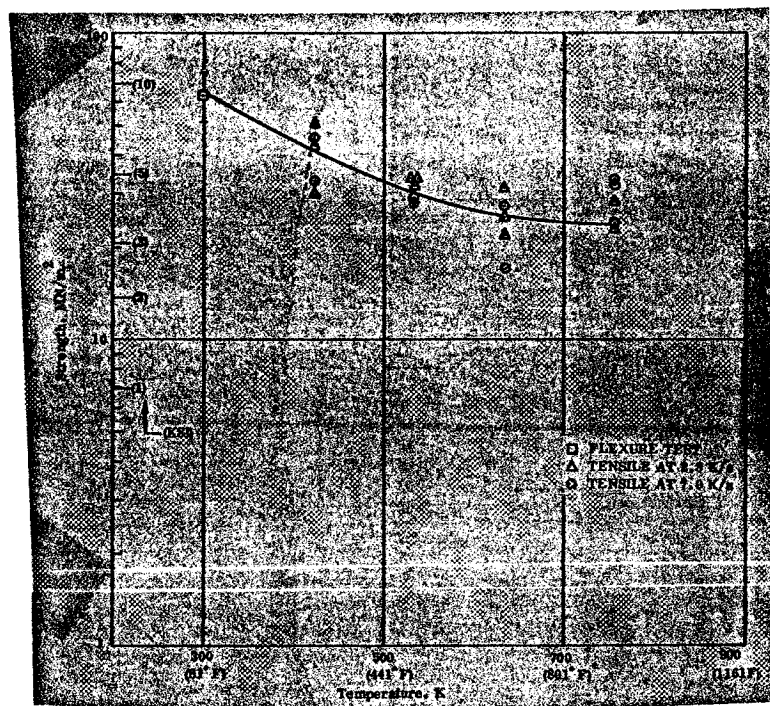


Figure 57. Strength Measurements, MX 2600, With Lamina

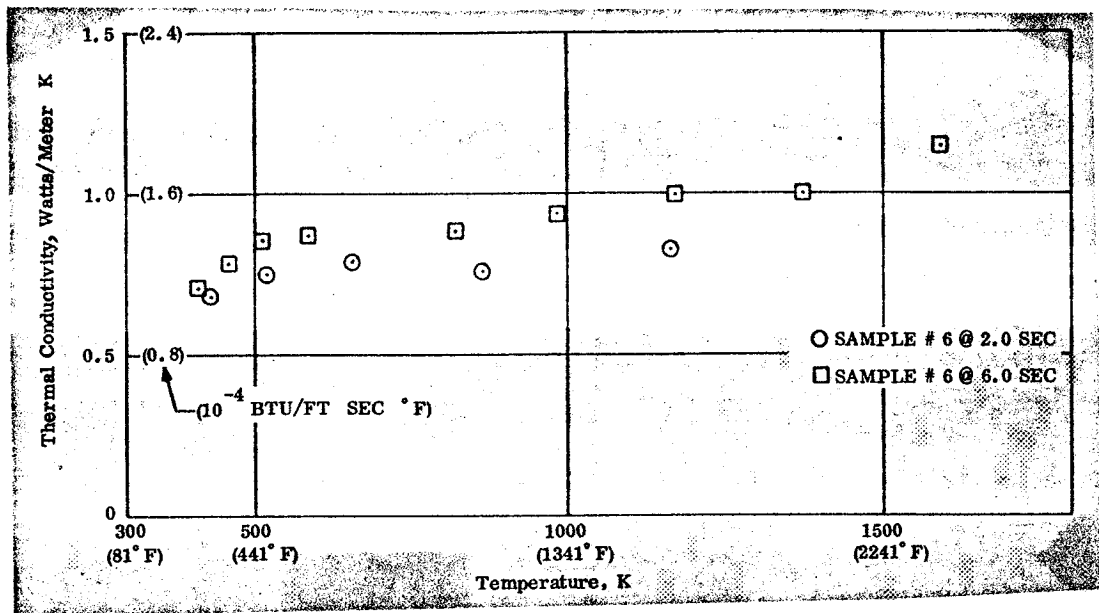


Figure 58. Thermal Conductivity of MX 2600 Silica Phenolic Char With Lamina, Transient Measurement

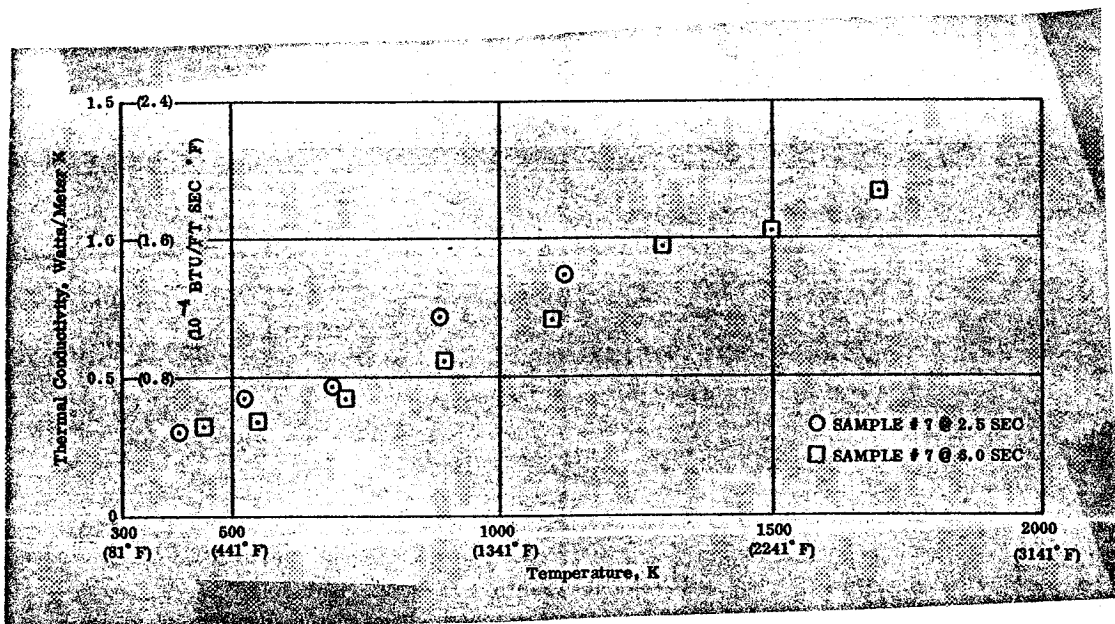


Figure 59. Thermal Conductivity of MX 2600 Silica Phenolic Char Across Lamina, Transient Measurement

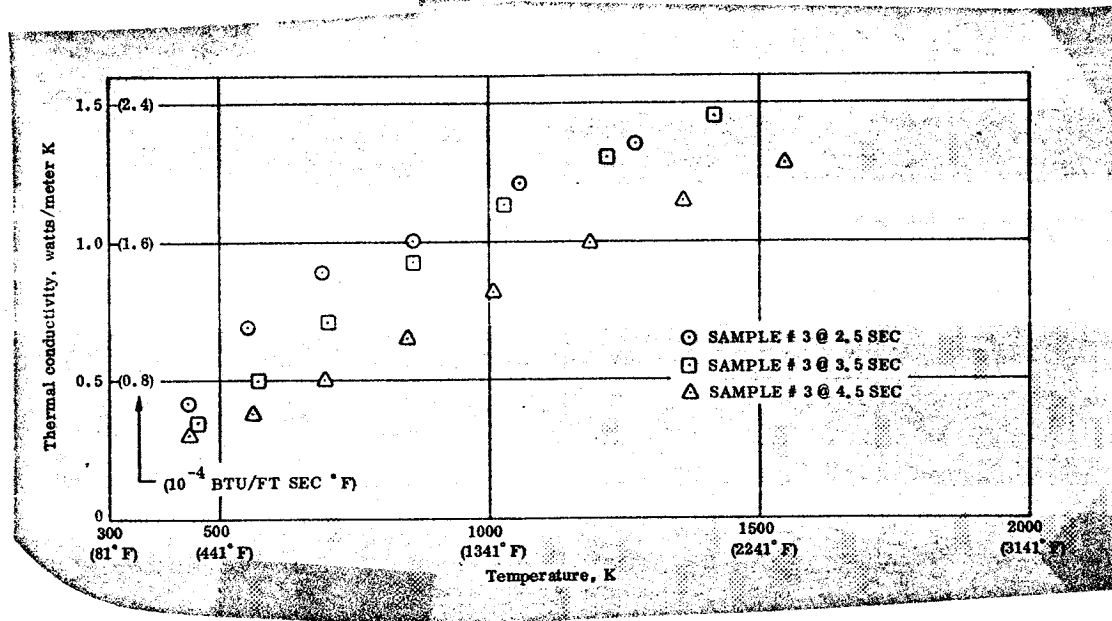


Figure 60. Thermal Conductivity of MX 2600 Silica Phenolic Char From Rocket Nozzle (Approx. 30-Degree Orientation)

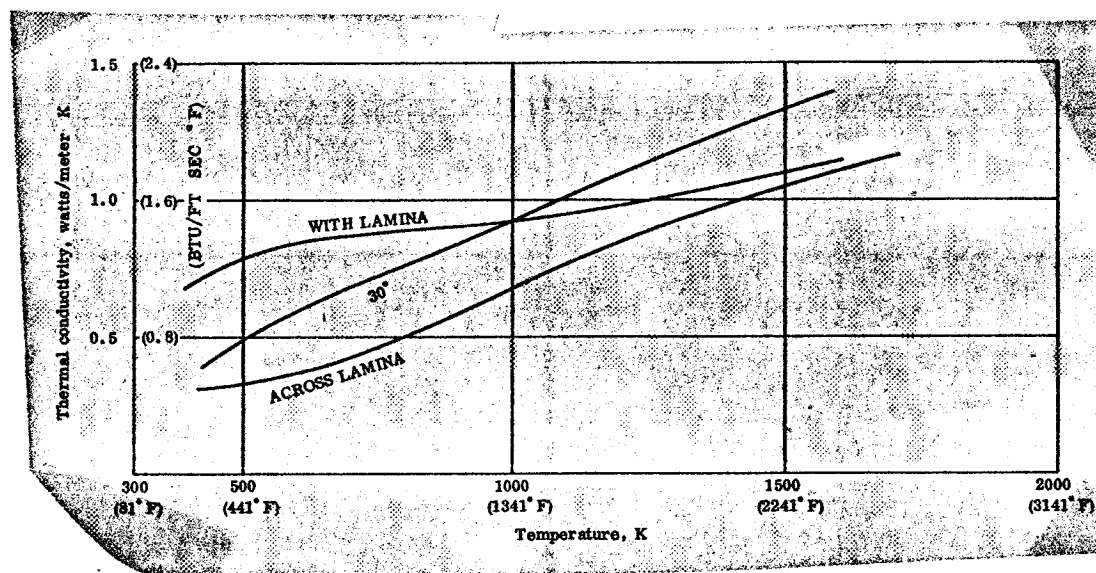


Figure 61. Thermal Conductivity of MX 2600 Silica Phenolic Char, Summary of Transient Data

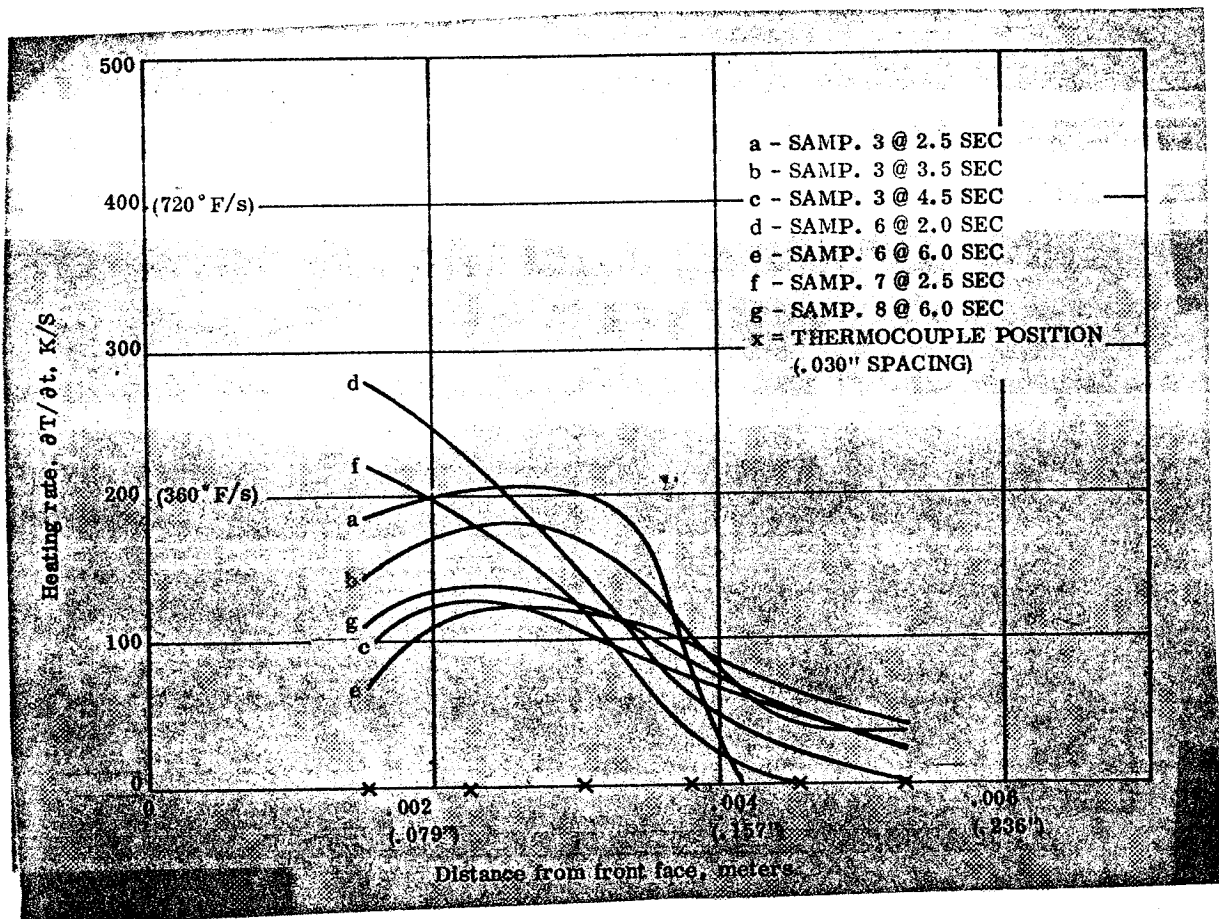


Figure 62. Thermal Conductivity of MX 2600 Silica Phenolic Char, Summary of Heating Rate Data

Figure 63. Thermal Expansion of FM 5272, Across Lamina, Low Heating Rate (0.033K/s) (3.6° F/min)

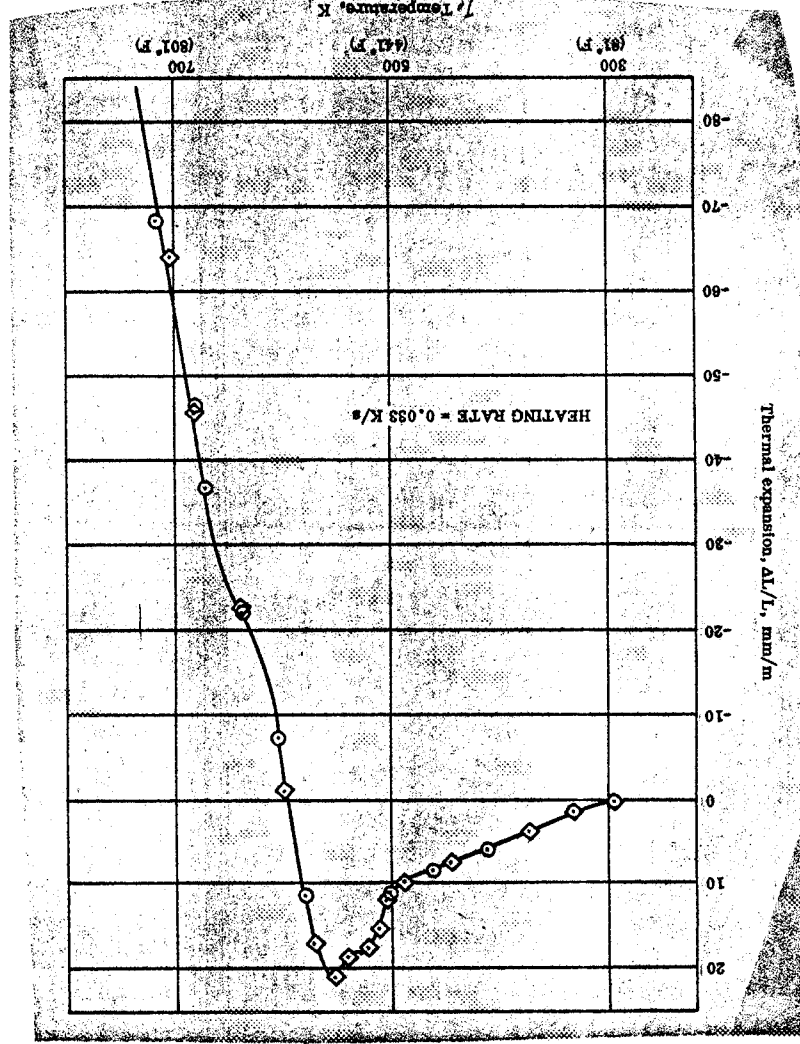


Figure 64. Thermal Expansion of FM 5272, With Lamina, Low Heating Rate (0.033K/s) (3.6° F/min)

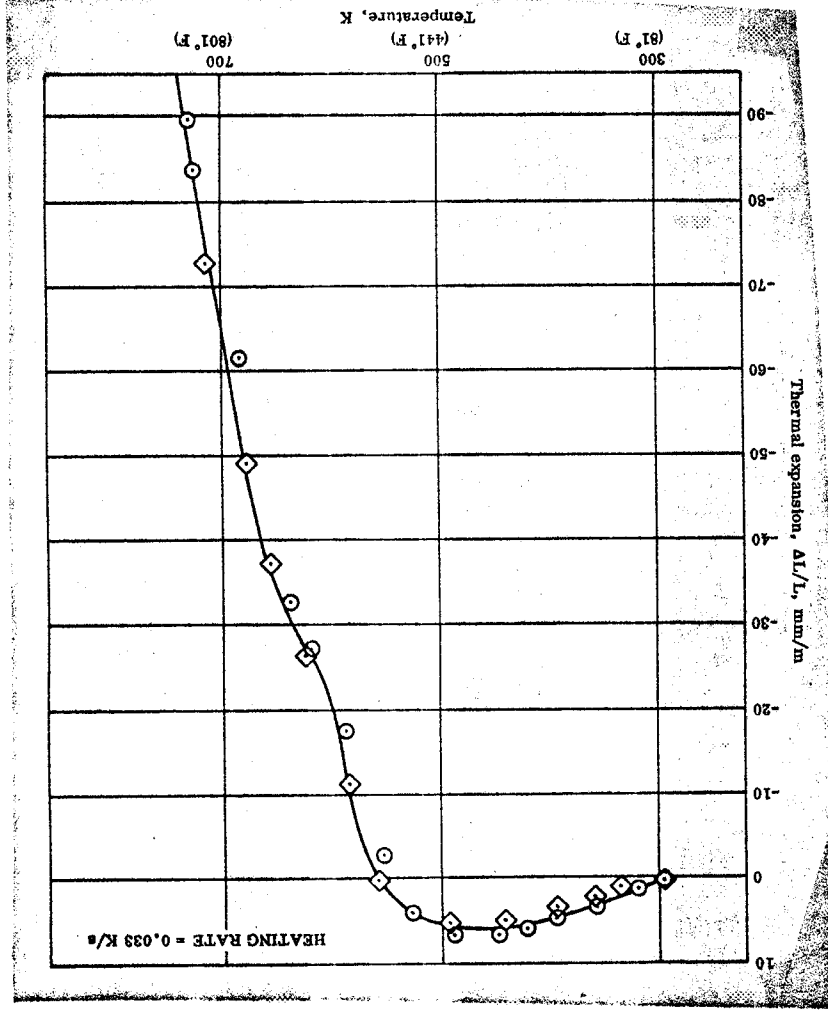


Figure 67. Thermal Expansion of FM 5272, With
Lamina at 5.55 K/s (1500° F/min)

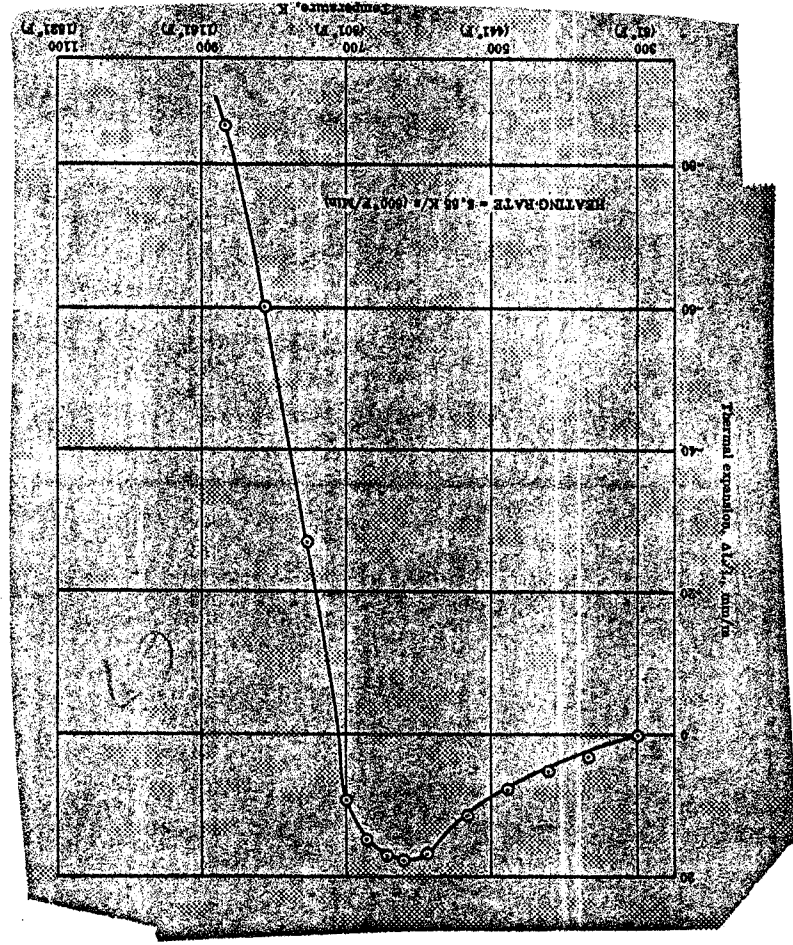
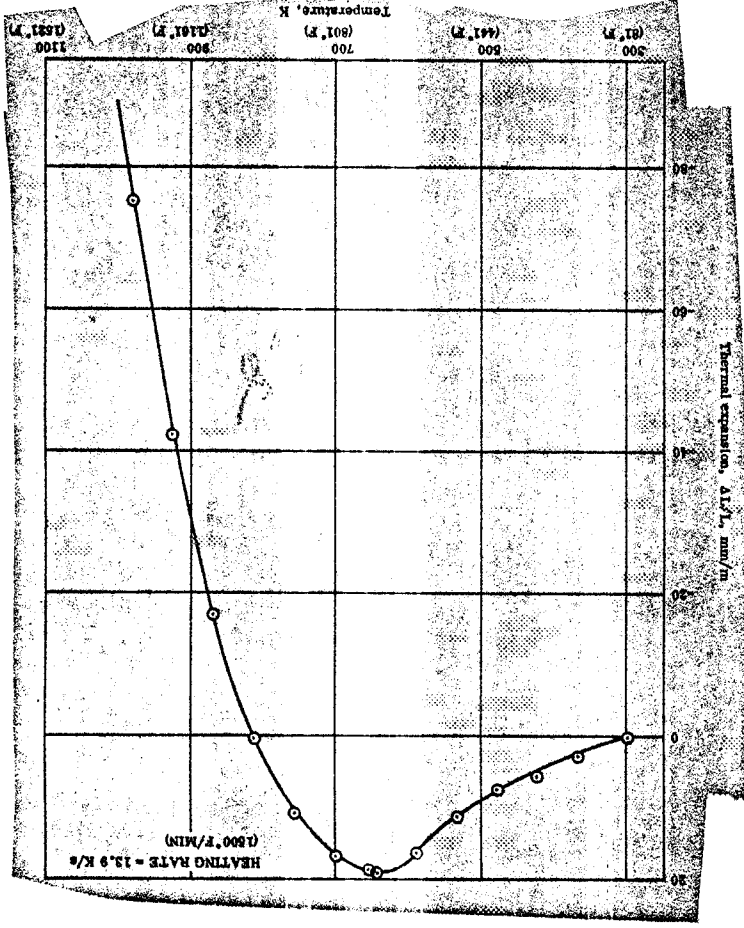


Figure 68. Thermal Expansion of FM 5272, With
Lamina at 13.9 K/s (1500° F/min)



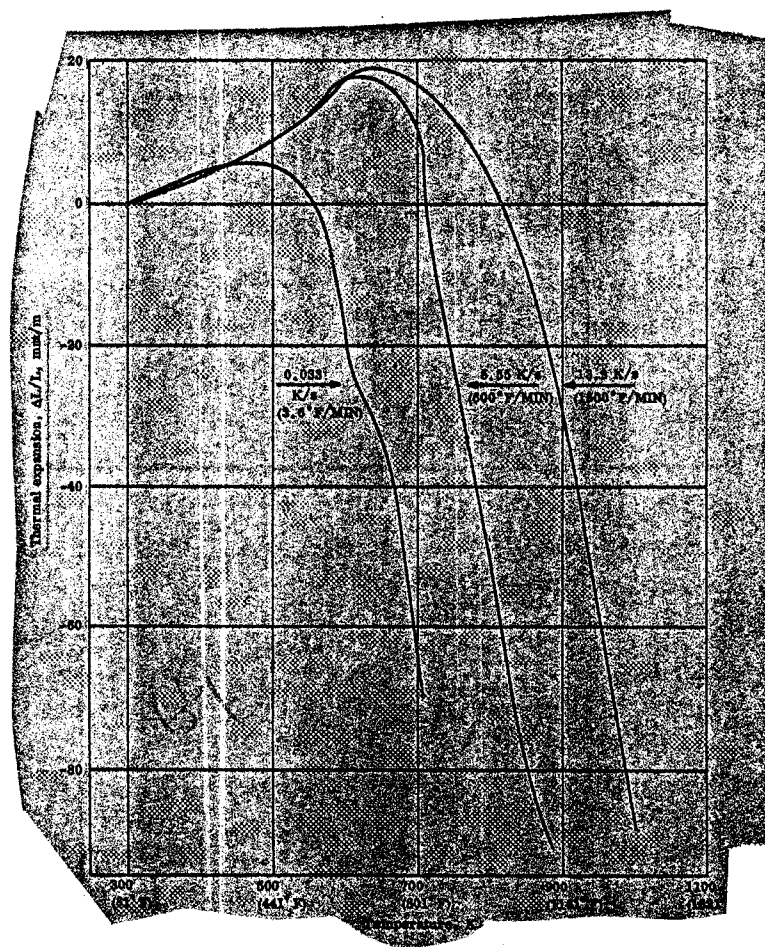


Figure 69. Thermal Expansion of FM 5272, Effect of Heating Rate

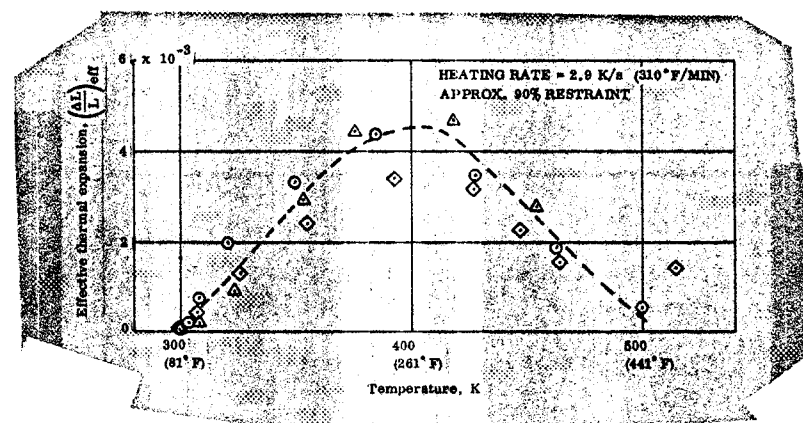


Figure 70. Restrained Expansion of FM 5272, With Lamina, Heating Rate = 2.9 K/s (310 ° F/min) R = 90%

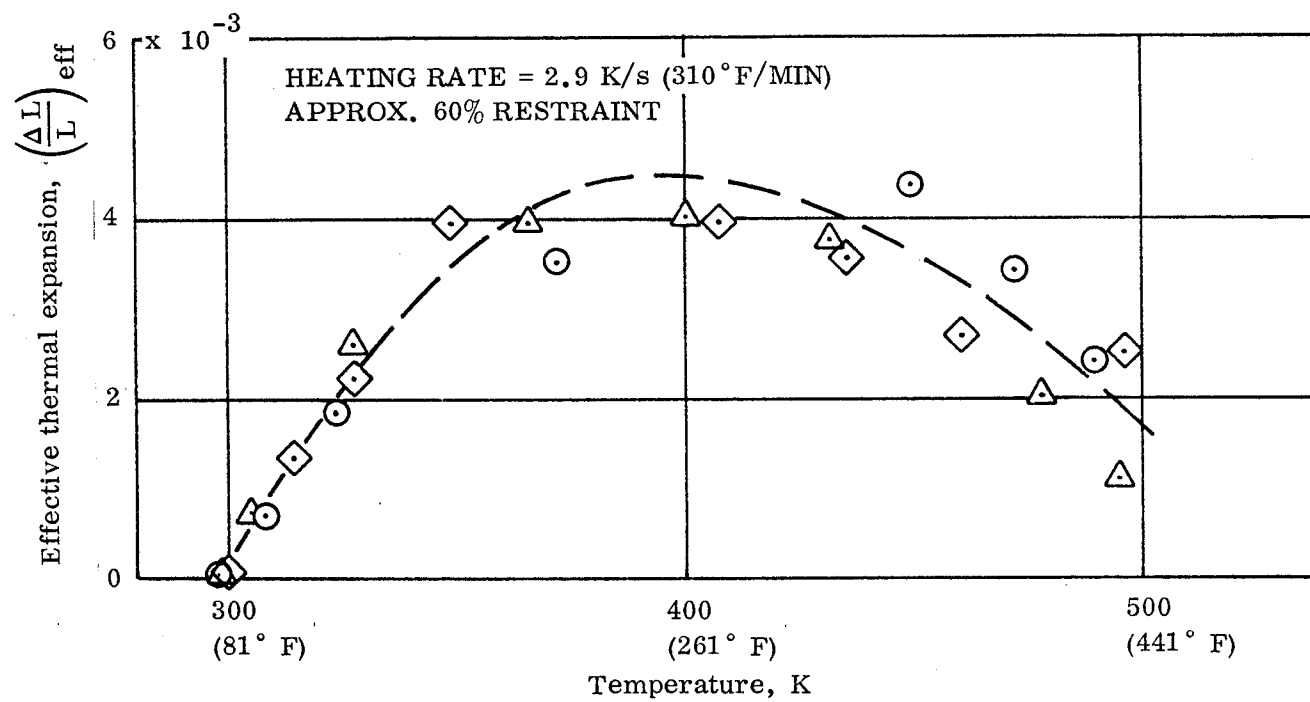


Figure 71. Restrained Expansion of FM 5272, With Lamina
Heating Rate = 5.0 K/s (540° F/Min) R = 90%

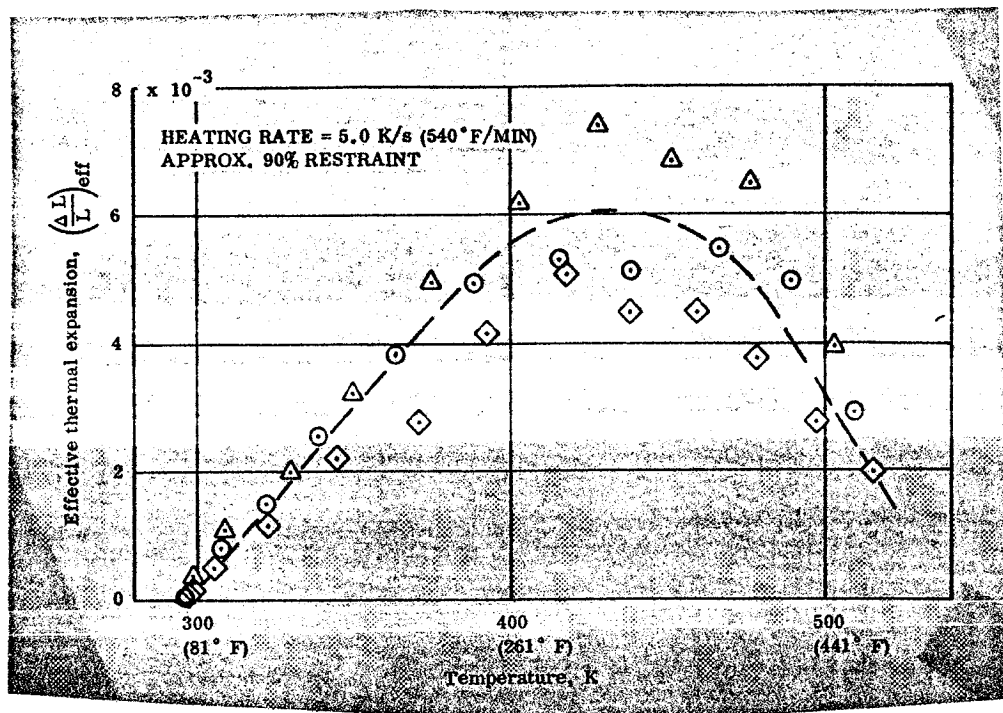


Figure 72. Restrained Expansion of FM 5272, With Lamina, Heating Rate = 5.0 K/s (540° F/min) R = 90%

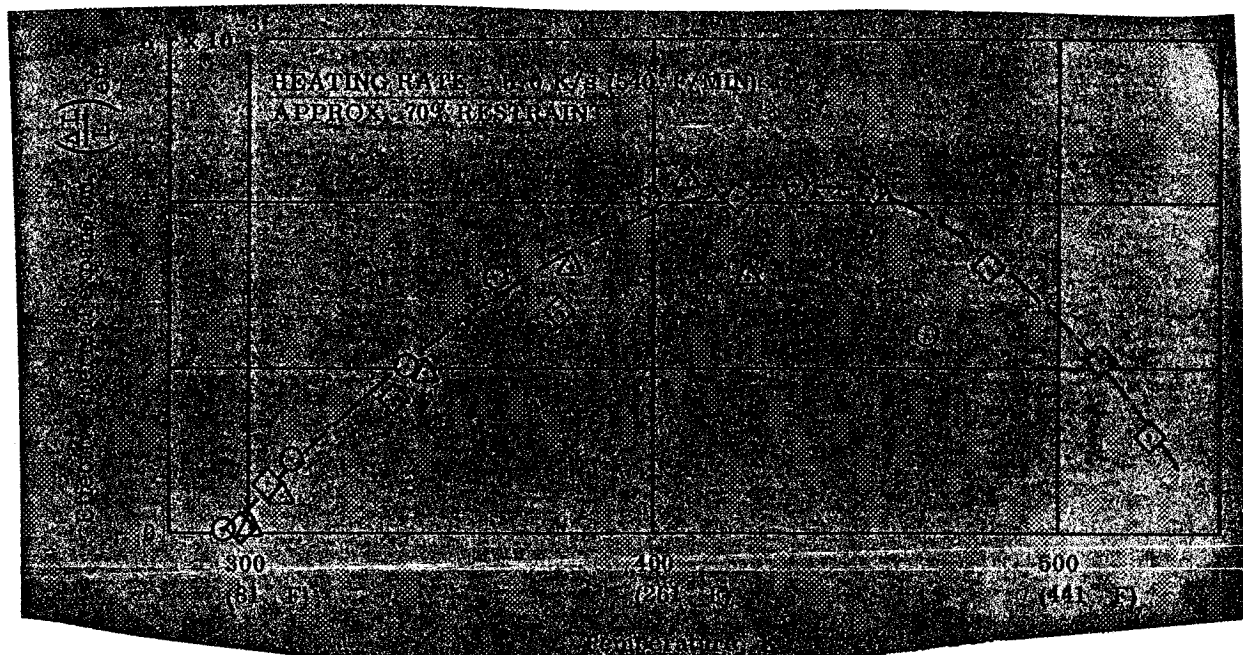


Figure 73. Restrained Expansion of FM 5272, With Lamina, Heating Rate = 5.0 K/s (540° F/min) R = 70%

than was obtained for free expansion at low heating rate. However, in the restrained cases the peaks occur at somewhat lower temperature. It may also be noted that the condition of high restraint plus high heating rate (90 percent and 5 K/s, Figure 72) results in a slightly higher effective expansion. This is similar to the effect seen with MX 2600 in the across laminate direction but the magnitude is much less.

Figures 74 through 79 give the result of the restrained thermal expansion tests in the across laminate direction. Surprisingly, the effective thermal expansions obtained are considerably less than were observed in the free expansion tests at low heating rate and again the peaks occur at lower temperature. In general, the effective thermal expansion obtained in the across laminate direction is very similar to that obtained in the with laminate direction and again it appears that high-restraint coupled with high heating rate can result in a somewhat higher effective thermal expansion.

Figure 80 gives the result of measurements on a thicker walled specimen to check for size effects. The peak expansion is possibly 20 percent greater than was observed with the thin wall specimens under the same conditions but this is actually a rather small difference.

Restrained expansion data are summarized in Figures 81 and 82.

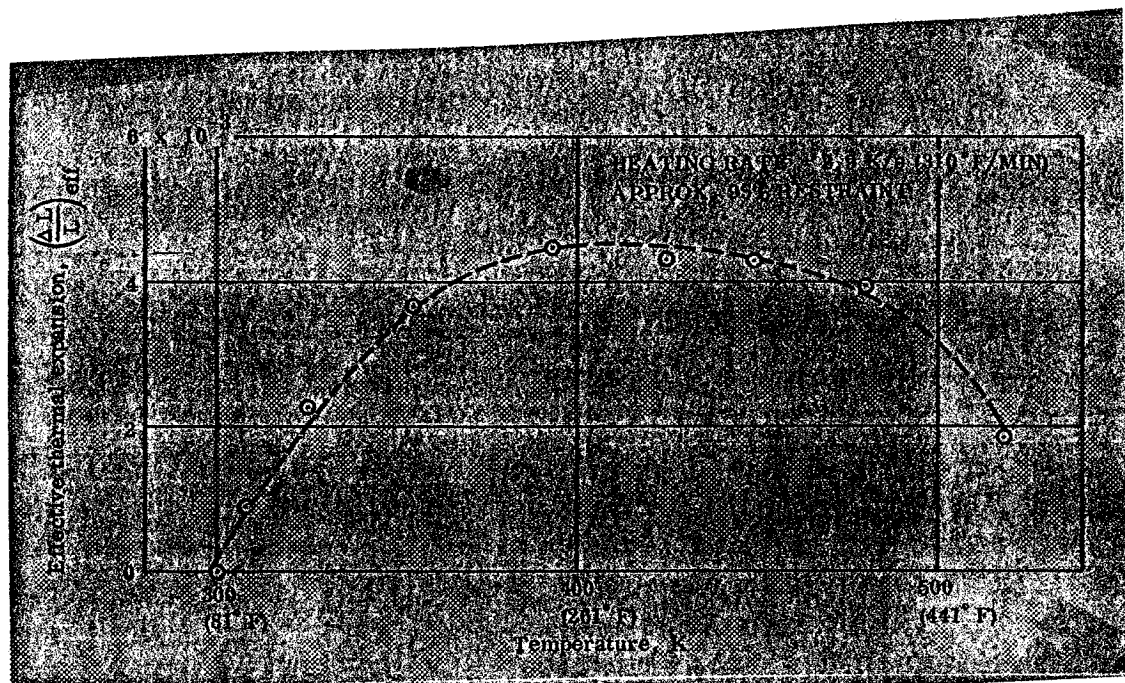


Figure 74. Restrained Expansion of FM 5272, Across Lamina
Heating Rate = 2.9 K/s (310° F/min) R = 95%

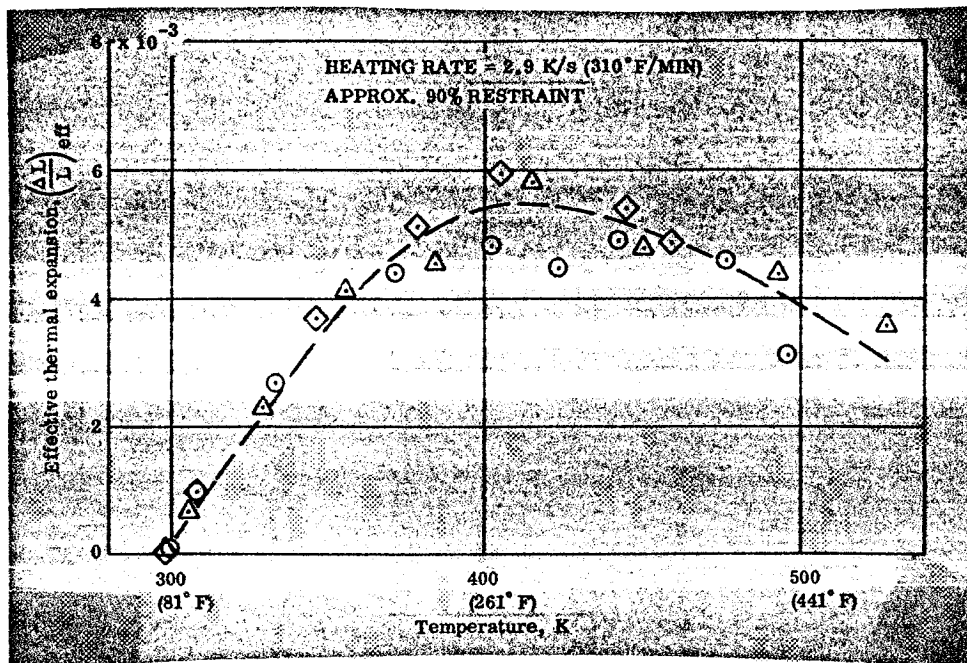


Figure 75. Restrained Expansion of FM 5272, Across Lamina
Heating Rate = 2.9 K/s (310° F/min) R = 90%

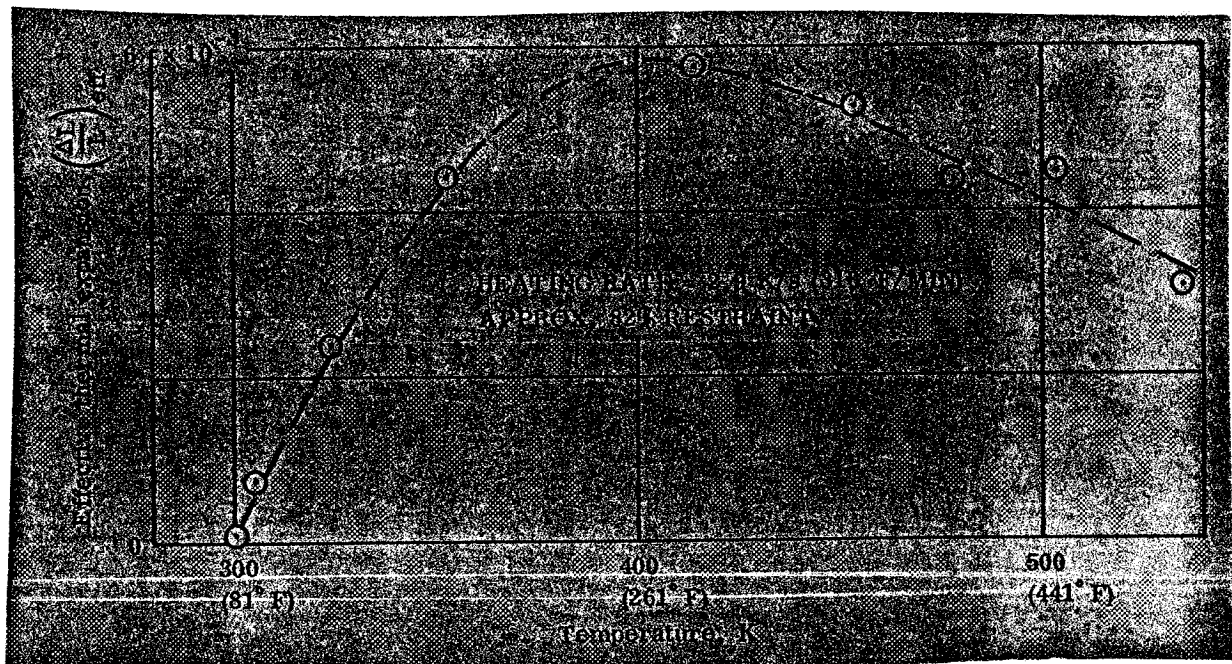


Figure 76. Restrained Expansion of FM 5272, Across Lamina
Heating Rate = 2.9 K/s (310° F/min) R = 82%

Figure 78. Restrained Expansion of FM 5272, Across Lamina
Heating Rate = 5.0 K/s (540° F/min) R = 90%

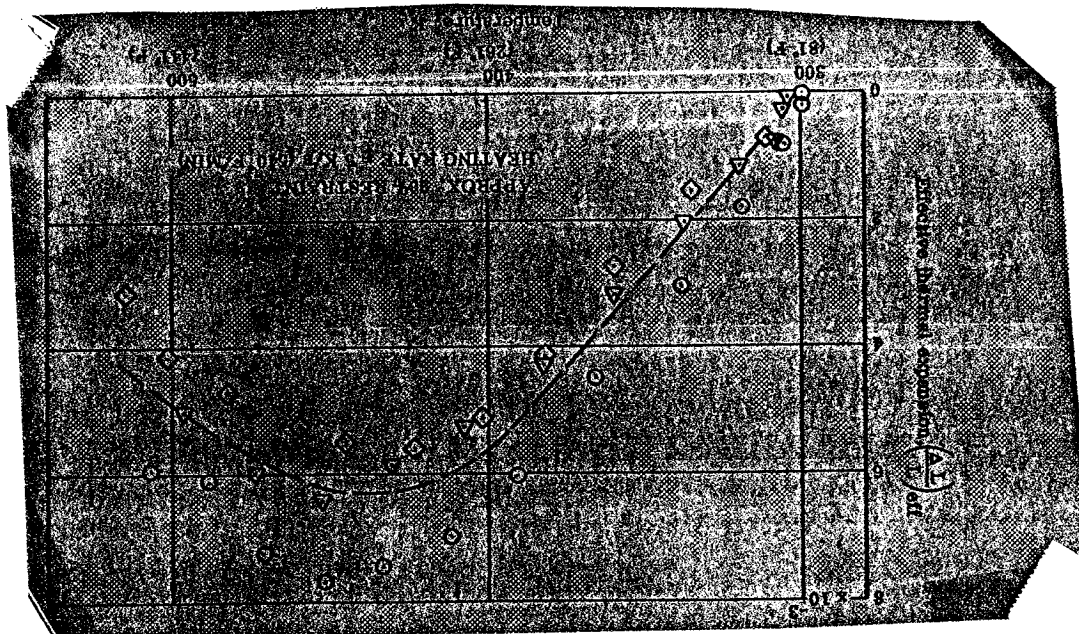
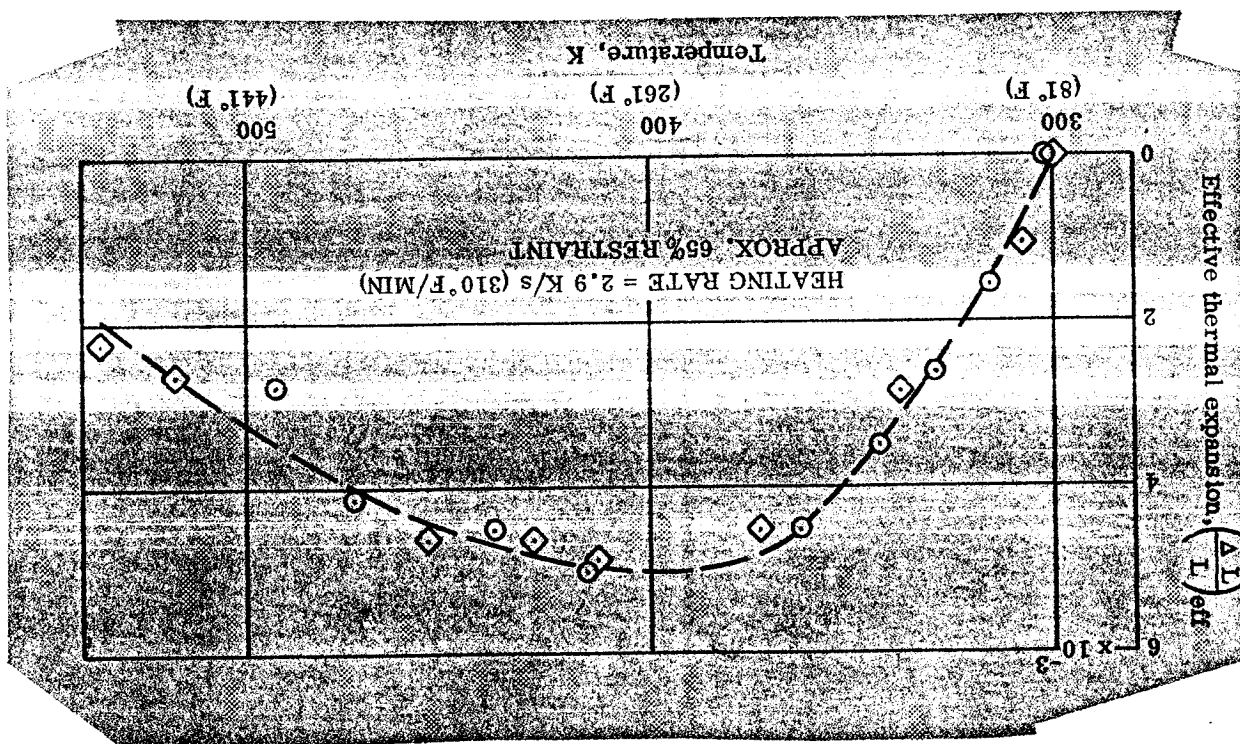


Figure 77. Restrained Expansion of FM 5272, Across Lamina
Heating Rate = 2.9 K/s (310° F/min) R = 65%



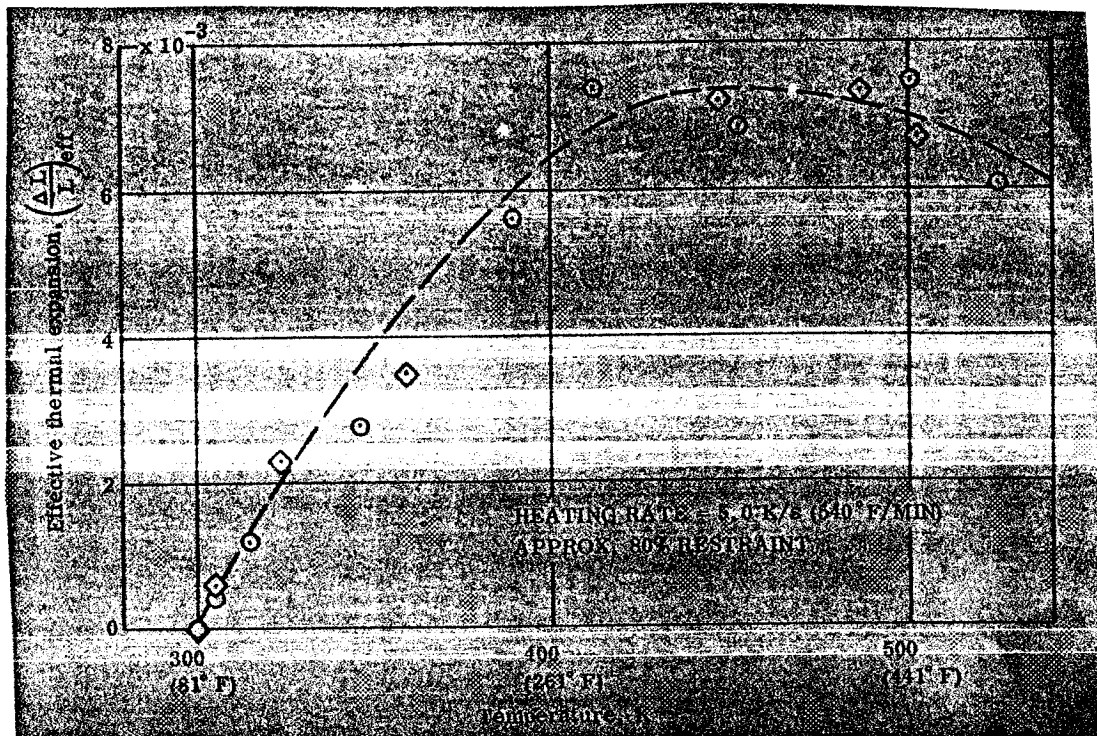


Figure 79. Restrained Expansion of FM 5272, Across Lamina
Heating Rate = 5.0 K/s (540° F/min) R = 80%

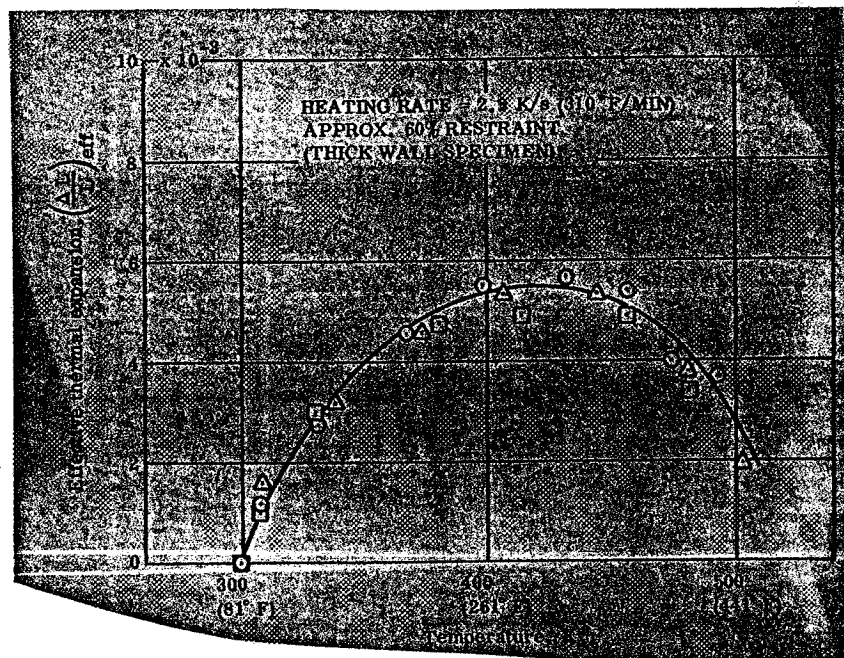


Figure 80. Restrained Expansion Tests on Thick Wall Specimen of
FM 5272 Heating Rate = 2.9 K/s (310° F/min) R = 60%

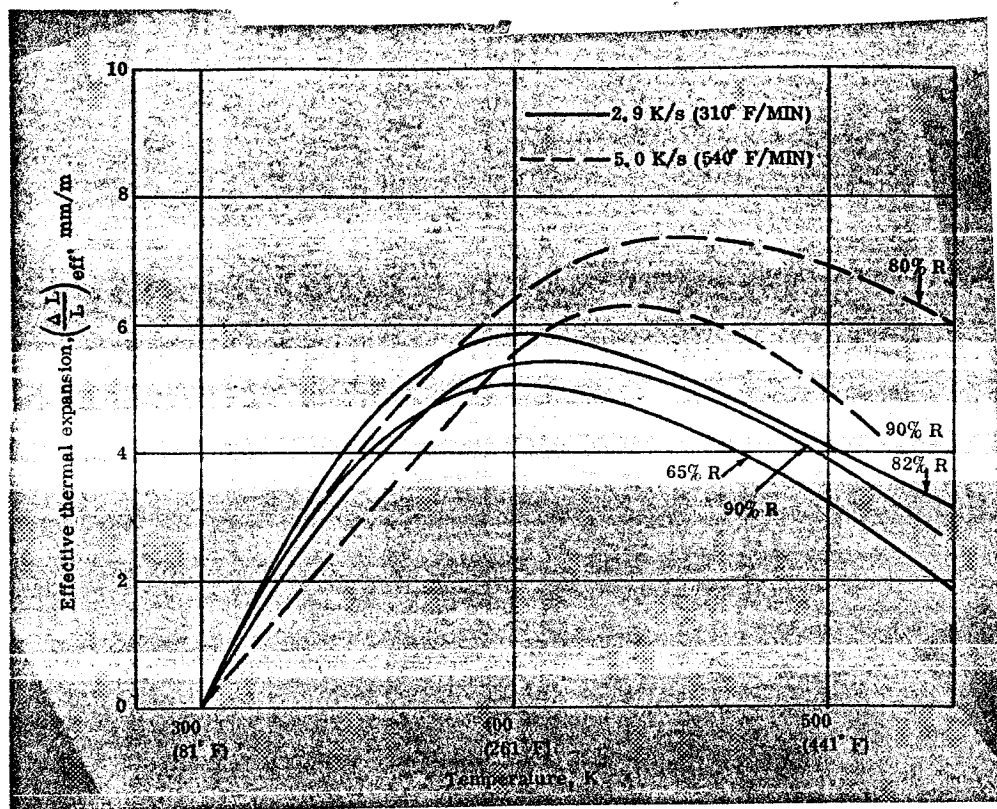


Figure 81. Summary of Restrained Expansion Data, FM 5272, Across Lamina

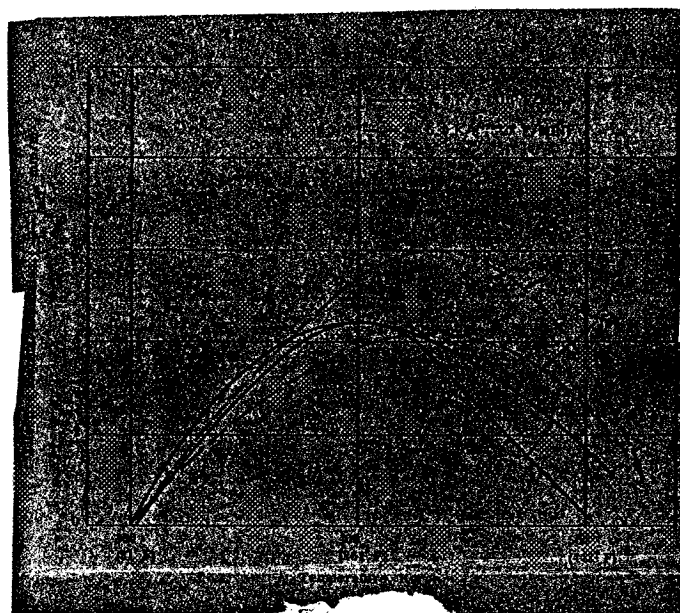


Figure 82. Summary of Restrained Expansion Data, FM 5272, With Lamina

Modulus data obtained during the restrained expansion tests are given in Figures 83 through 95. Just as there appeared to be little difference in the effective thermal expansion with test direction, direction also appears to have little effect on the modulus.

Figure 96 shows a typical charred specimen of FM 5272 after completion of a test. Note the fissures which develop in the surface. This differs greatly from the response of MX 2600 (fig. 44) as no such fissures developed in the silica phenolic. These fissures, and the low density, porous char which forms, may be responsible for the low effective thermal expansion as they provide paths for gases to escape and hence may help to keep stresses low.

Strength measurements on FM 5272. - Initial strength measurements were made by means of flexure tests at room temperature. Results were as follows (with laminate direction):

80.0 MN/m ²
84.9
71.9
81.4
80.7
78.6
Mean = 79.6 MN/m ² (11,500 psi)

With laminate strengths were measured at elevated temperatures by means of tensile tests, the results of which are given in Figure 97. At heating rates of 2.8 and 7.0 K/s the strengths obtained were essentially the same. However, increasing the heating rate to 13.9 K/s resulted in a significant loss of strength. Note that while heating MX 2600 to 700 K resulted in a loss of strength of about 2.5X, a similar temperature rise resulted in a 100X strength loss for the FM 5272.

Transient thermal conductivity of FM 5272 char. - Initially, an attempt was made to produce cellulose phenolic char with the Tandem Gerdien Arc facility, the same means by which the silica phenolic char was produced, but the char produced was very soft and crumbly and mechanically too weak to be machined or instrumented. One other attempt was made to produce char under transient conditions. A muffle furnace was preheated to 1033 K and a sample of cellulose phenolic was inserted in a argon atmosphere. This sample splintered during the charred process. Finally, mechanically sturdy char was produced by programming the furnace up at a rate of 5 K/minute to a temperature of 1033 K with the samples in an argon atmosphere.*

*Although this char would not be representative, it was hoped that an approximate conductivity could be obtained.

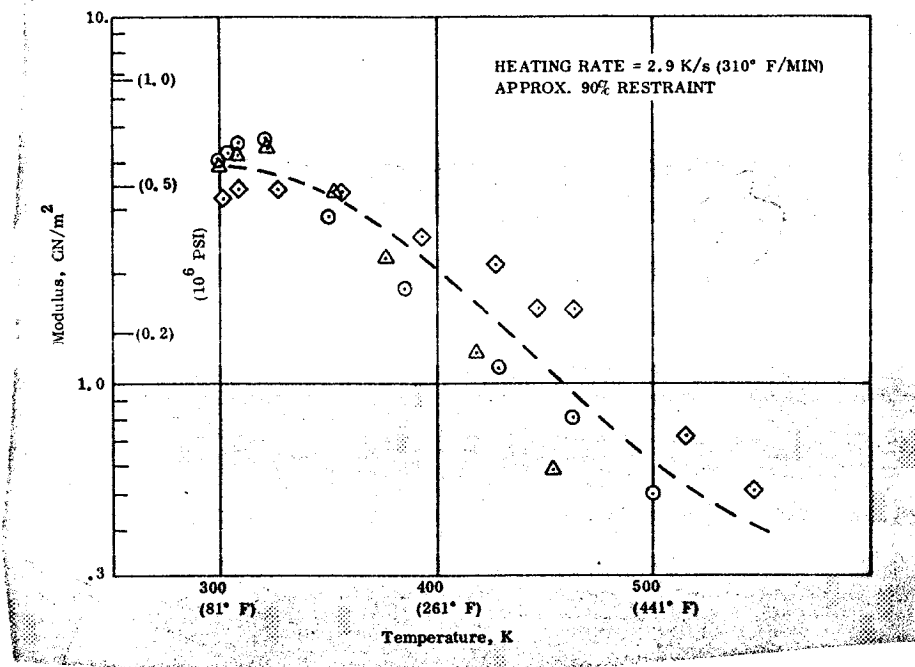


Figure 83. Modulus of Restrained FM 5272, With Lamina
Heating Rate = 2.9 K/s (310° F/min) R = 90%

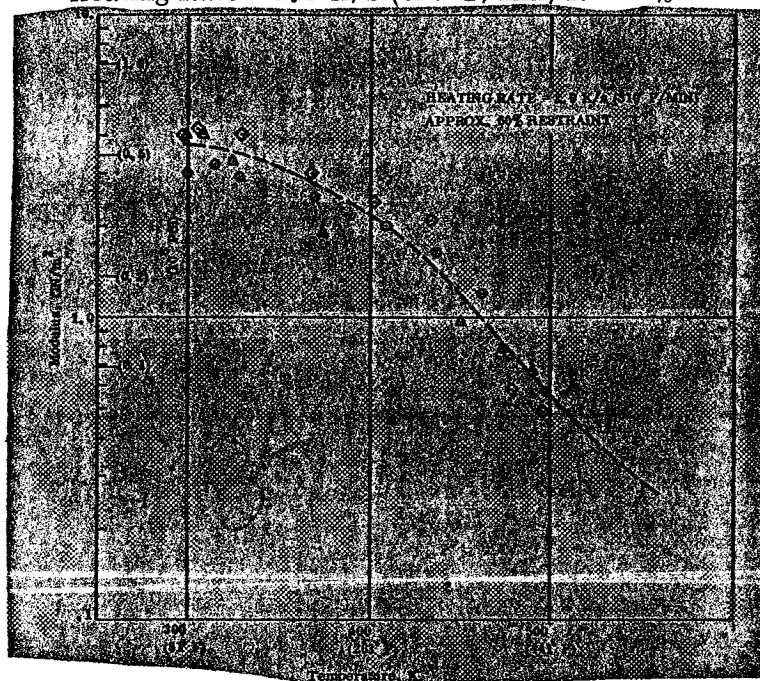


Figure 84. Modulus of Restrained FM 5272, With Lamina
Heating Rate = 2.9 K/s (310° F/min) R = 60%

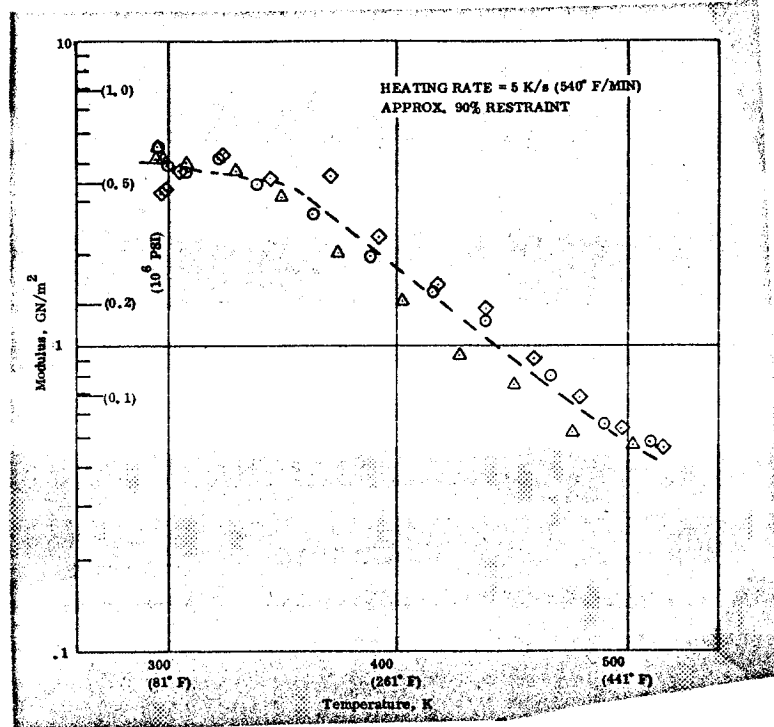


Figure 85. Modulus of Restrained FM 5272, With Lamina
Heating Rate = 5.0 K/s (540° F/min) R = 90%

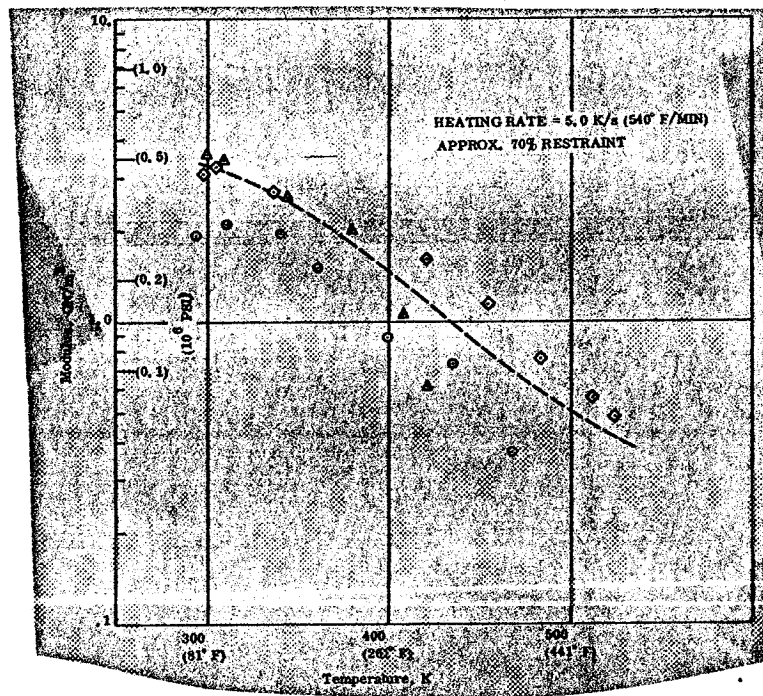


Figure 86. Modulus of Restrained FM 5272, With Lamina
Heating Rate = 5.0 K/s (540° F/min) R = 70%

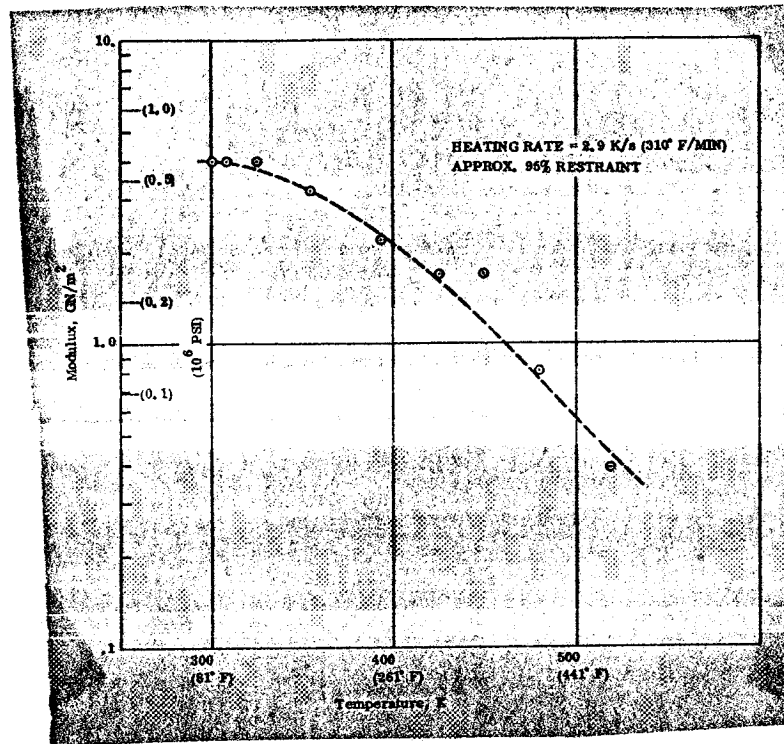


Figure 87. Modulus of Restrained FM 5272, Across Lamina
Heating Rate = 2.9 K/s (310° F/min) R = 95%

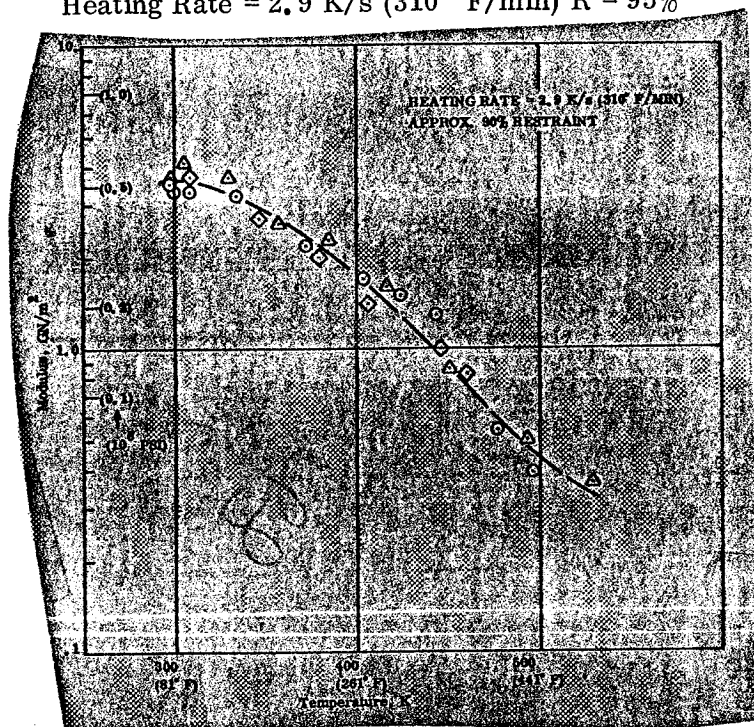


Figure 88. Modulus of Restrained FM 5272, Across Lamina
Heating Rate = 2.9 K/s (310° F/min) R = 90%

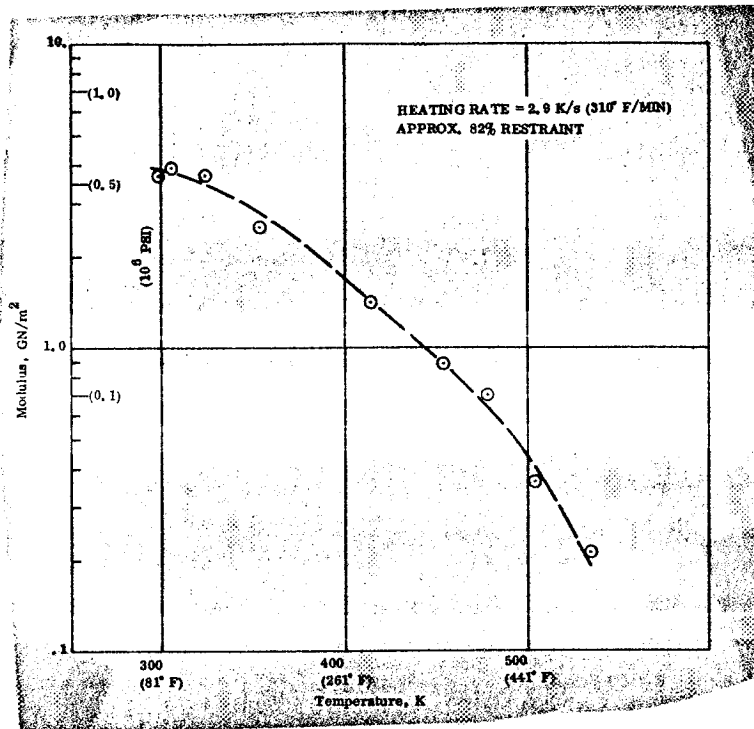


Figure 89. Modulus of Restrained FM 5272, Across Lamina
Heating Rate = 2.9 K/s (310° F/min) R = 82%

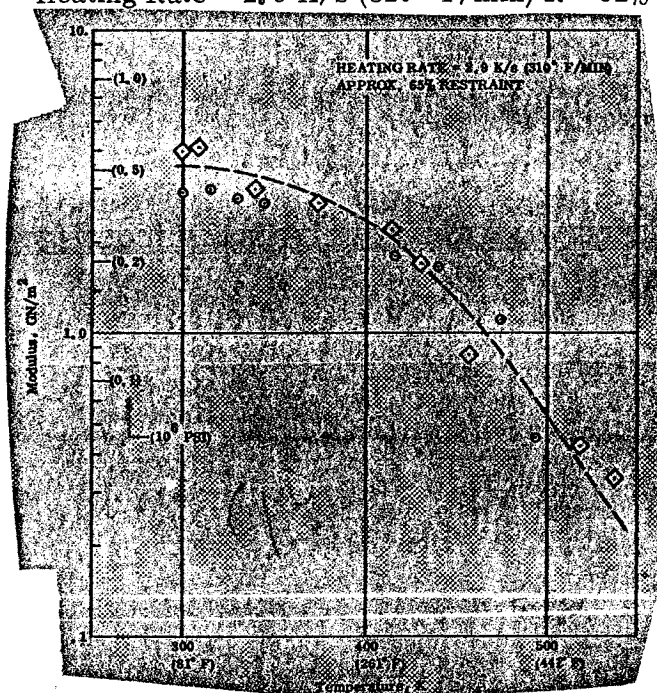


Figure 90. Modulus of Restrained FM 5272, Across Lamina
Heating Rate = 2.9 K/s (310° F/min) R = 65%

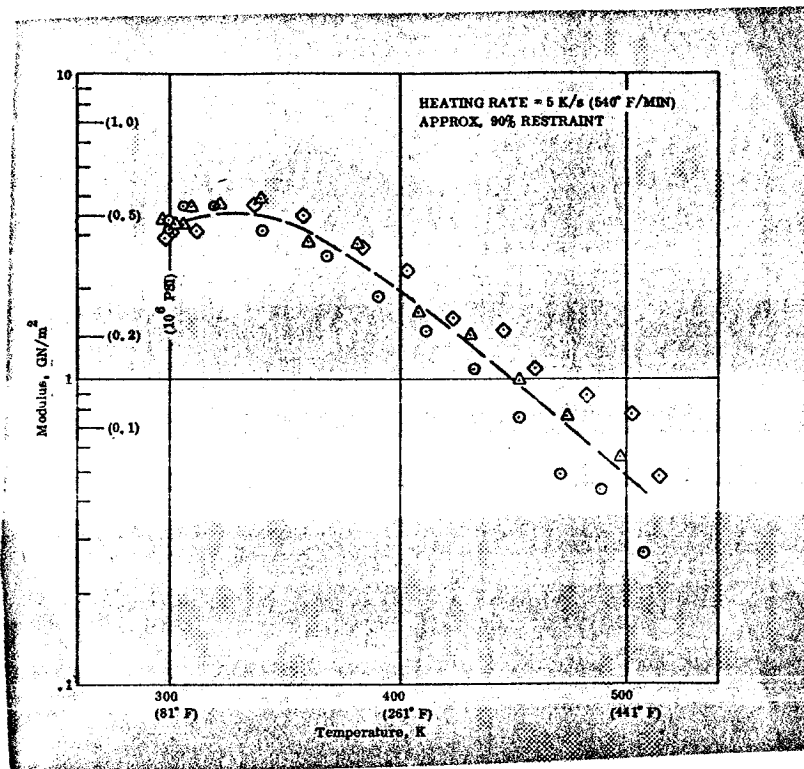


Figure 91. Modulus of Restrained FM 5272, Across Lamina,
Heating Rate = 5.0 K/s (540° F/min) R = 90%

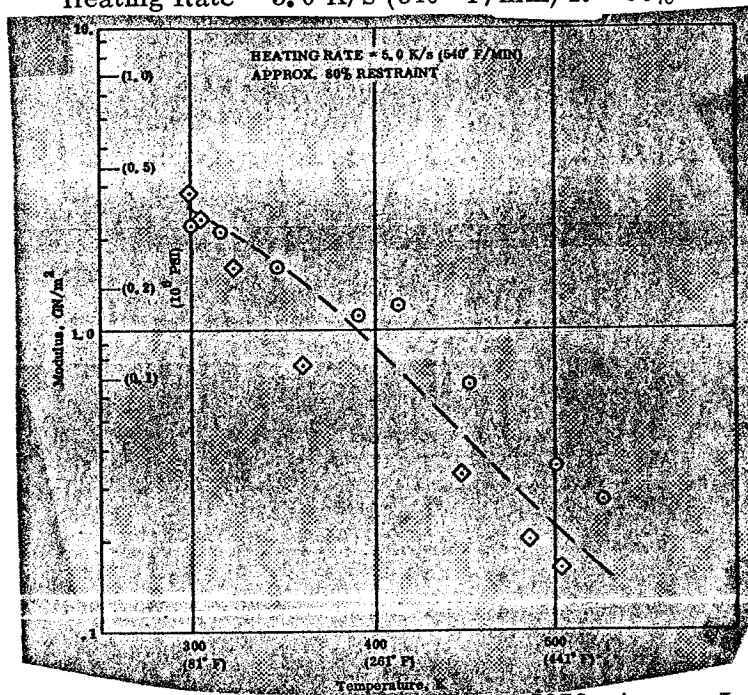


Figure 92. Modulus of Restrained FM 5272, Across Lamina,
Heating Rate = 5.0 K/s (540° F/min) R = 80%

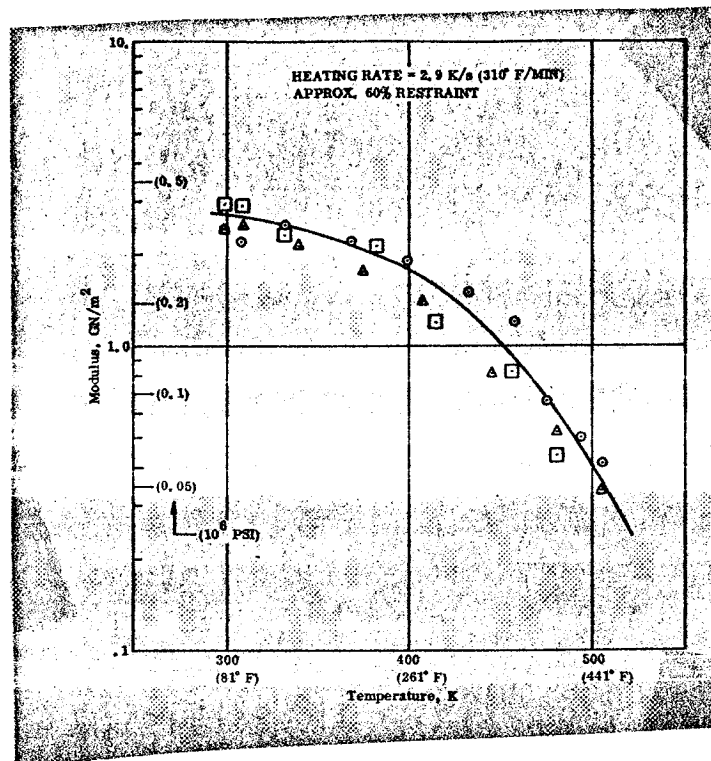


Figure 93. Modulus of Restrained FM 5272, With Lamina, Thick Wall Specimen
Heating Rate = 2.9 K/s (310° F/min) R = 70%

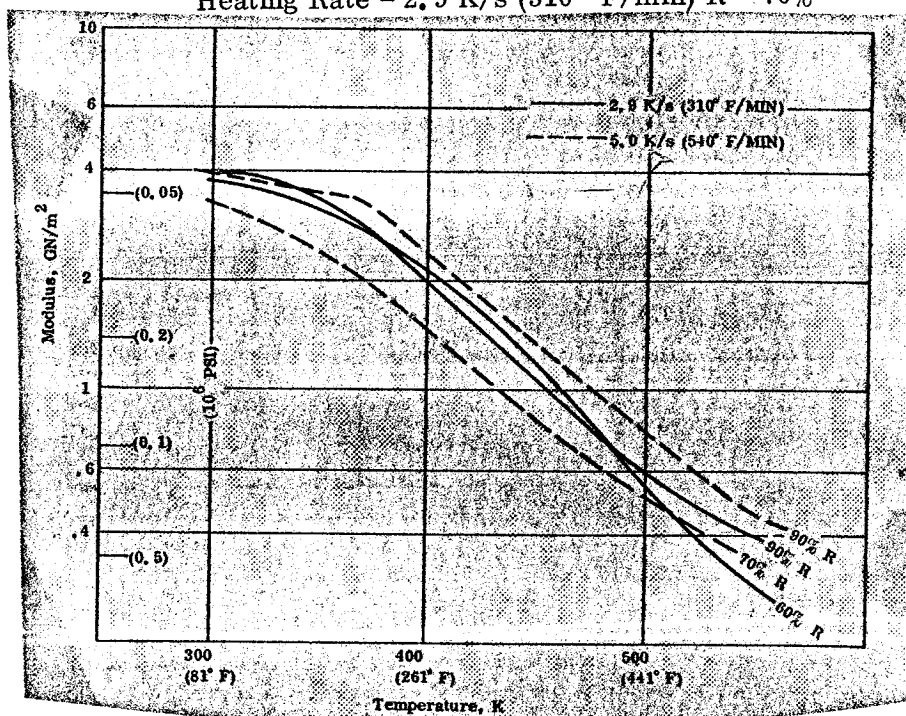


Figure 94. Summary of Modulus Data, FM 5272, With Lamina

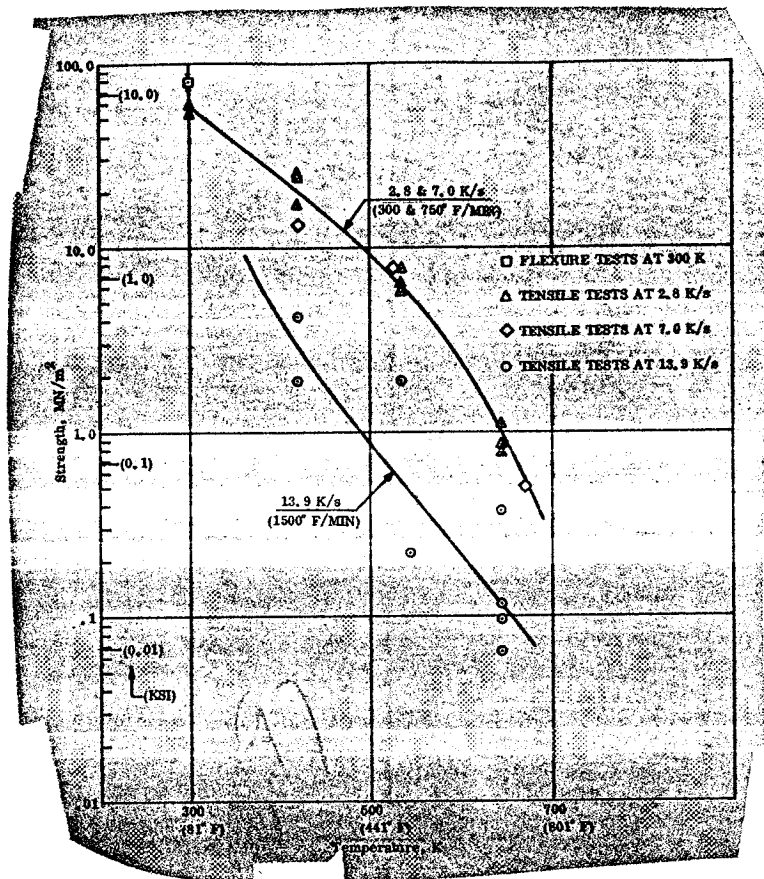


Figure 97. Strength Measurements, FM 5272 With Lamina

The samples were carefully machined and instrumented, and tested utilizing the Linde torch as a heat source. Initial effort consisted of testing a specimen at a heat flux 10^7 watts/meter² but it was found that the flow of the torch eroded the sample before any appreciable heat propagated into the specimen. Attempts were then made to test three more specimens at successively lower heat fluxes, down to a heat flux level of 2.5×10^6 watts/meter², with the same result. The material was not mechanically strong enough to survive heating with this type of heat source. The ideal type of heating source for fragile samples like this char, would be a high power CO₂ laser, which would produce no mechanical erosion. Unfortunately, as stated before, one was not available. However, the above indicates that the char would not survive in any area of a rocket motor where significant gas flow occurred.

Measurements on Carbitex 700

Density measurements on several specimens of the Carbitex 700 panel used on this program gave a density of 1510 kg/m³. This is somewhat higher than the value of 1420 indicated in the manufactures literature (The Carborundum Co., Bulletin No. A-2213-D).

Free thermal expansion of Carbitex 700. - Thermal expansion data for Carbitex 700, obtained under slow heating conditions (0.033 K/s) with the Brinkmann dilatometer are given in Figures 98 and 99.

With laminate thermal expansion data which were obtained under fast heating conditions are shown in Figures 100 and 101. The data given in Figure 100 were obtained at a rate of 13.9 K/s (1500 F/min) and the data in Figure 101 at 27.8 K/s (3000° F/min). Each of the high heating rate curves represents measurements on three long (5.08 cm) and three short (1.27 cm) specimens, the measurements on each length being averaged and the difference taken to eliminate and effects as described in the section on test methods. The curve shown in Figure 100 is practically identical to the slow heating data (Figure 99) as shown in Figure 102. The curve obtained at the highest heating rate is slightly lower at high temperature but the difference is not significant. Thus the expansion is independent of the heating rate. In view of the absence of any heating rate dependence of the ATJ, this result was expected.

Restrained thermal expansion of Carbitex 700. - The results of restrained expansion tests on Carbitex 700 in the with laminate direction are given in Figures 103, 104 and 105, where the effective thermal expansion is plotted as a function of temperature. The data given in Figures 103 and 104 are both for 55 percent restraint but the former is for a heating rate of 13.9 K/s (1500° F/min) and the latter for a rate of 27.8 K/s (3000° F/min). The result was essentially the same, again indicating no rate effect. If these data are compared with the data given in Figure 99 (slow heating, free expansion), it is seen that $(\Delta L/L)_{\text{eff}}$ runs slightly low at the higher temperatures (Fig. 106). As noted earlier, this may be the result of curvature (i. e. , non-linearity) of the stress-strain relation. It is also seen that the higher level of restraint (hence higher stress) results in a somewhat lower effective thermal expansion. This is in agreement with the results obtained on ATJ.

Modulus measurements from small cyclic loads imposed during restrained expansion are shown in Figure 107. These moduli at room temperature are somewhat lower than the with laminate moduli obtained from room temperature flexure tests. Flexure tests (3 point loading) yielded the following modulus data:

10.2 GN/m ²
8.9
9.9
11.0
10.5
12.3
11.6
<hr/>
Mean 10.6 GN/m ² (1.54 x 10 ⁶ psi)

This is roughly 10 percent higher than the starting moduli from the restrained expansion tests, but the latter are essentially compression moduli and, for some reason, compression moduli for graphitics seem to run somewhat lower than the tensile moduli.

Compressive stress-strain of Carbitex 700. - In view of the lack of any heating rate sensitivity of the Carbitex 700, a number of compressive stress-strain tests were conducted rather than additional restrained expansion tests as it appeared that more of the latter tests would provide no additional information. As explained in an earlier section of this report, these tests were not conducted to failure because of the high risk of damage to the apparatus. The resultant compression data are given in Figures 108 and 109 and in Table 1. According to the manufacturer, the compressive strengths at room temperature are:

With laminate: 41.4 MN/m^2 (6000 psi)

Across laminate: 103.5 MN/m^2 (15,000 psi)

However, in some preliminary experiments in connection with the set-up of these tests, one of the with laminate specimens failed at a strain of 0.0045 m/m. Because of this it appeared that to test to higher strains was a high risk situation which had to be avoided. In addition, the WL thermal expansion is only about 0.005 m/m at the highest temperature available (1900 K) so that it would appear that for thermal analyses the portion of the stress-strain curve up to this strain would be of the greatest interest.

Strength measurements on Carbitex 700. - Preliminary flex strength measurements on Carbitex 700 gave the following result (with laminate direction strength):

54.5 MN/m^2

53.8

56.6

63.1

58.6

60.0

56.6

Mean: 57.5 MN/m^2 (8350 psi)

This result is in good agreement with the flex strength of 62 MN/m^2 (9000 psi) given in the manufacturer's literature.

The results of with laminate tensile measurements at elevated temperatures are given in Table 2 for two heating rates.

TABLE 1. COMPRESSIVE MODULUS OF CARBITEX 700 (GN/m²)

Temperature	With Lamina	Across Lamina
300 K (81° F)	6.2	1.67
	6.3	1.77
	6.3	1.72 (0.25)*
	6.4	
	6.4 (0.93)*	
1200 K (1701° F)	7.4	1.55
	7.7	1.65
	7.8	1.60 (0.23)
	7.6 (1.10)	
1400 K (2061° F)	5.75	1.47
	5.85	1.57
	5.80 (0.84)	1.52 (0.22)
1600 K (2421° F)	6.6	1.55
	6.8	1.65
	6.7 (0.97)	1.75
		1.65 (0.24)
1800 K (2781° F)	6.4	1.40
	6.6	1.44
	6.5 (0.94)	1.42 (0.21)

* - (10⁶ psi)

It is seen that there is no apparent effect due to heating rate or to temperature over the range of 1370 K to 1920 K. It may also be noted that these values run somewhat higher than the value of 38.0 MN/m² (5500 psi) reported by the manufacturer (Bulletin No. A-2213-D).

Transient thermal conductivity of Carbitex 700. - The specimens were instrumented with a thermocouple spacing of 0.15 cm and were tested at the Hyperthermal arc facility. The resultant data is shown in Figures 110 through 112. The variation in conductivity between the with laminate and across laminate directions is what would be expected of a laminate material. Also, the trend of the conductivity to decrease with increasing temperature is what is expected of a graphite type material. The data spread in the across grain direction is normal, but not so in the with grain direction. The reason for

TABLE 2. TENSILE STRENGTH OF CARBITEX 700, WITH LAMINATE (MN/m²)

Heating Rate K/s	Temperature		
	1370 K	1650 K	1920 K
13.9 (1500 F/Min)	47.2	45.9	40.0
13.9 (1500 F/Min)	45.3	46.0	41.4
13.9 (1500 F/Min)	<u>45.9</u>	<u>45.9</u>	<u>45.9</u>
Mean:	46.1 (6.70)	45.9 (6.65)	42.4 (6.15 KSI)
27.8 (3000 F/Min)	42.1	47.5	48.9
27.8 (3000 F/Min)	45.4	46.2	47.2
27.8 (3000 F/Min)	<u>47.7</u>	<u>47.2</u>	<u>46.6</u>
Mean:	45.1 (6.55)	47.0 (6.80)	47.6 (6.90 KSI)
Overall Mean:	45.6 (6.60)	46.5 (6.75)	45.0 (6.55 KSI)

this unusual spread is believed to be as follows: in the with grain direction, there are high conductive fibers which are lying in a less conductive media and are aligned in the direction of heat flow. This would give rise to a non-uniform temperature distribution in a plane perpendicular to the direction of heat flow. Simply stated, the heat will flow down the fibers faster than through the matrix. Since we are measuring the temperature almost at a point (because of the miniature thermocouple) and are not obtaining an average over the plane, the apparent temperature distribution can be something other than realistic. Hence, anomalies in the computed thermal conductivity would result. In the across laminate direction, this would not happen because all of the highly conductive fibers would be perpendicular to the direction of heat flow.

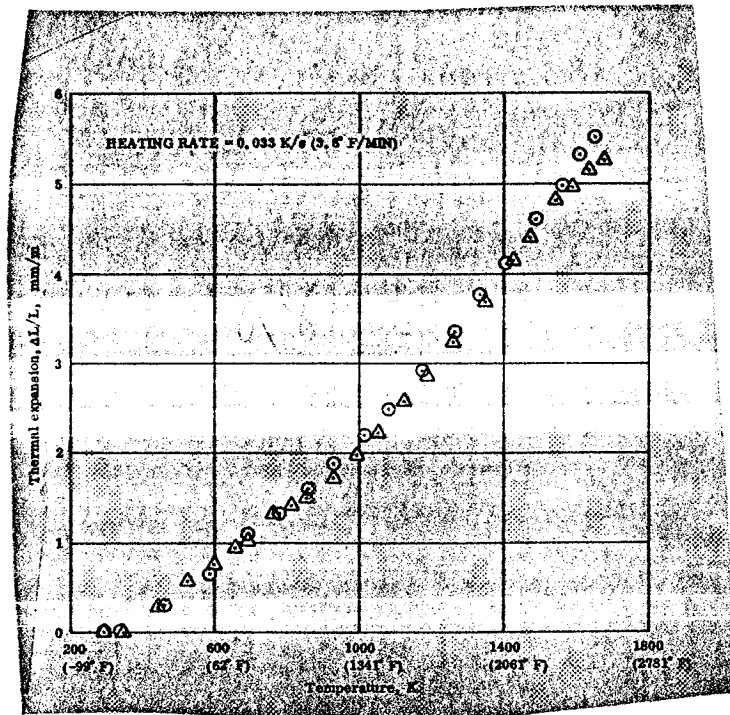


Figure 98. Thermal Expansion of Carbitex 700 Across Lamina, 0.033K/s (3.6° F/min)

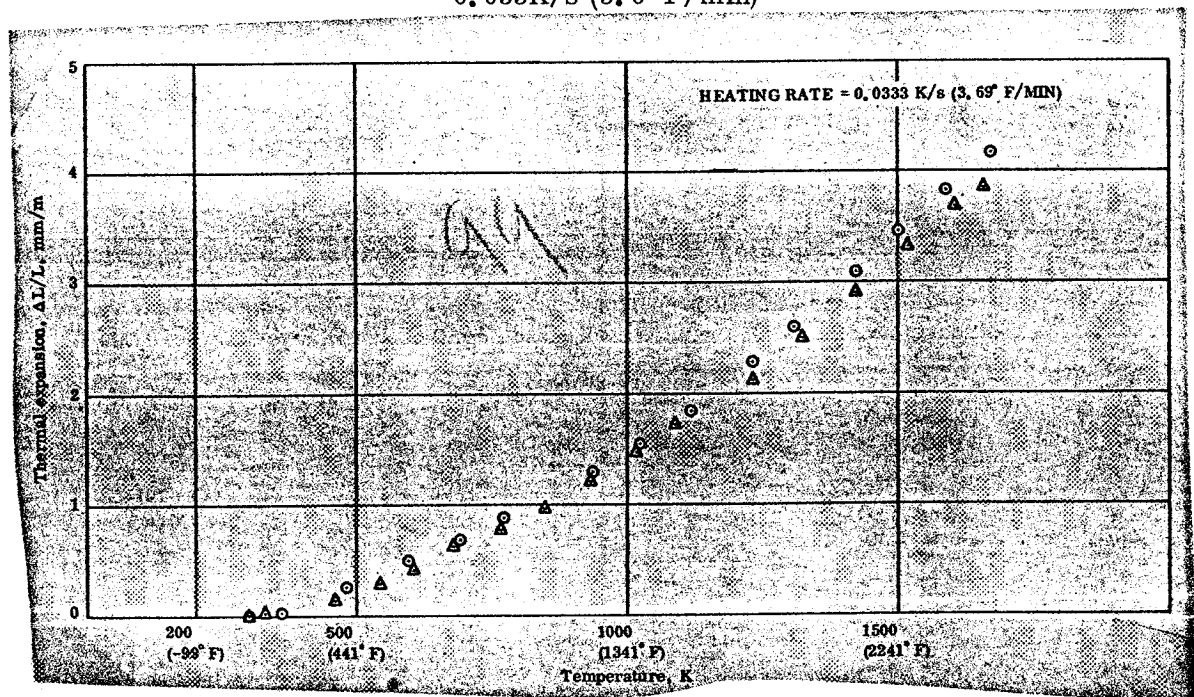


Figure 99. Thermal Expansion of Carbitex 700 With Lamina, 0.033K/s (3.6° F/min)

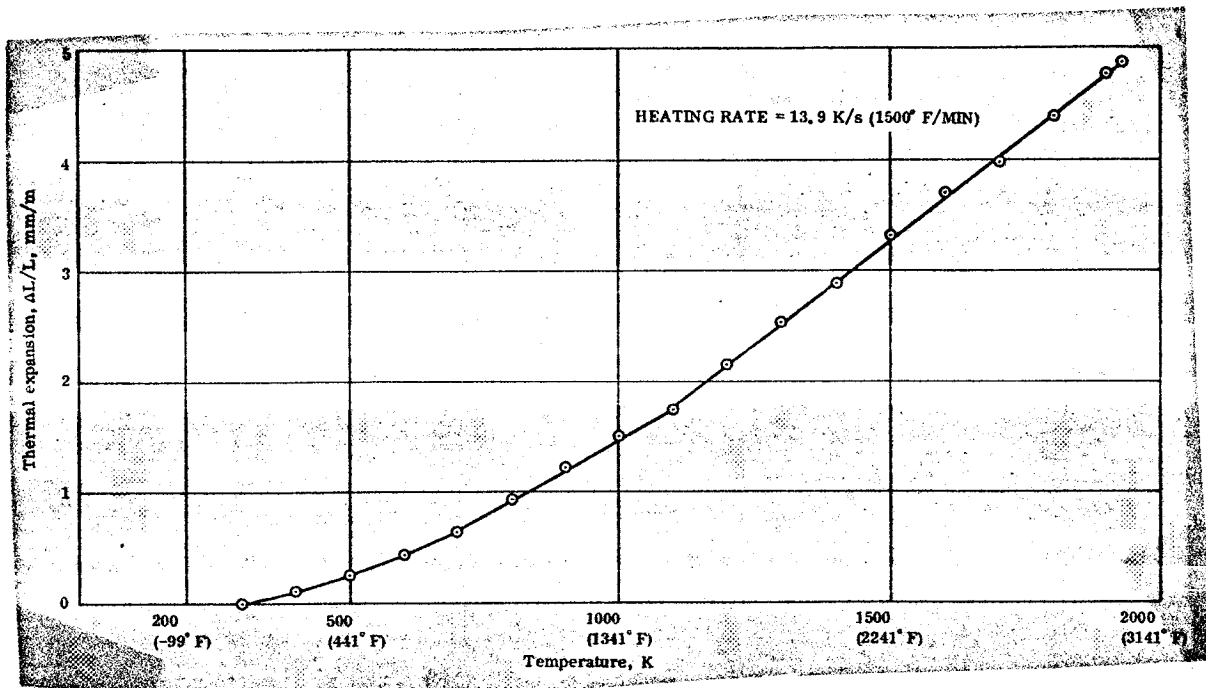


Figure 100. Thermal Expansion of Carbitex 700 With Lamina, 13.9 K/s (1500° F/min)

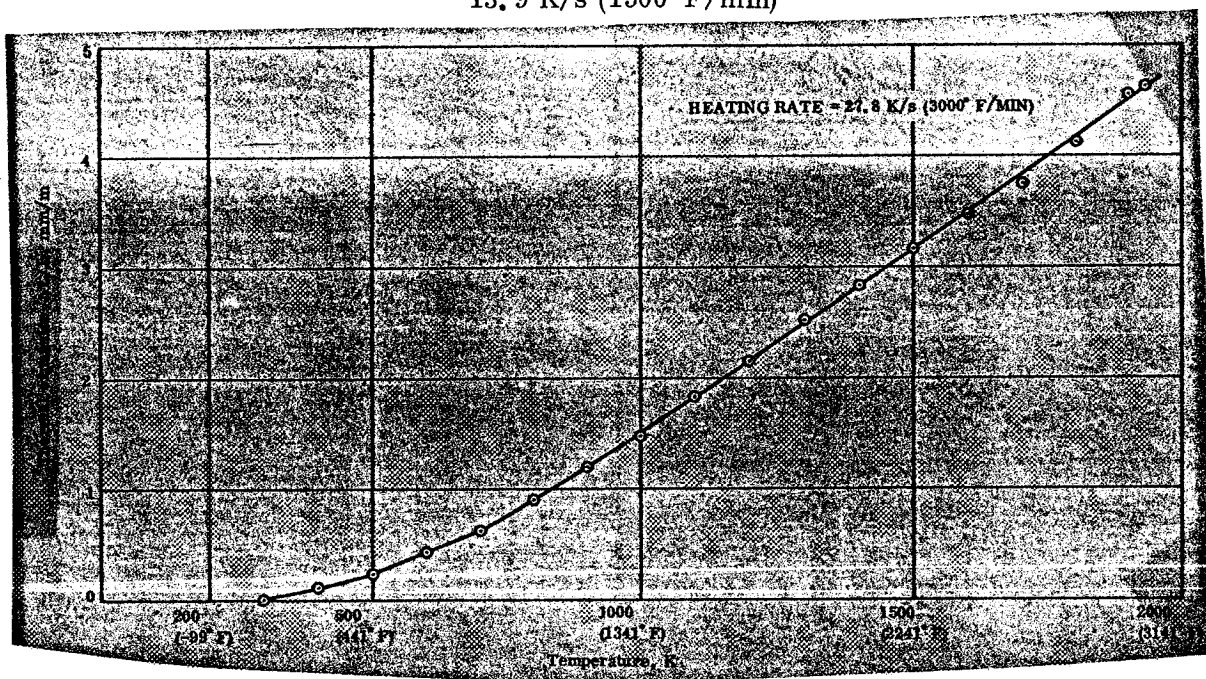


Figure 101. Thermal Expansion of Carbitex 700 With Lamina, 27.8 K/s (3000° F/min)

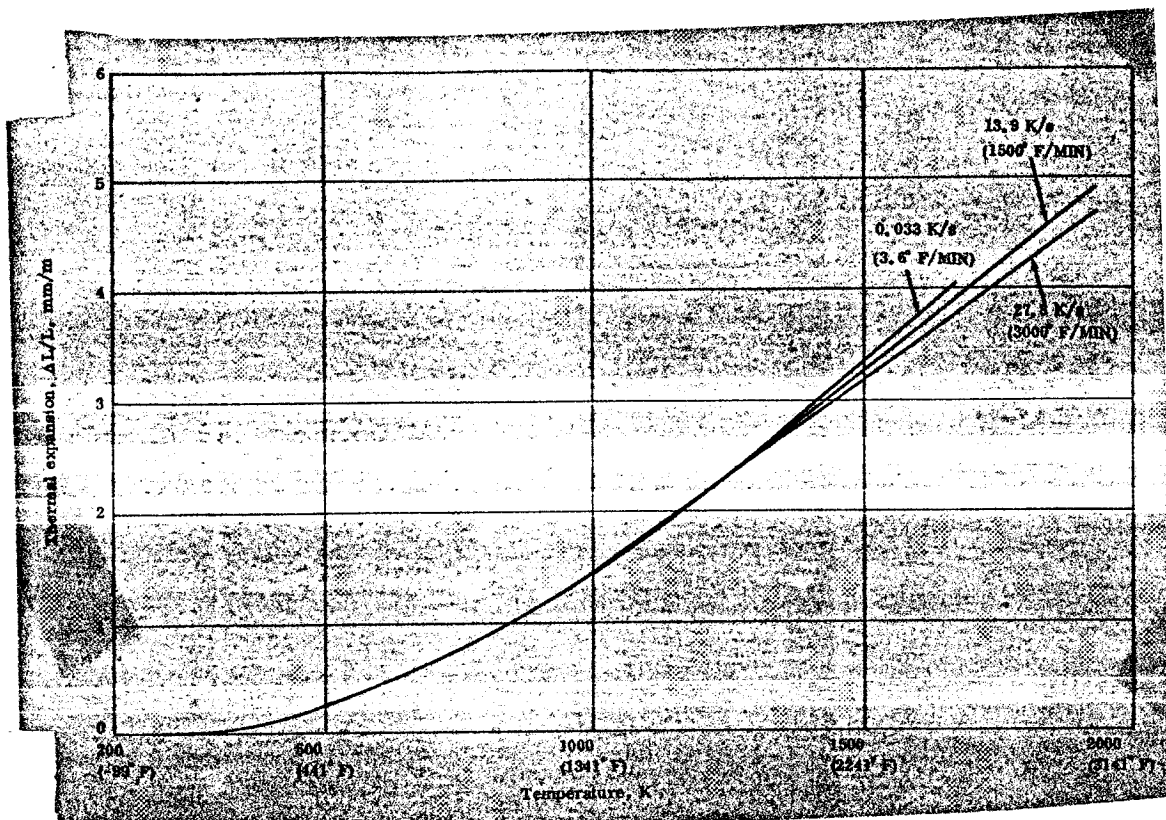


Figure 102. Summary of Free Thermal Expansion Data, Carbitex 700, With Lamina

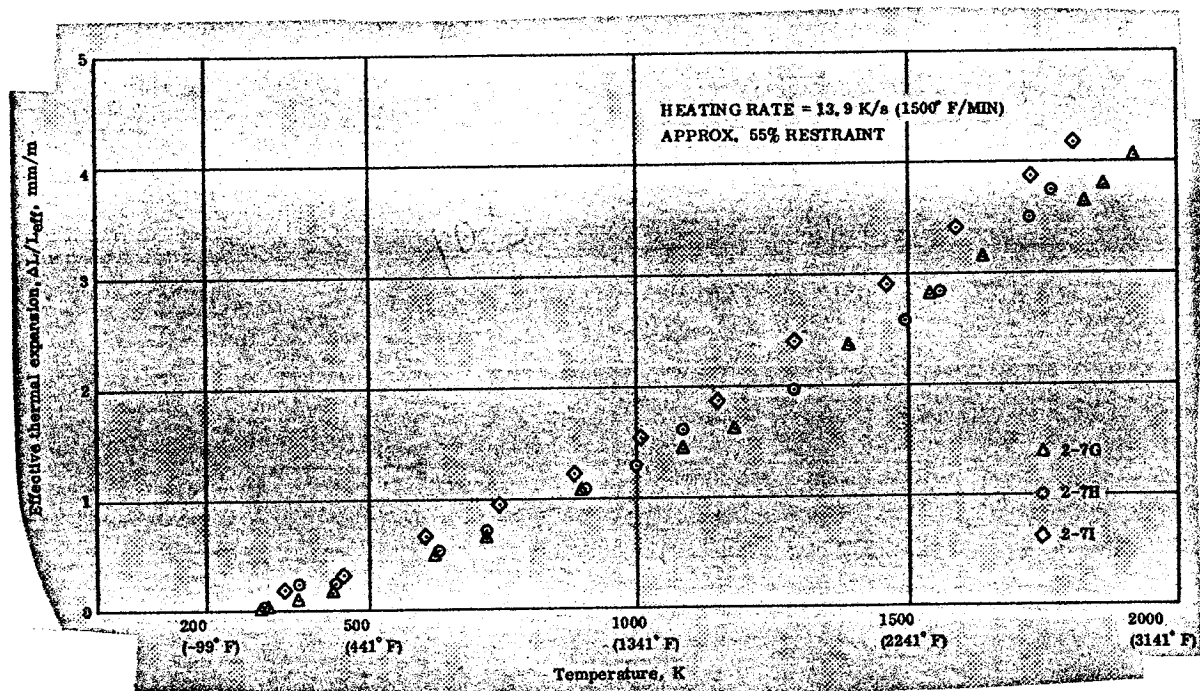


Figure 103. Restrained Expansion of Carbitex 700, With Lamina
Heating Rate = 13.9 K/s (1500° F/min) R = 55%

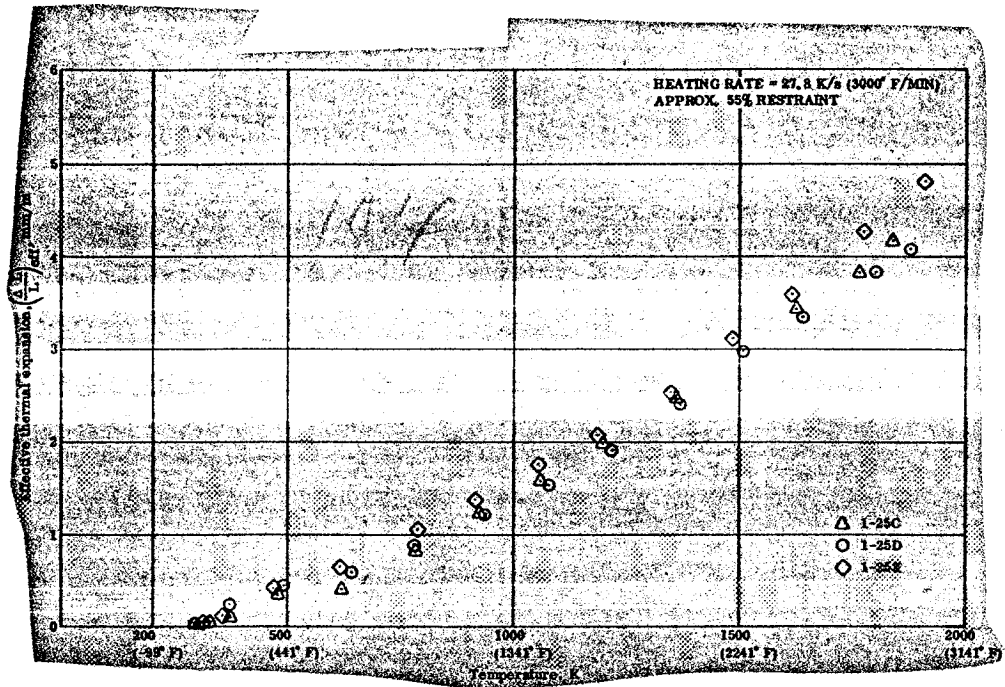


Figure 104. Restrained Expansion of Carbitex 700, With Lamina
Heating Rate = 27.8 K/s (3000° F/min) R = 55%

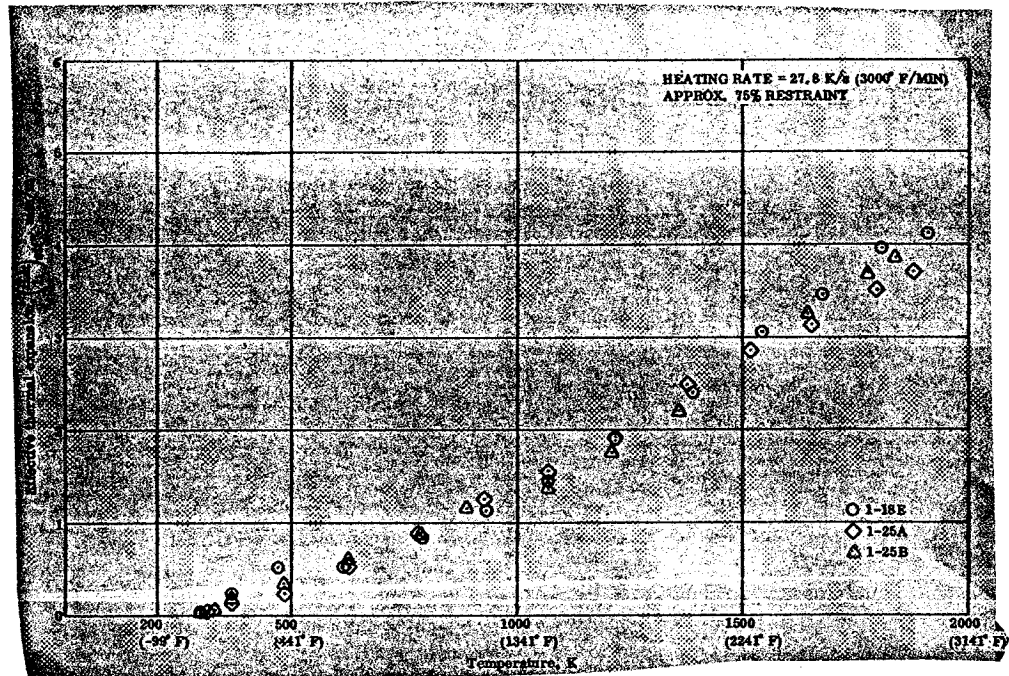
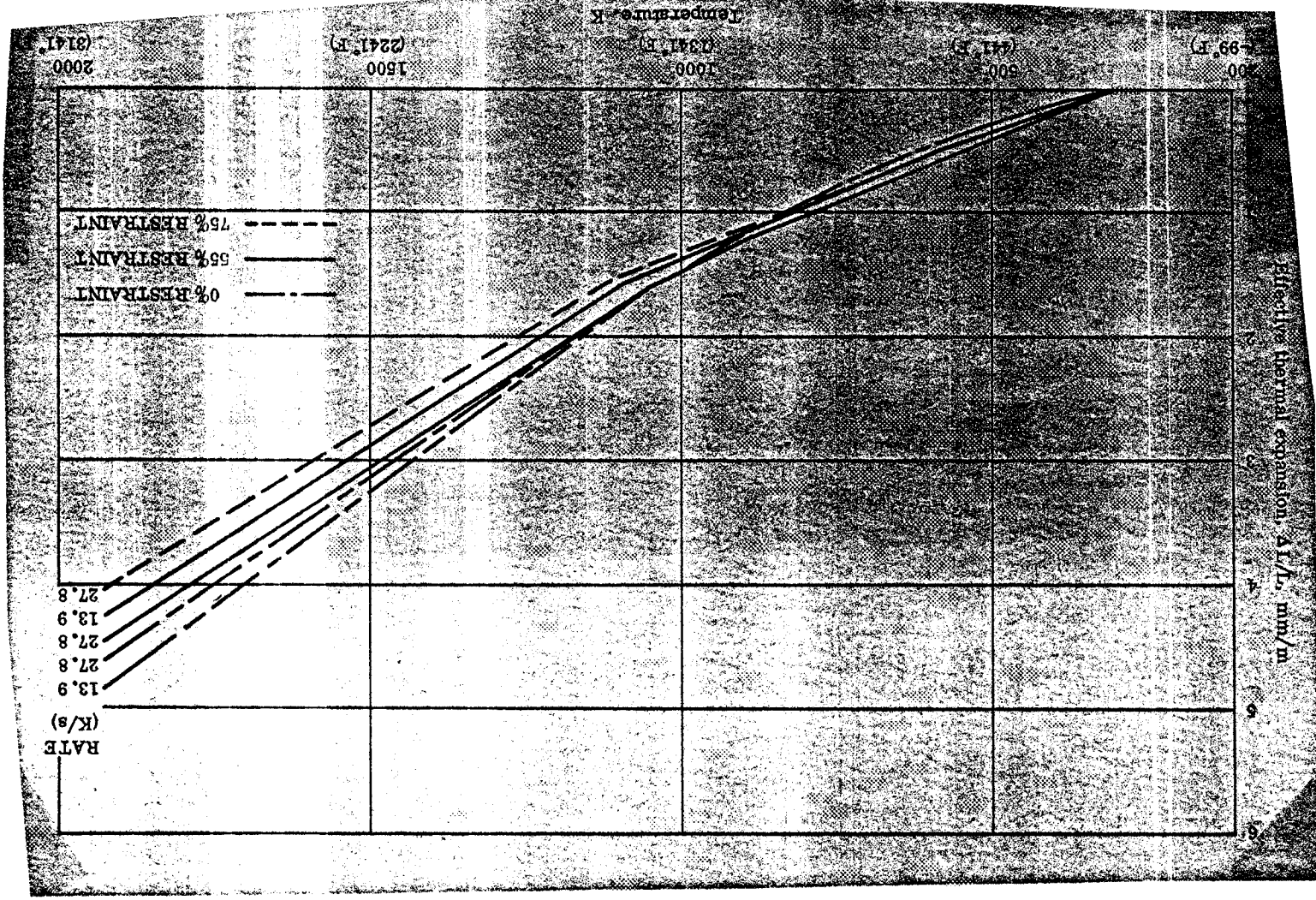


Figure 105. Restrained Expansion of Carbitex 700, With Lamina
Heating Rate = 27.8 K/s (3000° F/min) R = 75%

Figure 106. Summary of Restrained Expansion Data, Carbitex 700, With Lamina



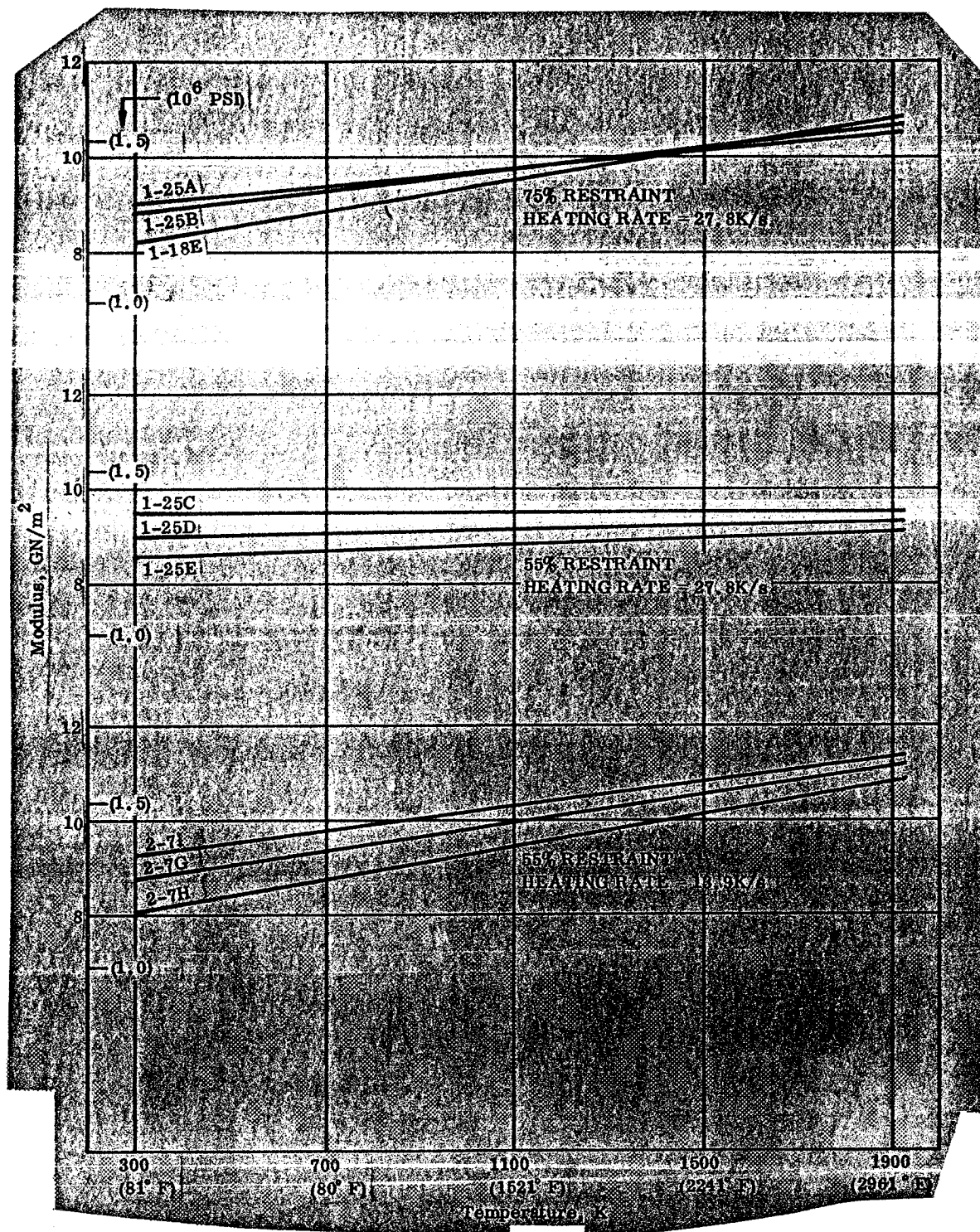


Figure 107. Modulus of Restrained Carbitex 700, With Lamina

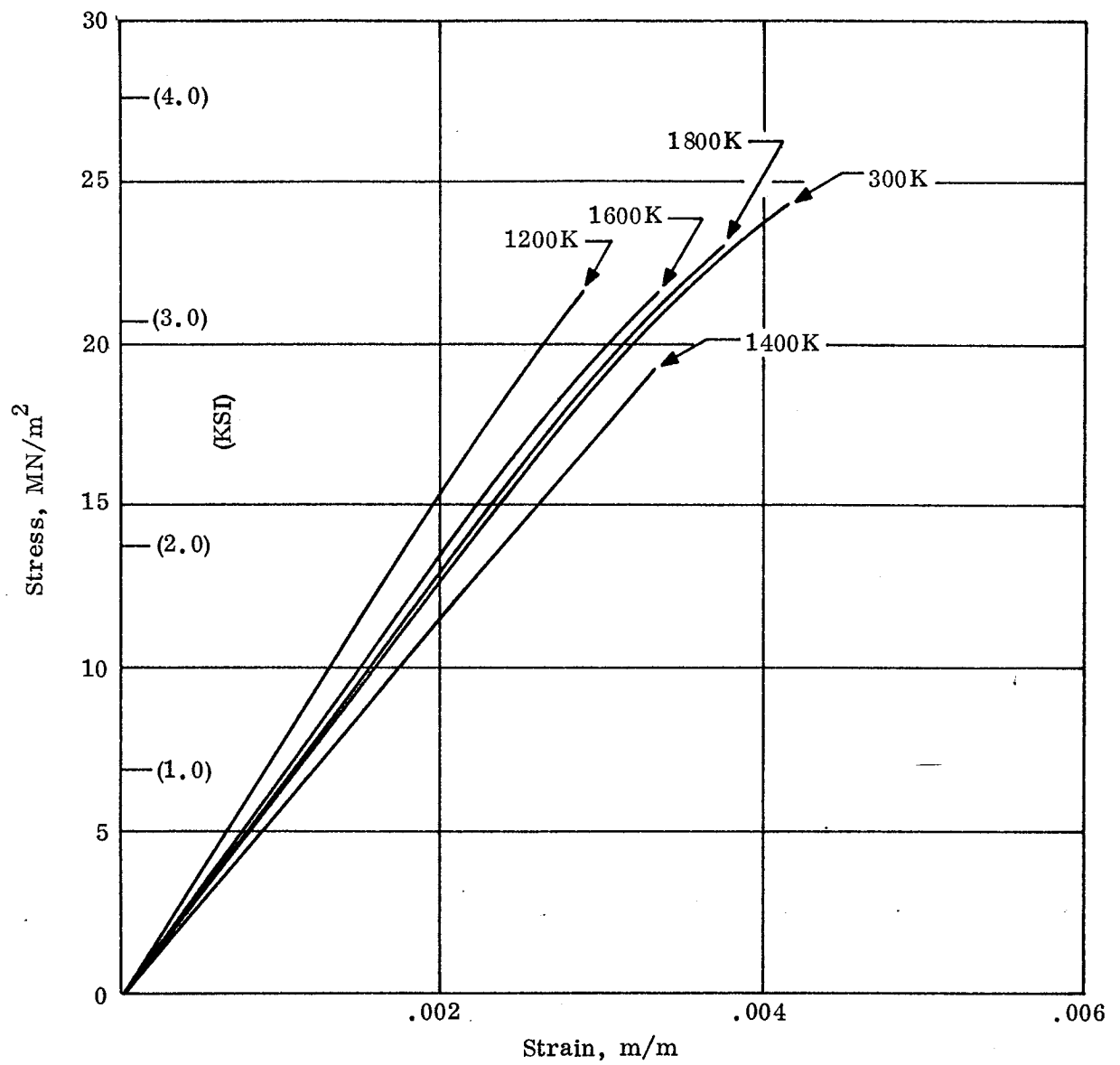


Figure 108. Compressive Stress-Strain Behavior of Carbitex 700 to 1800 K With Lamina (Average curves, not loaded to failure)

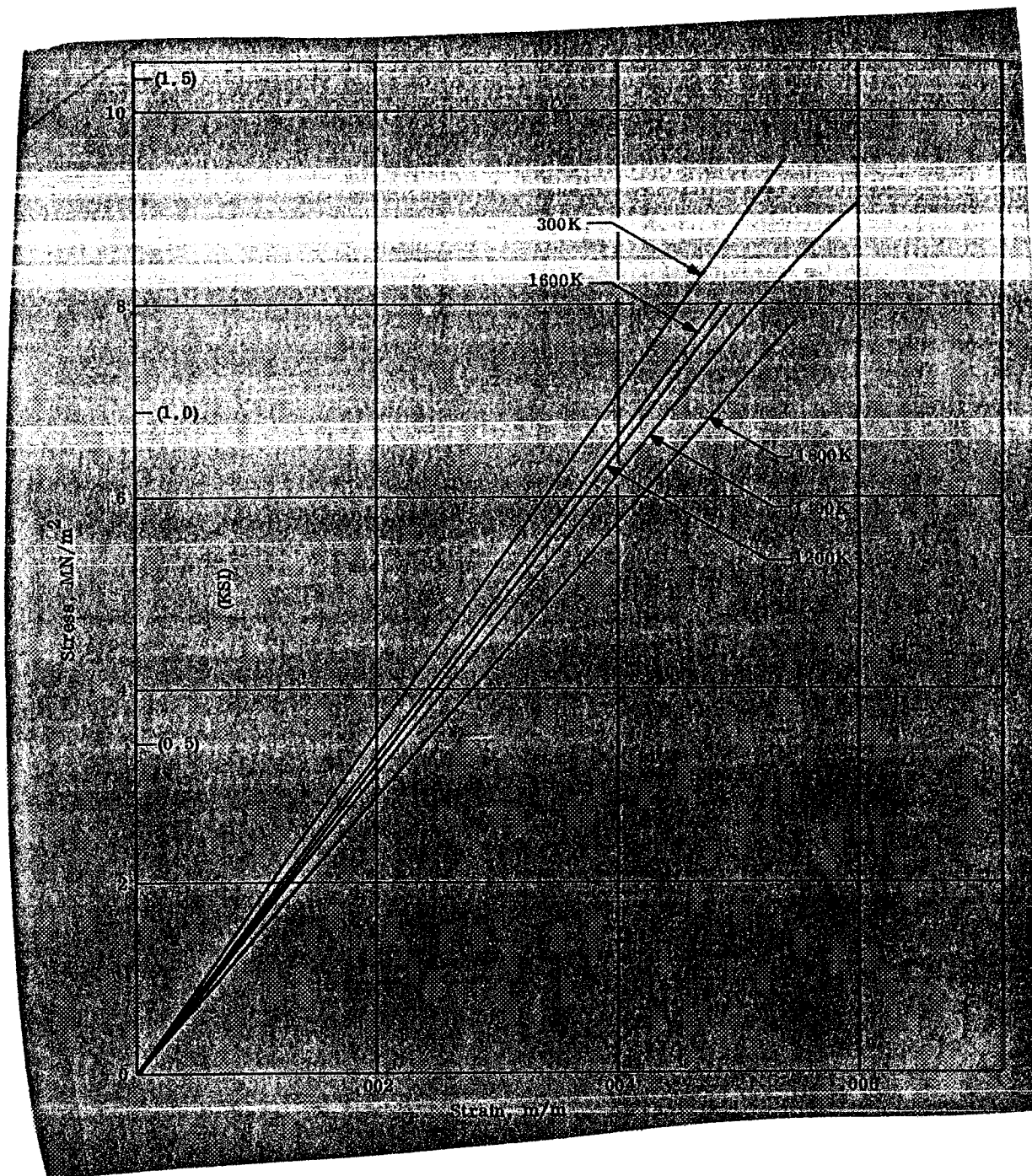


Figure 109. Compressive Stress-Strain Behavior of Carbitex 700 to 1800 K Across Lamina (Average curves, not loaded to failure)

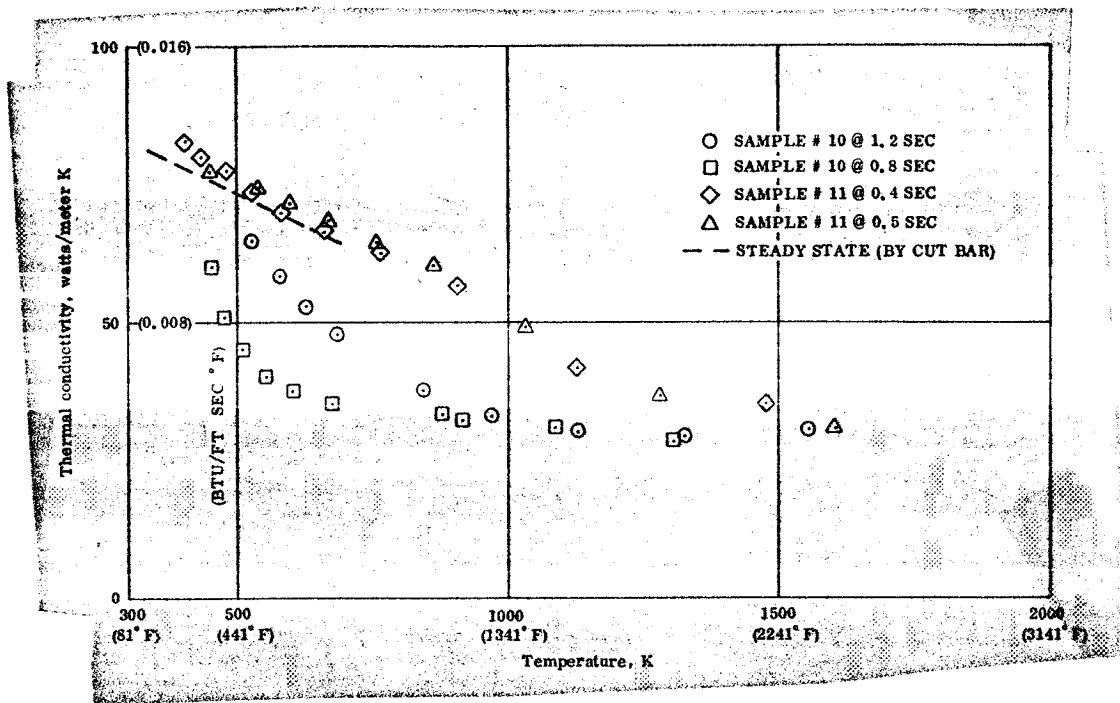


Figure 110. Thermal Conductivity of Carbitex 700, Transient Test With Lamina

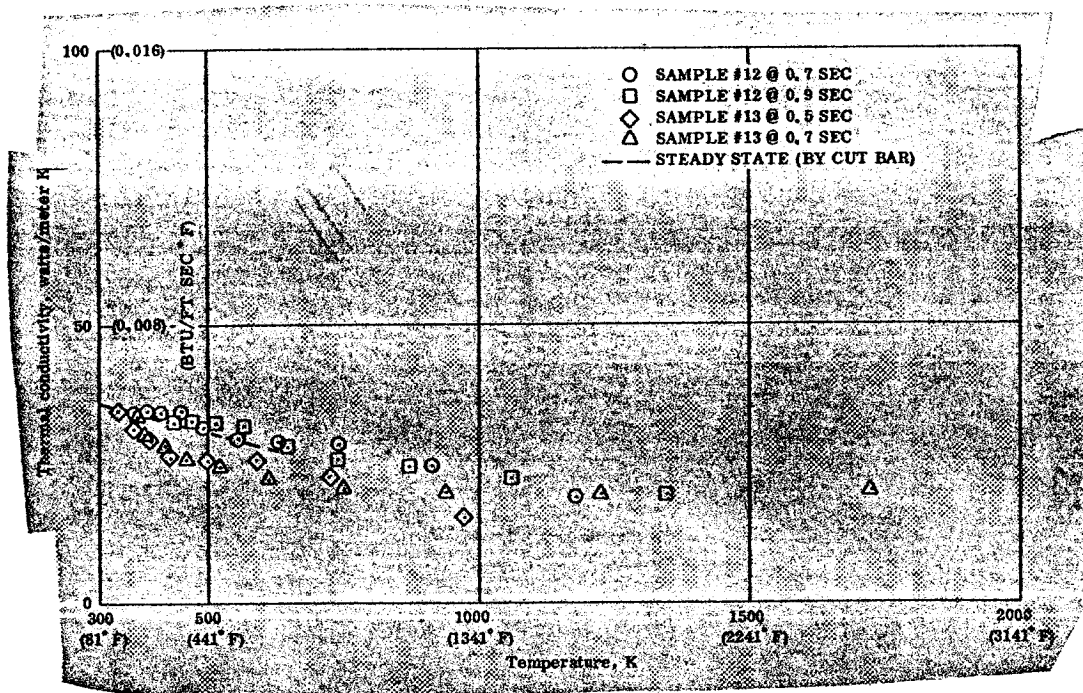


Figure 111. Thermal Conductivity of Carbitex 700, Transient Test Across Lamina

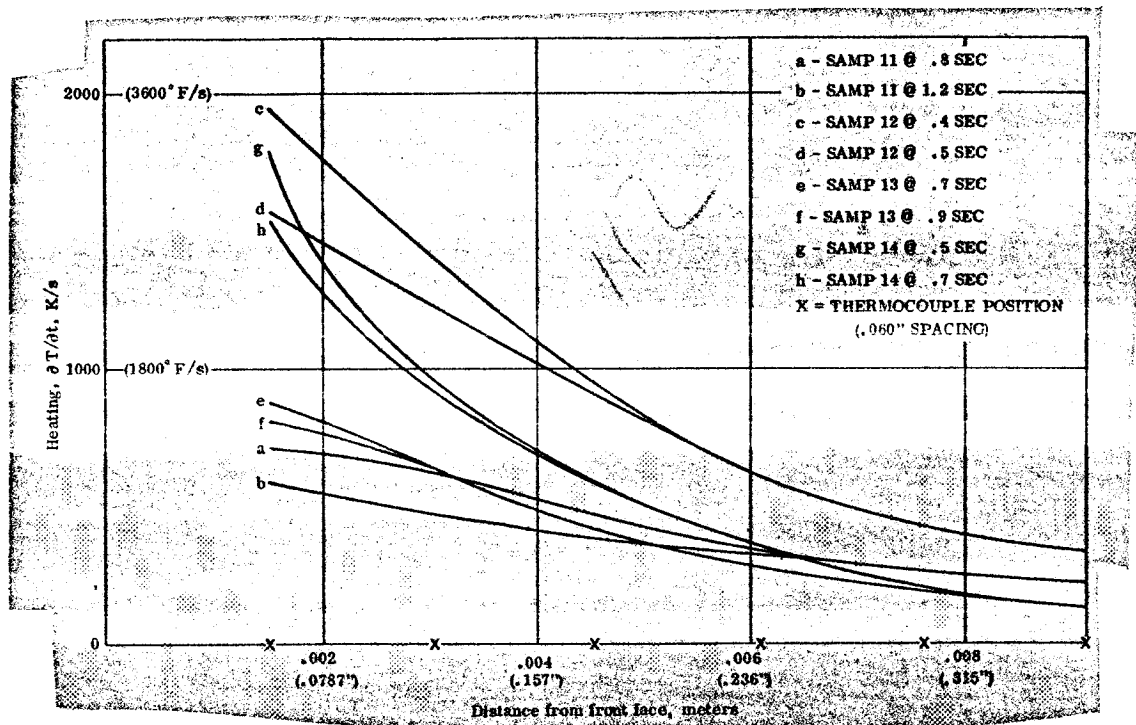


Figure 112. Thermal Conductivity of Carbitex 700, Transient Test
Summary of Heating Rate Data

Measurements on RPP-4

Density of the RPP-4 carbon-carbon composite was measured as $1446 \pm 11 \text{ kg/m}^3$ (from measurements on three of the restrained expansion specimens). This is somewhat lower than the density obtained on the Carbitex panel.

Free thermal expansion of RPP-4. -Slow heating rate thermal expansion data for RPP-4 are shown in Figure 113. Note that there is a considerable difference between the expansions for the two directions. At 1300 K, the AL and WL expansions are 5.85 and 2.25 mm/m respectively, a ratio of 2.6. This compares with a ratio of about 1.4 for Carbitex 700. Whether there is any advantage to having a higher or lower anisotropy in this respect probably depends on the specific application and the difference is noted here simply as one of the respects in which these two laminated carbon-carbons differ.

Figures 114 and 115 show the results of the high heating rate free thermal expansion measurements, each of which is again obtained from measurements on three long (5.08 cm) and three short (1.26 cm) specimens. One of these falls slightly above and the other slightly below the curve obtained at low heating rate. This is also seen if one considers the mean thermal expansion coefficient (fig. 116). From these curves it is concluded that no significant heating rate effect exists.

Restrained thermal expansion of RPP-4. - The results of restrained thermal expansion measurements are shown in Figures 117 and 118. There appears to be no significant difference between these two sets of data other than that considerably more scatter occurred at the higher heating rate. Thus there again is no evidence of any effect due to heating rate.

Comparing the effective thermal expansion obtained from the restrained expansion tests with the thermal expansion obtained from the free or unrestrained tests at comparable rates (fig. 119), it initially appears that a significant difference exists at the higher temperatures with the expansion obtained from the restrained tests running somewhat lower than the free expansion. The reason for this difference is not known. In the case of ATJ graphite and Carbitex 700 a similar deviation was also noted at the higher levels of restraint and, particularly in the case of ATJ, it was thought that this might be due to non-linearity of the stress-strain relation. However, in the case of RPP-4 the stress-strain curves are, for the most part, remarkably linear and it appears that this could not be the reason. As will be noted below (i. e., in the section on compression tests) there is sufficient variability indicated by the stress-strain curves that what appears to be a significant difference may only be a result of material variability and an insufficient number of replicate tests to establish a reliable mean curve. Note, for example, that the two free expansion curves (fig. 119), each of which is based on six tests, differ by about 0.50 mm/m. The mean of these two curves differs from the restrained expansion curve by about 0.75 mm/m, which would also suggest that this difference may not be as significant as it first appears or that the real difference between the two methods may be less than is indicated by this limited number of tests. On the other hand, considering all of the tests on the three graphitic materials (i. e., ATJ, Carbitex and RPP-4), it appears quite certain that the restrained expansion tests do indicate an effective expansion which is somewhat lower when the degree of restraint is high.

The with laminate modulus determinations made as a part of the restrained expansion tests are shown in Figure 120. Compared to the corresponding measurements on Carbitex 700 (fig. 107), it is seen that the starting values are about the same but the RPP-4 shows a larger increase with increase in temperature.

Compression stress-strain tests on RPP-4. - As was the case with Carbitex, the RPP-4 showed no significant heating rate effect. Therefore a number of compressive stress-strain tests were run rather than additional restrained expansion tests. The results of these measurements are given in Table 3 and Figures 121 and 122. As with the Carbitex, and for the same reason, the specimens were not loaded to failure.

Considering the with laminate curves, there does not appear to be any trend with increasing temperature. In general, the modulus of graphitics tend to increase somewhat with increase in temperature over the temperature range covered in these

TABLE 3. COMPRESSIVE MODULUS OF RPP-4 (GN/m²)

	<u>With Lamina</u>	<u>Across Lamina</u>
300 K (81 °F)	6.0 8.5 <u>8.9</u> 7.8 (1.13)*	2.5 2.9 <u>3.0</u> 2.9 (0.42)*
1200 K (1701 °F)	5.6 5.1 5.4 <u>6.8</u> 5.7 (0.83)	2.45 2.50 <u>2.55</u> 2.50 (0.36)
1400 K (2061 °F)	6.2 6.3 <u>6.4</u> 6.3 (0.91)	2.2 2.2 <u>2.6</u> 2.3 (0.33)
1600 K (2421 °F)	7.3 7.3 8.0 <u>9.2</u> 7.9 (1.14)	2.65 <u>2.75</u> 2.70 (0.39)
1800 K (2781 °F)	4.9 5.6 6.0 <u>6.7</u> 5.8 (0.84)	2.0 2.0 <u>2.1</u> 2.0 (0.29)

* - (10⁶ psi)

tests. For these five sets of curves, the modulus appears to first decrease, then increase and finally again decrease. Considering all temperatures, the values range from 5.0 to 9.3 GN/m² (0.72 to 1.35 x 10⁶ psi) with the lowest value occurring at 1800 K and the highest at 1600 K. At 300 K, the range was from 6.0 to 8.9 GN/m² (0.87 to 1.27 x 10⁶ psi). In the case of the Carbitex (Figures 108 and 109), there again is no consistent trend with temperature, but the total range is from 5.9 to 7.9 GN/m² (0.86 to 1.15 x 10⁶ psi), or about half the total scatter. In the across laminate direction, a somewhat similar situation exists but the modulus of the RPP-4 in this direction is about double that of the Carbitex 700 although the density of the RPP-4 is lower. Thus the difference appears to be due to some structural difference, possibly a difference in degree of graphitization due to differences in final graphitization temperature. It may be advisable to ascertain that the graphitization temperature exceeds the maximum temperature to which the material will be exposed in a rocket nozzle (i. e., over 3600 K, if possible) to avoid possible heating rate effects which may occur if the graphitization temperature is exceeded.

Strength measurements on RPP-4. - The results of room temperature flexure measurements (3 point loading) on RPP-4 are given in Table 4. The strengths obtained are considerably higher than were obtained on Carbitex; the modulus is only slightly higher.

TABLE 4. FLEX STRENGTH AND MODULUS OF RPP-4

@ 300 K (with laminate direction)

Strength (MN/m ²)	Modulus (GN/m ²)
104.2	11.6
118.0	13.5
104.9	13.5
64.2	9.0
64.9	9.0
73.8	9.7
122.1*	11.6*
124.2*	13.5*
Mean 97.2 (14.0 ksi)	11.4 (1.65 x 10 ⁶ psi)

Note: * - See text.

In conducting flex tests, the specimens are usually prepared such that the load is applied in the across laminate direction and the outer-fiber tensile and compressive stresses are in the with laminate direction. This yields the strength and modulus in the with laminate direction. However, it is also possible to apply the load in the with laminate direction and also develop the outer fiber stress in the with laminate direction (since two of the three directions are "with laminate"). This should also yield the "with laminate" strength and modulus. In the above reported tests, six were conducted using the first method of loading and two (those marked with the asterisks) using the second method.

The results of tensile tests on RPP-4 at elevated temperatures and fast heating rates are given in Table 5. These results were interesting in that the specimens appear to consist of two groups with about 35 to 40 percent of the specimens being much stronger than the others. In conducting the tests it was noted that one of two types of failures occurred. These were:

- (1) A tensile failure in the gage section at a stress level of about 55 MN/m^2 (8000 psi) or
- (2) A shear failure (interlaminar) in the grips at a tensile stress (based on gage cross-section) of about 90 MN/m^2 (13000 psi).

The second type of failure could possibly be avoided by a slightly modified specimen design, in which case 40 percent of the specimens would be expected to show strengths comparable to those obtained in the flex tests.

In considering the flex tests, it will be noted that two of the flex test results (25 %) were quite low also and a third was interintermediate. Thus the scatter is present there also but the stronger specimens are dominant.

TABLE 5. TENSILE STRENGTH MEASUREMENTS ON RPP-4 (MN/m^2)

Heating Rate (K/s)	Temperature		
	1370 K	1640 K	1920 K
13.9	56.6	48.0	49.0
13.9	53.8	55.9	54.9
13.9	>91.8	53.8	>89.7
13.9			>93.2
27.8	58.0	58.0	53.5
27.8	>83.8	>96.2	>81.5
27.8	54.2	55.3	>81.5

It is quite common for flex tests to yield higher strengths for graphitics than do tensile tests. This is sometimes because it is more difficult to perform a tensile test as a small amount of bending can result in premature failure if the ultimate strain of the material is low. However, it has also been suggested that, since only the outer fibers are at high tensile stress in the flex test, the effective volume of the flex specimen is small compared to that of a tensile specimen of similar cross-section area. Thus if there are any flaws present in the material which might act as stress-risers, these would be more apt to affect the tensile test than the flex test, with resultant lower tensile strengths.

Transient thermal conductivity of RPP-4. - The samples were instrumented with a thermocouple spacing of 0.15 cm and were tested at the Hyperthermal Arc facility. The resultant data are shown in Figures 123, 124 and 125. The conductivity in both directions is slightly less than the conductivity of the corresponding direction of Carbitex 700 with the exception of the higher temperatures in the with grain direction. It would be particularly interesting to see if the data scatter from specimen to specimen in the with grain direction is larger than the across grain direction for this material as it was for the Carbitex.

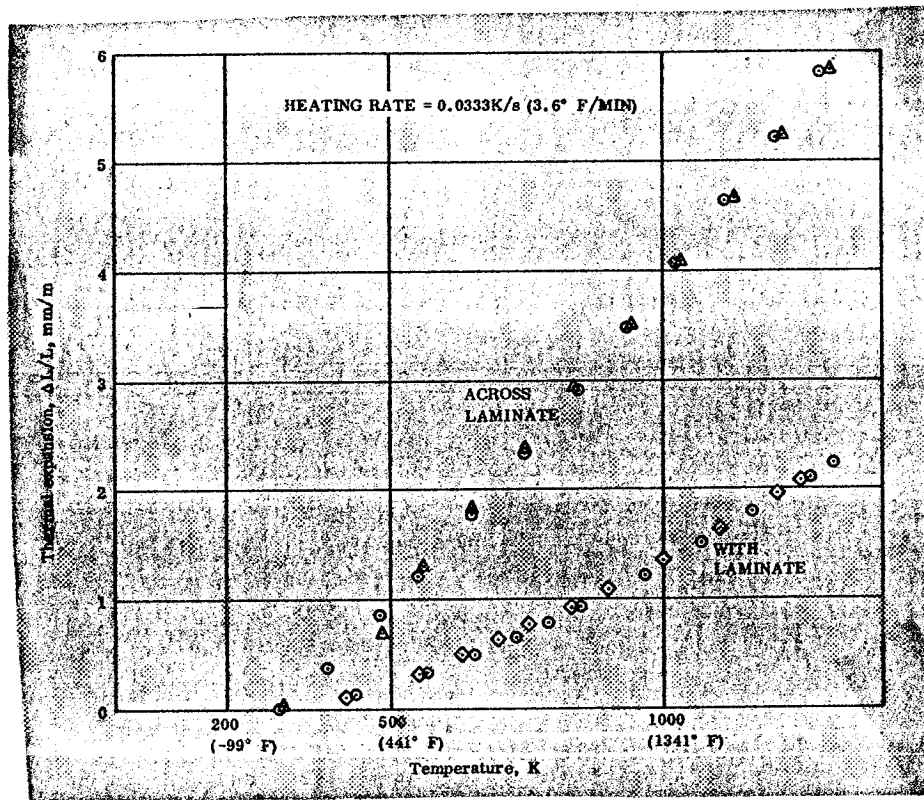


Figure 113. Thermal Expansion of RPP-4 With and Across Lamina at 0.033 K/s (3.6° F/min)

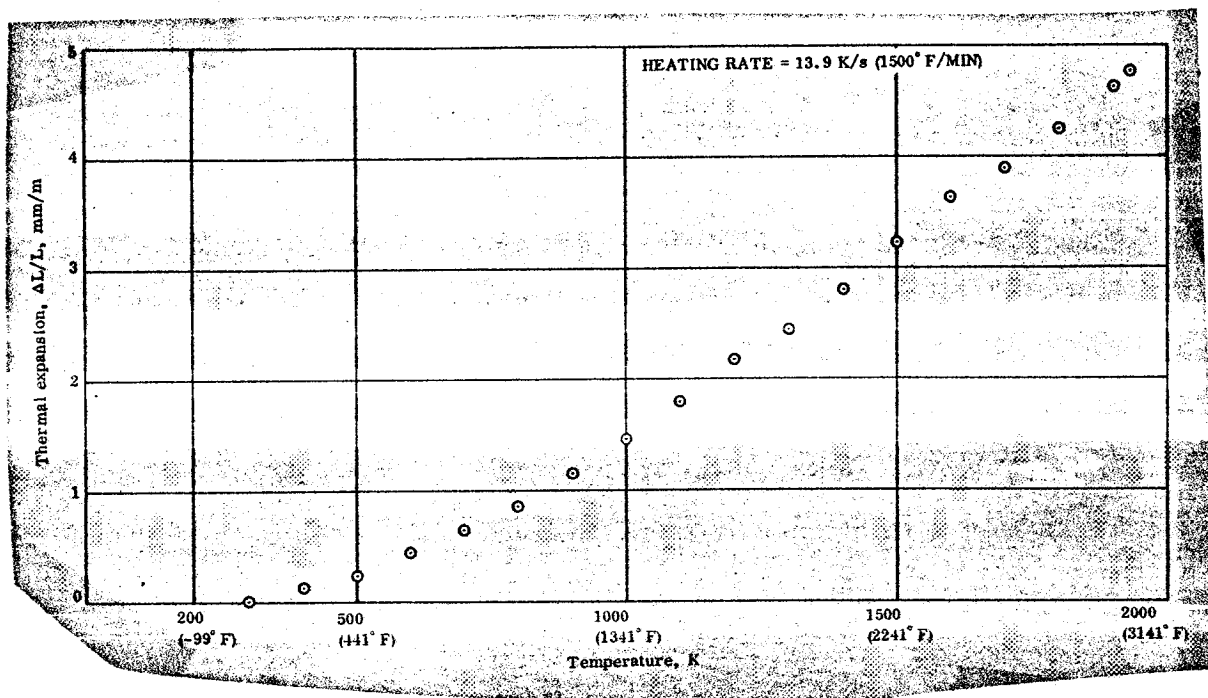


Figure 114. Thermal Expansion of RPP-4 With Lamina, 13.9 K/s (1500° F/min)

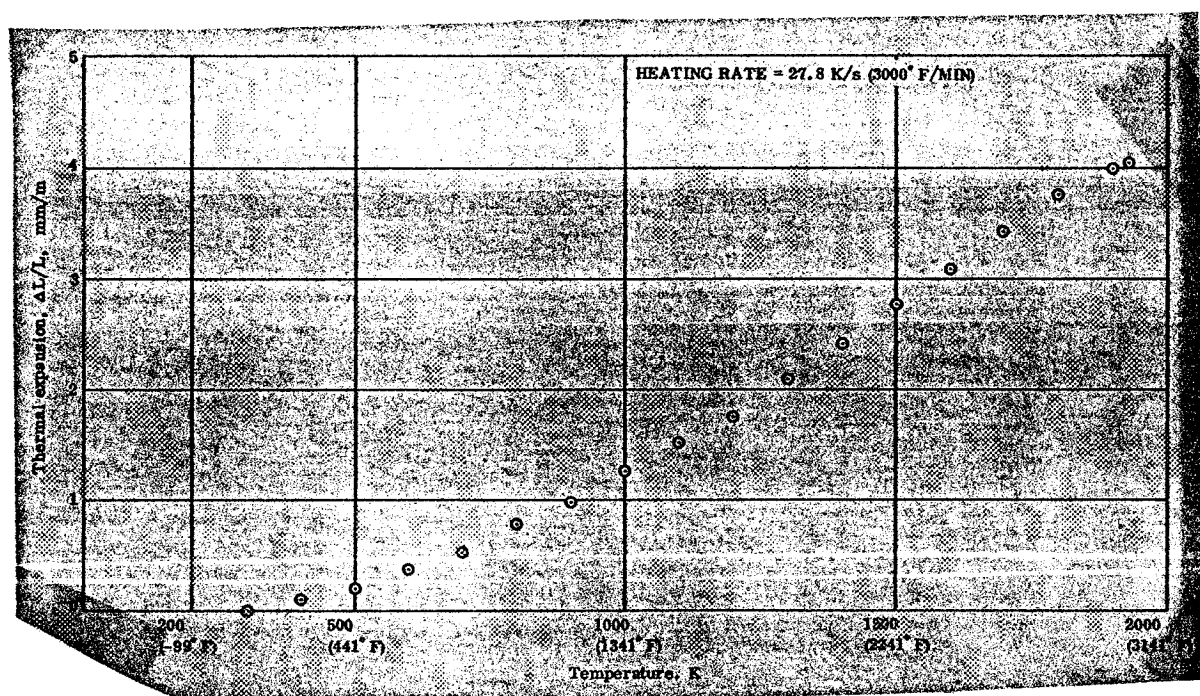


Figure 115. Thermal Expansion of RPP-4 With Lamina, 27.8 K/s (3000° F/min)

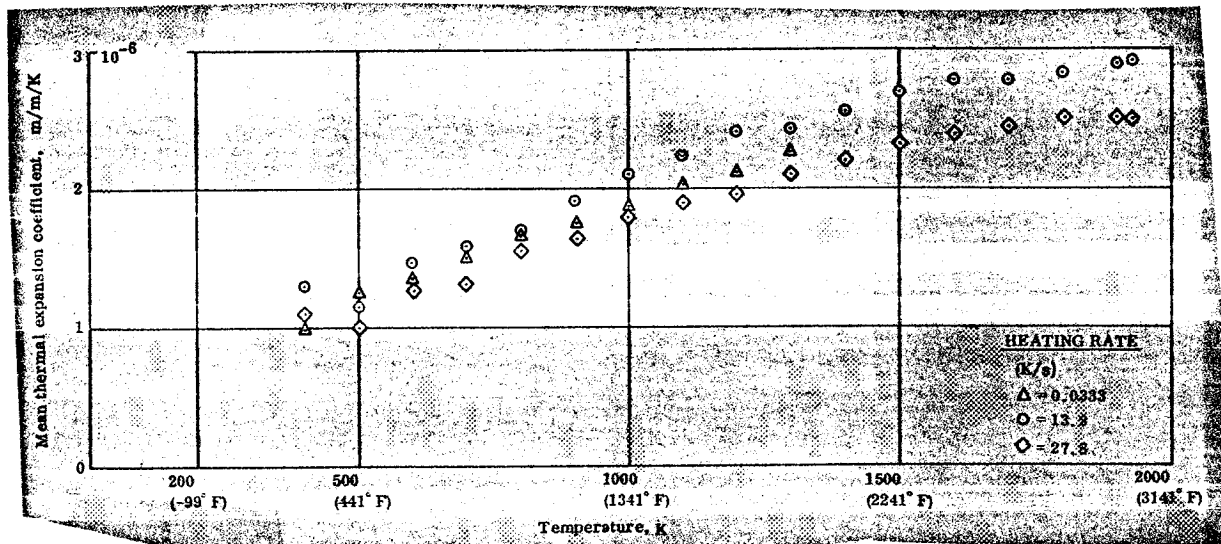


Figure 116. Mean Thermal Expansion Coefficient of RPP-4, With Lamina

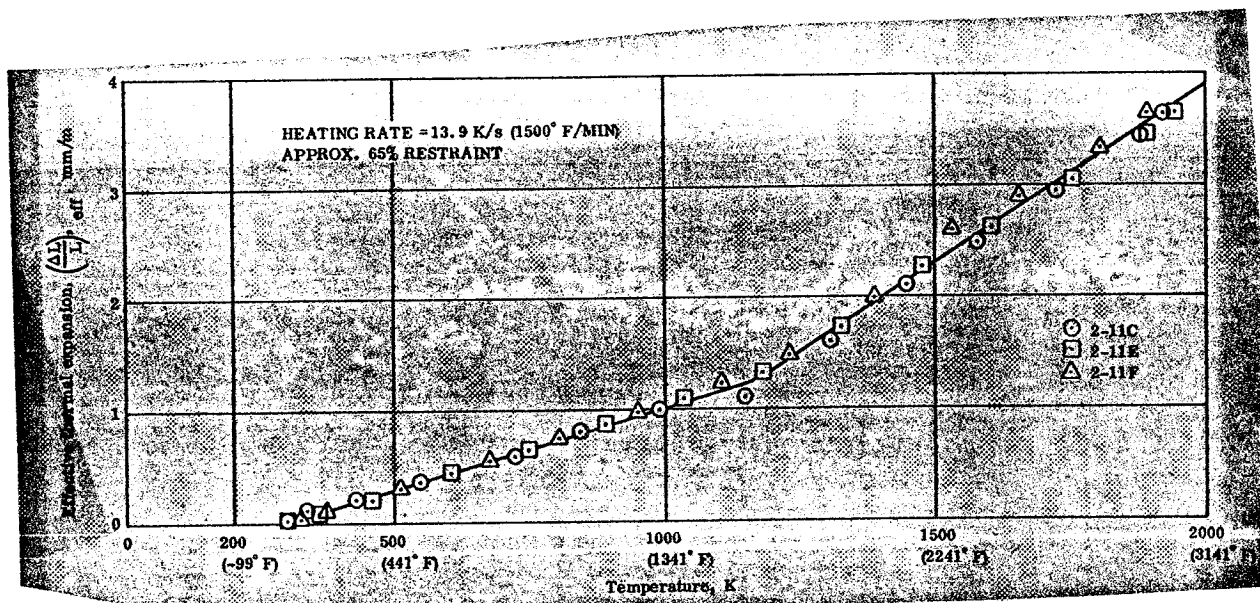


Figure 117. Restrained Thermal Expansion of RPP-4, With Lamina
Heating Rate = 13.9 K/s (1500° F/min) R = 65%

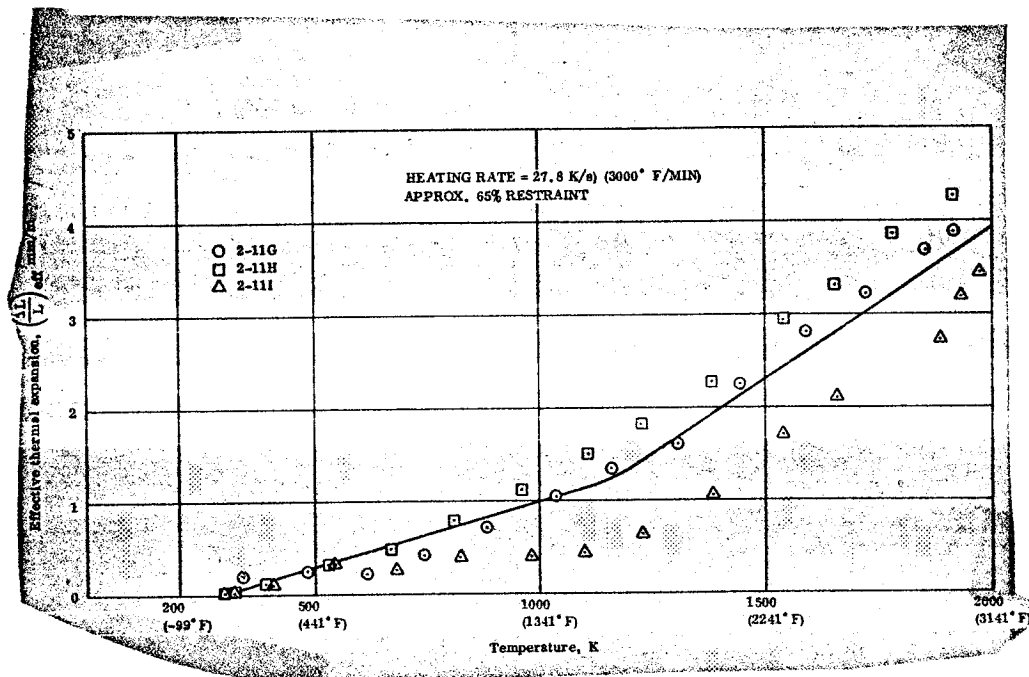


Figure 118. Restrained Thermal Expansion of RPP-4, With Lamina
Heating Rate = 27.8 K/s (3000° F/min) R = 65%

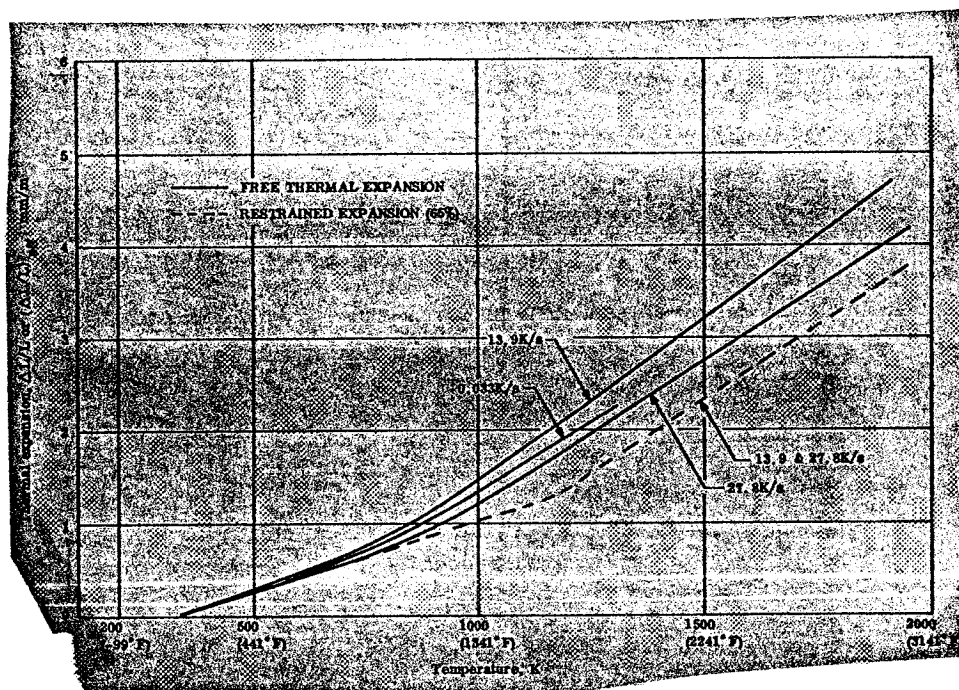


Figure 119. Summary of Free and Restrained Thermal Expansion
Data, RPP-4, With Lamina

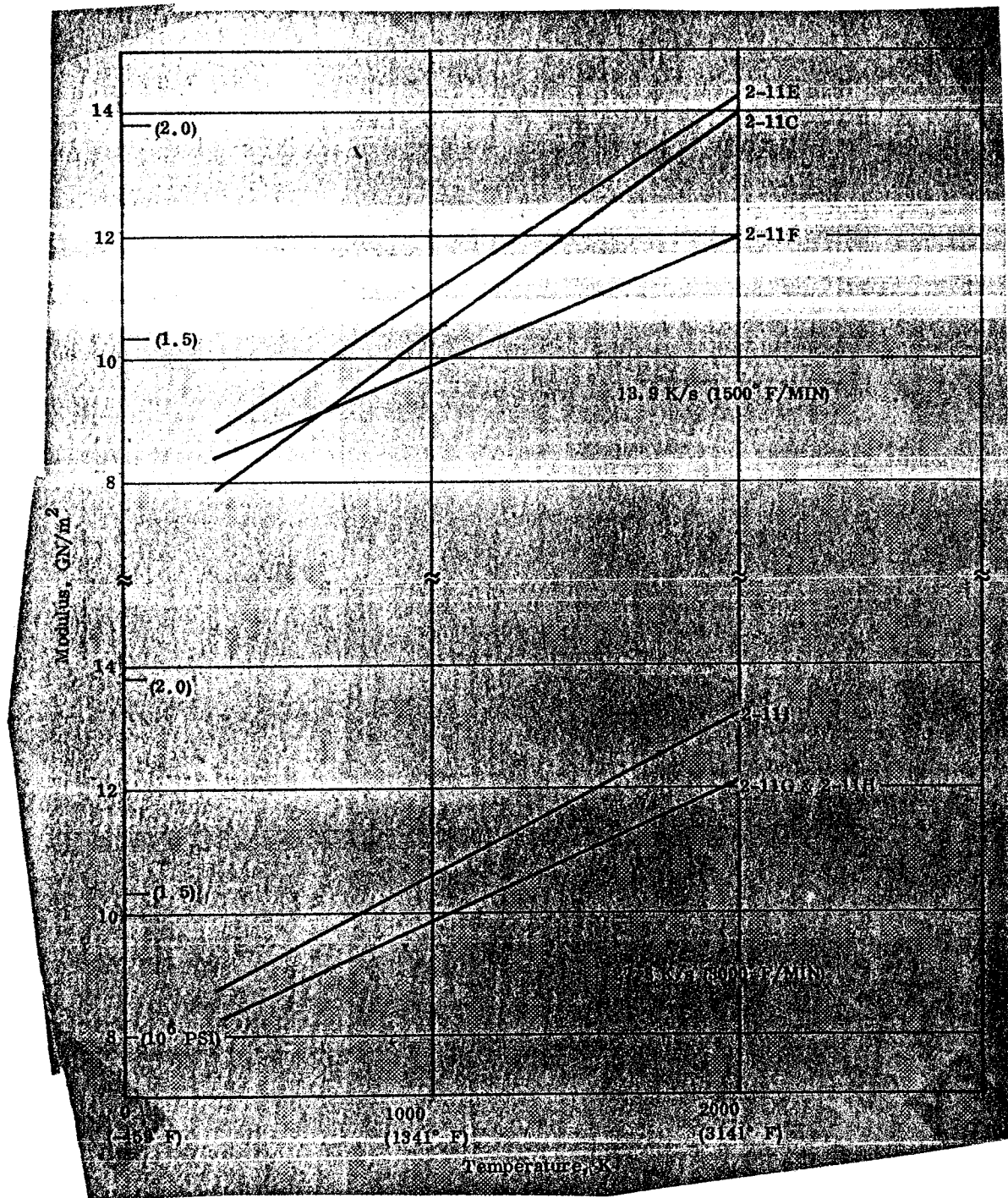


Figure 120. Modulus of Restrained RPP-4, With Lamina, R = 65%

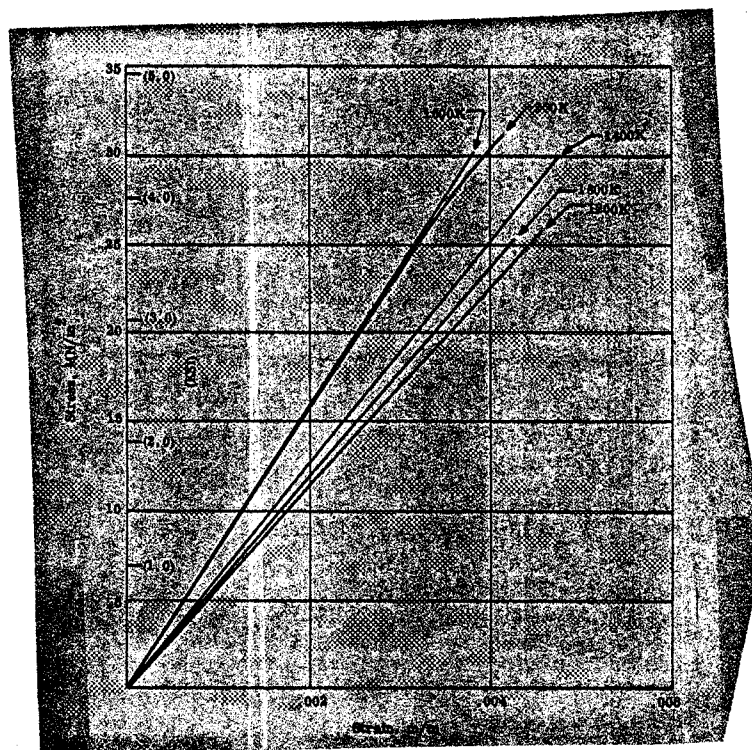


Figure 121. Compressive Stress-Strain Behavior of RPP-4 to 1800 K (Average curves, not loaded to failure) With Lamina

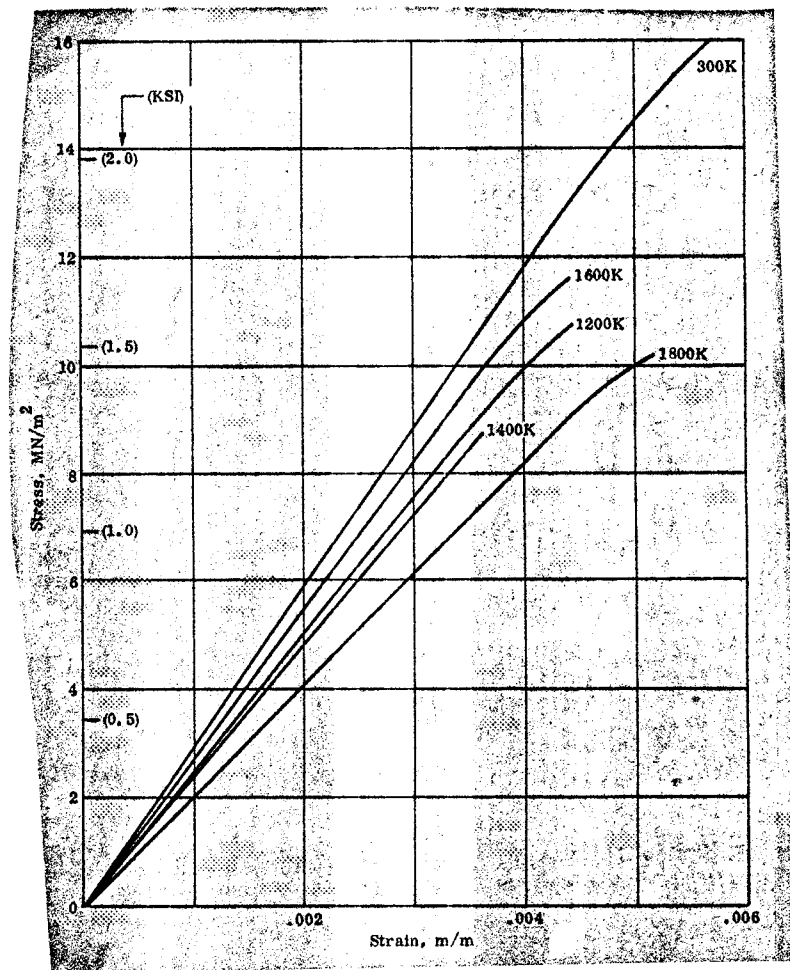


Figure 122. Compressive Stress-Strain Behavior of RPP-4 to 1800 K (Average curves, not loaded to failure) Across Lamina

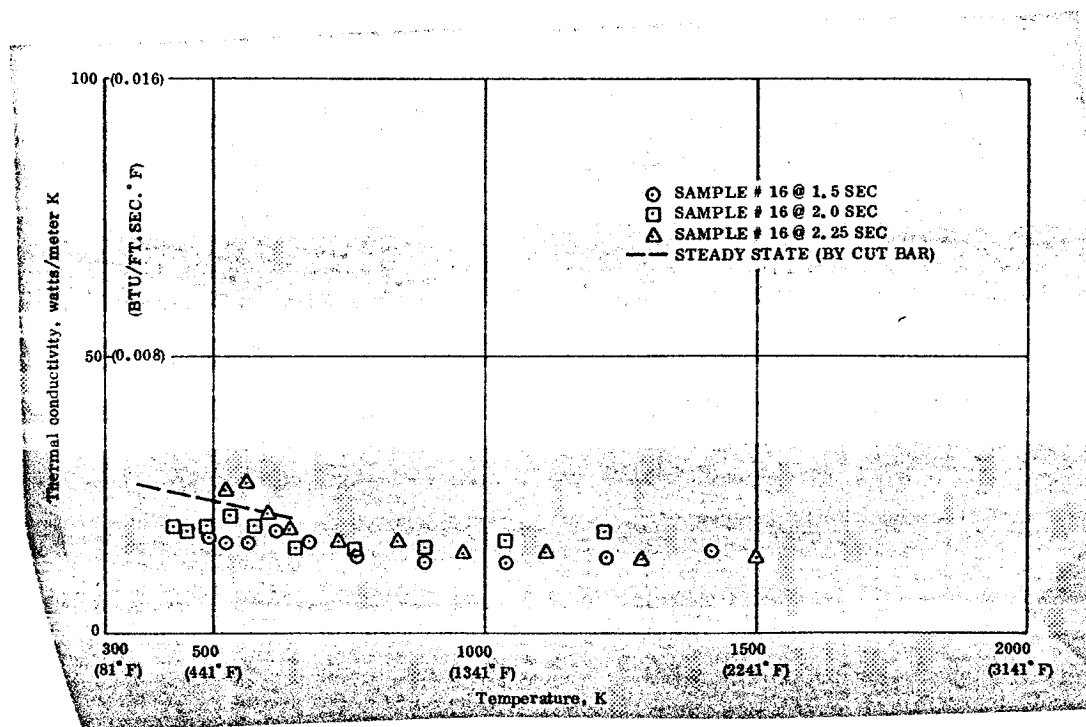


Figure 123. Thermal Conductivity of RPP-4, Transient Tests Across Lamina

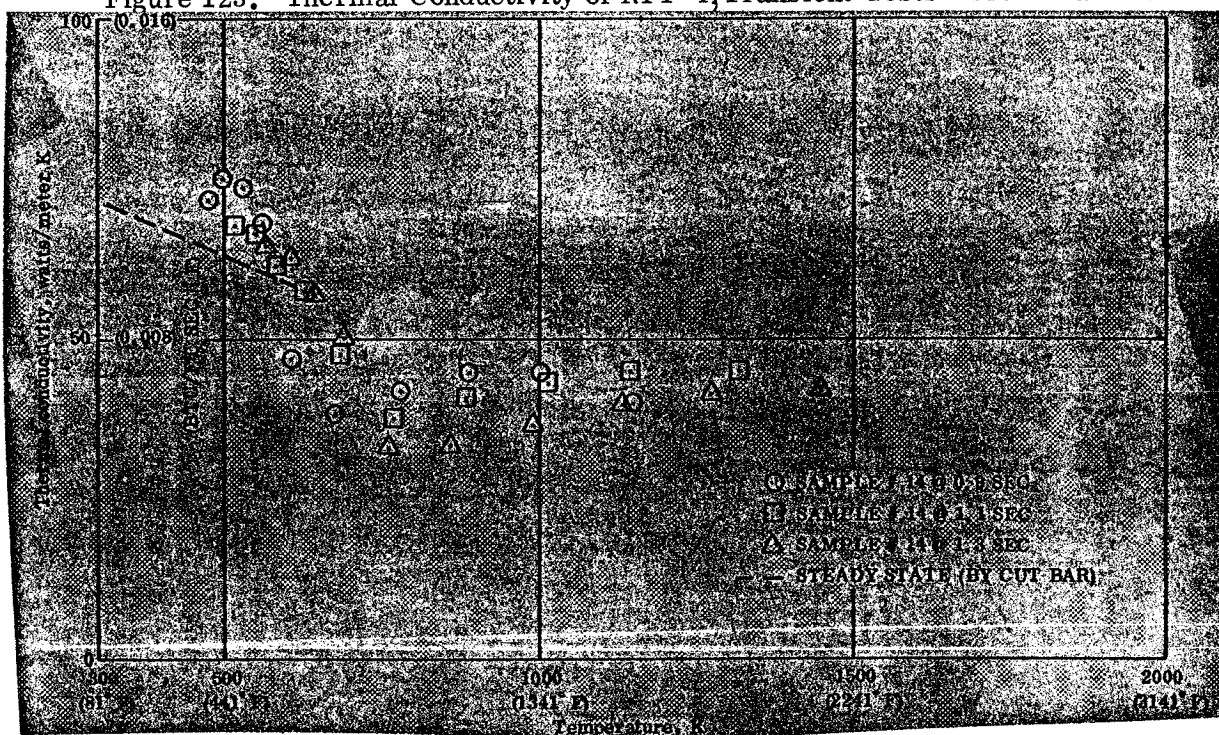


Figure 124. Thermal Conductivity of RPP-4, Transient Tests With Lamina

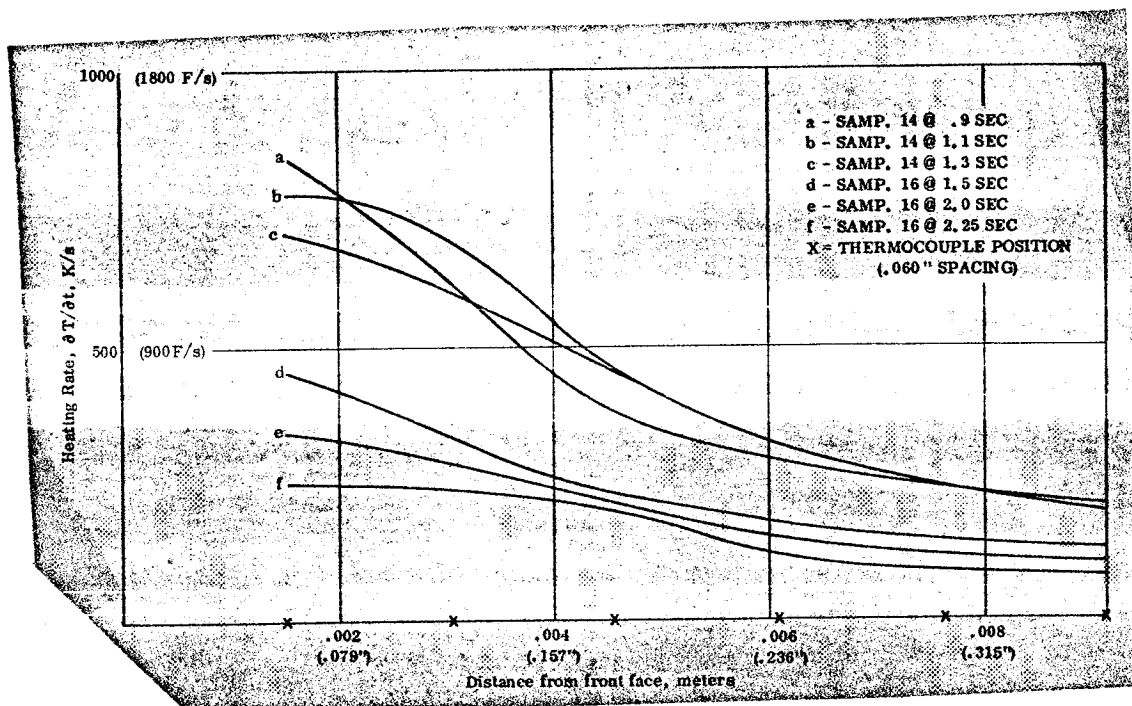


Figure 125. Thermal Conductivity of RPP-4, Transient Tests
Summary of Heating Rate Data

UTILIZATION OF TRANSIENT DATA IN THERMO-STRUCTURAL ANALYSIS

As additional knowledge of material behavior becomes available, the designer/structural analyst must answer the question, "How can recent understandings of material behavior best be factored into the present design/analysis techniques?" For loading rate sensitive materials, one must estimate the loading rate, then determine the suitable properties for analysis of the resulting stresses and deformation.

In the present work, thermal expansion has been found to be dependent on constraint and rate of change in temperature. Consequently, before predicting thermal stresses, one must determine the rate of change of temperature at a given location, along with the relative physical constraints. The appropriate thermal expansion curves may then be used to determine the thermal expansion for use in thermal stress calculations. In relatively simple geometric problems the constraint on the material may be easily characterized and one need only determine thermal expansion as a function of the given rate of change of temperature. Stated more simply, material properties such as thermal expansion must now be considered as a function of the material, the rate of change of temperature, and the physical constraints on the material. That is, thermal expansion becomes:

$$\frac{\Delta L}{L} = f\left(\frac{dT}{dt}, \sigma, \text{constraint}\right)$$

Given the temperature history of a material, the time rate of change of temperature can be determined rather easily for any point in the material. However, except for simple geometries, the constraint at a given point is not so easily determined. For highly constraint sensitive materials one must first estimate the final stress levels (hence constraint), then calculate a stress solution for the assumed constraint. A comparison of the resulting constraints with those assumed will determine the accuracy of the results. A few iterations of the analysis should be sufficient to define a final stress state which reflects the proper material properties.

CONCLUSIONS

ATJ Graphite

1. Thermal expansion under free or unrestrained conditions is independent of heating rate for rates up to 27.8 K/s (3000° F/min.) and temperatures up to 1900 K (2961° F).
2. Effective thermal expansion, obtained from restrained expansion tests, is essentially the same as the free expansion for restraints up to at least 55 percent. High restraint (75%) appears to yield a slightly low result.
3. Thermal conductivity obtained from the transient test agrees with earlier static data, indicating a lack of any heating rate sensitivity.
4. No significant heating rate effects were anticipated for ATJ graphite and the agreement between static and transient techniques indicates the validity of the transient techniques.

MX 2600 Silica Phenolic

1. Heating rate has a significant effect upon the free thermal expansion. Increasing the heating rate results in higher peak expansion and the return to zero expansion occurs at higher temperature.
2. The peak in the effective thermal expansion versus temperature curve (with lamina direction) is shifted to lower temperatures and the expansion returns to zero at lower temperature as the degree of restraint is increased. Thus, increased restraint has essentially the opposite effect of increasing heating rate.
3. Across lamina restraint appears to have a similar effect. However, the combination of high restraint with high heating rate can result in high stress (due to gas pressure) and hence, a high effective thermal expansion. This condition can result in large pieces of material being blown off of the surface as gases escape. Thus, in end use, a combination of high heating rate and high restraint could lead to a high ablation rate.
4. Within a limited range of heating rates (2.9 and 5.0 K/s), heating rate and restraint did not appear to have a significant effect upon the modulus obtained under restrained conditions.

5. Strength decreased with increase in temperature. Heating rate did not have a significant effect within the narrow range of 2.8 to 7.0 K/s but these could differ from static data.

6. Density of char formed by exposure to the plasma from a tandem Gerdien arc was somewhat lower (8%) than char obtained from a fired SCOUT motor.

7. Thermal conductivity of the char from a SCOUT motor (30 degree lay-up) was intermediate to the with and across-lamina data obtained on arc formed char, as would be expected, at low temperatures. However, at high temperatures the conductivity of the motor formed char was higher than either of the arc-formed chars. This could be due to the somewhat higher density.

FM 5272 Cellulose Phenolic

1. Thermal expansion of FM 5272 is significantly affected by heating rate. Peak expansion is increased and the peak is shifted to higher temperature as the heating rate is increased.

2. The peak effective thermal expansion (restrained test) is considerably less than the expansion obtained from a free or unrestrained test at a comparable heating rate and the peaks occur at lower temperature.

3. Within a narrow range of heating rates, heating rate and restraint do not appear to affect the modulus which is obtained under restrained conditions.

4. Strength decreases significantly with increase in temperature. Heating rates of 2.8 and 7 K/s gave comparable results but increasing the rate to 13.9 K/s (1500° F/min) resulted in lower strengths and considerably more scatter.

5. Char formed in the Gerdien arc facility was so weak that transient thermal conductivity models disintegrated almost instantly upon subsequent exposure to the arc. Char formed under slower heating conditions was stronger but still could not survive the plasma flow of the arc (or even the gas flow from a Linde torch) long enough to provide useful data.

Carbitex 700

1. Thermal expansion is independent of heating rate within the range of rates and temperatures employed.

2. As with the ATJ graphite, the restrained expansion tests gives an effective expansion which is slightly low at the higher temperatures with the deviation increasing as the restraint is increased. Up to about 55 percent restraint the deviation is minor.

3. Heating rate and temperature had no effect upon strength within the range of rates and temperatures employed.

4. At low temperatures, thermal conductivities were the same for both the transient and cut-bar techniques, indicating no rate effect.

5. Thermal conductivity in the with-lamina direction shows considerable scatter (transient technique). This may be related to the fact that fiber bundles have higher conductivities than surrounding matrix material and the thermocouples are very small in diameter and measure temperature in a very localized region.

RPP-4

1. Thermal expansion is independent of heating rate within the range of rates and temperatures employed.

2. Effective thermal expansion obtained from restrained expansion tests runs somewhat lower than the free expansion. However, restrained expansion tests were only run at 65 percent restraint and the other graphities also showed such a deviation at restraints above about 55 percent.

3. Compressive stress-strain curves showed greater variability as compared with the Carbitex 700.

4. With lamina tensile strength appeared to be independent of heating rate and temperature within the ranges employed.

5. About 60 percent of the tensile specimens had tensile strengths of about 55 MN/m² (8,000 psi). The other 40 percent had strengths in excess of 90 NM/m² (13,000 psi).

6. At low temperature, the transient and cut-bar techniques gave essentially the same thermal conductivity, thus indicating no rate effect.

7. As with the Carbitex 700, transiently determined thermal conductivity in the with-lamina direction shows anomalies which may be related to the difference in conductivities of the fibers and matrix.

General

1. Graphite materials generally would not be expected to show significant heating rate effects at temperatures below their graphitization temperature. This has been true of the materials tested. As a result, material properties determined under static heating conditions should be adequate.

2. Reinforced polymeric materials exhibit significant heating rate effects on properties. As a result, thermal expansion data in particular should be determined under conditions of heating rate and restraint which approach, as near as possible, the conditions expected in the end-use application.

APPENDIX

Conversion Factors

<u>To Convert</u> <u>From</u>	<u>To</u>	<u>Multiply By</u>
K/s	°F/sec	1.8
K/s	°F/min	108
m/m	in/in	1.0
mm/m	in/in	0.001
N/m ²	psi	0.000145
GN/m ²	psi	145,000
MN/m ²	psi	145

REFERENCES

1. Anon.: Study of Improved Materials for use in SCOUT Solid Rocket Motor Nozzles, Phase I Report. Report No. 23.412, LTV Aerospace Corp., 6 Sept., 1969.
2. Holt, D.L., et al: The Strain Rate Dependence of the Flow Stress in Some Aluminum Alloys. Report No. TR66-75, General Motors Defense Research Laboratories, November 1966.
3. Glasstone, S.; Laidler, K.J.; and Eyring, H.: The Theory of Rate Processes. pp. 480-483, McGraw-Hill, N.Y. (1941).
4. Roetling, J.A.: Yield Stress Behavior of Some Thermoplastic Polymers. TIS Report No. 67SD325, General Electric Missile and Space Division, 1967.
5. Brazel, J.P.; Tanzilli, R.A.; and Begany, A.R.: Determination of the Thermal Performance of Char under Heating Conditions Simulating Atmospheric Entry. paper in Thermophysics and Temperature Control of Spacecraft and Entry Vehicles, Vol. 18 in Progress in Astronautics and Aeronautics, AIAA series, 1966, Academic Press.
6. Andrew, James F.: Elastic Properties of Carbons and Graphite. PhD Thesis, State University of N.Y. at Buffalo, 1963.
7. Roetling, J.A.; and Rosicky, E.: Response of Transducers in Short Duration Tests. High Speed Testing Vol. VI: The Rheology of Solids; Applied Polymer Symposia No. 5, Interscience, 1967.
8. Kratsch, K.M.; Hearne, L.F.; and McChesney, H.R.: Thermal Performance of Heat Shield Composites during Planetary Entry. AIAA/NASA Engineering Problems of Manned Interplanetary Exploration, American Institute of Aeronautics and Astronautics, New York, 1963.
9. Shaw, T.E.; Garner, D.C.; and Florence, D.E.: Effects of Uncertainties in Thermophysical Properties in Ablation Efficiency. Thermophysics and Temperature Control in Spacecraft and Entry Vehicles, Vol. 18 in Progress in Astronautics and Aeronautics, AIAA, 1966.
10. Parker, W.J.; Jenkins, R.J.; Butler, C.P.; and Abbott, G.L.: Flash Method of Determining Thermal Diffusivity, Heat Capacity and Thermal Conductivity. J. Appl. Phys., 32, p. 1679, 1961.
11. Cunnington, G.R.; Smith, F.J.; and Bradshaw, W.: Thermal Diffusivity Measurements of Graphites and Chars using a Pulsed Laser. Thermophysics and Temperature Control in Spacecraft and Entry Vehicles, Vol. 18 in Progress in Astronautics and Aeronautics, AIAA, 1966.

12. Hiltz, A.A.; Florence, D.E.; and Lowe, D.L.: Selections, Development and Characterization of a Thermal Protection System for a Mars Entry Vehicle. Journal of Spacecraft and Rockets.
13. Brazel, J.P.; and Nolan, E.J.: Non-Fourier Effects in the Transmission of Heat. Proceedings of the Sixth Thermal Conductivity Conference, Dayton, Ohio AFML, 1966.